



Design, Development and Optimization of a Low Cost System for Digital Industrial Radiology



IAEA

International Atomic Energy Agency

IAEA RADIATION TECHNOLOGY SERIES PUBLICATIONS

One of the main objectives of the IAEA Radioisotope Production and Radiation Technology programme is to enhance the expertise and capability of IAEA Member States in utilizing the methodologies for radiation processing, compositional analysis and industrial applications of radioisotope techniques in order to meet national needs as well as to assimilate new developments for improving industrial process efficiency and safety, development and characterization of value-added products, and treatment of pollutants/hazardous materials.

Publications in the IAEA Radiation Technology Series provide information in the areas of: radiation processing and characterization of materials using ionizing radiation, and industrial applications of radiotracers, sealed sources and non-destructive testing. The publications have a broad readership and are aimed at meeting the needs of scientists, engineers, researchers, teachers and students, laboratory professionals, and instructors. International experts assist the IAEA Secretariat in drafting and reviewing these publications. Some of the publications in this series may also be endorsed or co-sponsored by international organizations and professional societies active in the relevant fields.

There are two categories of publications: the **IAEA Radiation Technology Series** and the **IAEA Radiation Technology Reports**.

IAEA RADIATION TECHNOLOGY SERIES

Publications in this category present guidance information or methodologies and analyses of long term validity, for example protocols, guidelines, codes, standards, quality assurance manuals, best practices and high level technological and educational material.

IAEA RADIATION TECHNOLOGY REPORTS

In this category, publications complement information published in the IAEA Radiation Technology Series in the areas of: radiation processing of materials using ionizing radiation, and industrial applications of radiotracers, sealed sources and NDT. These publications include reports on current issues and activities such as technical meetings, the results of IAEA coordinated research projects, interim reports on IAEA projects, and educational material compiled for IAEA training courses dealing with radioisotope and radiopharmaceutical related subjects. In some cases, these reports may provide supporting material relating to publications issued in the IAEA Radiation Technology Series.

All of these publications can be downloaded cost free from the IAEA web site:

<http://www.iaea.org/Publications/index.html>

Further information is available from:

Marketing and Sales Unit
International Atomic Energy Agency
Vienna International Centre
PO Box 100
1400 Vienna, Austria

Readers are invited to provide feedback to the IAEA on these publications. Information may be provided through the IAEA web site, by mail at the address given above, or by email to:

Official.Mail@iaea.org

DESIGN, DEVELOPMENT AND
OPTIMIZATION OF A LOW COST
SYSTEM FOR DIGITAL
INDUSTRIAL RADIOLOGY

The following States are Members of the International Atomic Energy Agency:

AFGHANISTAN	GUATEMALA	PANAMA
ALBANIA	HAITI	PAPUA NEW GUINEA
ALGERIA	HOLY SEE	PARAGUAY
ANGOLA	HONDURAS	PERU
ARGENTINA	HUNGARY	PHILIPPINES
ARMENIA	ICELAND	POLAND
AUSTRALIA	INDIA	PORTUGAL
AUSTRIA	INDONESIA	QATAR
AZERBAIJAN	IRAN, ISLAMIC REPUBLIC OF	REPUBLIC OF MOLDOVA
BAHRAIN	IRAQ	ROMANIA
BANGLADESH	IRELAND	RUSSIAN FEDERATION
BELARUS	ISRAEL	RWANDA
BELGIUM	ITALY	SAUDI ARABIA
BELIZE	JAMAICA	SENEGAL
BENIN	JAPAN	SERBIA
BOLIVIA	JORDAN	SEYCHELLES
BOSNIA AND HERZEGOVINA	KAZAKHSTAN	SIERRA LEONE
BOTSWANA	KENYA	SINGAPORE
BRAZIL	KOREA, REPUBLIC OF	SLOVAKIA
BULGARIA	KUWAIT	SLOVENIA
BURKINA FASO	KYRGYZSTAN	SOUTH AFRICA
BURUNDI	LAO PEOPLE'S DEMOCRATIC REPUBLIC	SPAIN
CAMBODIA	LATVIA	SRI LANKA
CAMEROON	LEBANON	SUDAN
CANADA	LESOTHO	SWAZILAND
CENTRAL AFRICAN REPUBLIC	LIBERIA	SWEDEN
CHAD	LIBYA	SWITZERLAND
CHILE	LIECHTENSTEIN	SYRIAN ARAB REPUBLIC
CHINA	LITHUANIA	TAJIKISTAN
COLOMBIA	LUXEMBOURG	THAILAND
CONGO	MADAGASCAR	THE FORMER YUGOSLAV REPUBLIC OF MACEDONIA
COSTA RICA	MALAWI	TOGO
CÔTE D'IVOIRE	MALAYSIA	TRINIDAD AND TOBAGO
CROATIA	MALI	TUNISIA
CUBA	MALTA	TURKEY
CYPRUS	MARSHALL ISLANDS	UGANDA
CZECH REPUBLIC	MAURITANIA	UKRAINE
DEMOCRATIC REPUBLIC OF THE CONGO	MAURITIUS	UNITED ARAB EMIRATES
DENMARK	MEXICO	UNITED KINGDOM OF GREAT BRITAIN AND NORTHERN IRELAND
DOMINICA	MONACO	UNITED REPUBLIC OF TANZANIA
DOMINICAN REPUBLIC	MONGOLIA	UNITED STATES OF AMERICA
ECUADOR	MONTENEGRO	URUGUAY
EGYPT	MOROCCO	UZBEKISTAN
EL SALVADOR	MOZAMBIQUE	VENEZUELA
ERITREA	MYANMAR	VIETNAM
ESTONIA	NAMIBIA	YEMEN
ETHIOPIA	NEPAL	ZAMBIA
FIJI	NETHERLANDS	ZIMBABWE
FINLAND	NEW ZEALAND	
FRANCE	NICARAGUA	
GABON	NIGER	
GEORGIA	NIGERIA	
GERMANY	NORWAY	
GHANA	OMAN	
GREECE	PAKISTAN	
	PALAU	

The Agency's Statute was approved on 23 October 1956 by the Conference on the Statute of the IAEA held at United Nations Headquarters, New York; it entered into force on 29 July 1957. The Headquarters of the Agency are situated in Vienna. Its principal objective is "to accelerate and enlarge the contribution of atomic energy to peace, health and prosperity throughout the world".

DESIGN, DEVELOPMENT AND
OPTIMIZATION OF A LOW COST
SYSTEM FOR DIGITAL
INDUSTRIAL RADIOLOGY

COPYRIGHT NOTICE

All IAEA scientific and technical publications are protected by the terms of the Universal Copyright Convention as adopted in 1952 (Berne) and as revised in 1972 (Paris). The copyright has since been extended by the World Intellectual Property Organization (Geneva) to include electronic and virtual intellectual property. Permission to use whole or parts of texts contained in IAEA publications in printed or electronic form must be obtained and is usually subject to royalty agreements. Proposals for non-commercial reproductions and translations are welcomed and considered on a case-by-case basis. Enquiries should be addressed to the IAEA Publishing Section at:

Marketing and Sales Unit, Publishing Section
International Atomic Energy Agency
Vienna International Centre
PO Box 100
1400 Vienna, Austria
fax: +43 1 2600 29302
tel.: +43 1 2600 22417
email: sales.publications@iaea.org
<http://www.iaea.org/books>

© IAEA, 2013

Printed by the IAEA in Austria

July 2013

STI/PUB/1561

IAEA Library Cataloguing in Publication Data

Design, development and optimization of a low cost system for digital industrial radiology. — Vienna : International Atomic Energy Agency, 2013.

p. ; 30 cm. — (IAEA radiation technology reports series, ISSN 2225-8833 ; no. 2)

STI/PUB/1561

ISBN 978-92-0-129310-7

Includes bibliographical references.

1. Radiography, Industrial — Instruments. 2. Nondestructive testing — Cost effectiveness. 3. Radiation — Safety measures. I. International Atomic Energy Agency. II. Series.

IAEAL

13-00827

FOREWORD

The International Atomic Energy Agency (IAEA) promotes industrial applications of non-destructive testing (NDT) technology. In its regular programme, it supports continuous and effective transfer of NDT technology to developing countries. These efforts have led to a stage of maturity and self-sufficiency in this area in many countries. NDT methods are primarily used for detection, location and sizing of surface and internal defects in welds, castings, forging composite materials, concrete, etc. NDT methods are also used in preventive maintenance of components in the nuclear, aircraft and other industries, and in civil engineering structures. Thus, NDT technology contributes significantly to the improvement of the quality of industrial products and the integrity of equipment and plant components. It is especially important in developing Member States where resources are scarce and life extension of components is critical. This has had a positive impact on the quality of industrial goods and services.

The introduction of powerful computers and reliable imaging technologies has had a significant impact on traditional radiation based NDT techniques. In particular, digitization of images provides economy of storage, efficiency of communication, and increased speed of inspection and evaluation. NDT laboratories in developed countries are progressing rapidly with digitization of radiation inspection data. New imaging techniques using image intensifier systems, imaging plates and flat panel detectors have increased the capacity for visualization of defects and revealed new potential for accurate evaluation of defects by radiation techniques.

To review the new developments in digital industrial radiography (DIR) and to recognize the significant potential of DIR techniques in the life assessment and extension of components, facilities and products, a meeting of experts was convened at the IAEA in November 2005. Based on the results of this meeting, the IAEA conducted several regional training courses in which participants from Member States were given training in DIR techniques. The IAEA also supported establishing facilities for DIR techniques in some Member States.

Realizing the need for easy construction and assembly of a low cost, more economically viable system for DIR technology, the IAEA conducted a coordinated research project (CRP) during 2007–2010 for research and development in the field of digital radiology, with the participation of 12 Member State laboratories. The current publication on design, development and optimization of a low cost DIR system is based on the findings of this CRP and inputs from other experts. The report provides guidelines to enable interested Member States to build their own DIR system in an affordable manner.

The IAEA wishes to thank the authors and CRP participants who contributed to this report. In particular, the IAEA is grateful to U. Ewert and U. Zscherpel (Federal Institute for Materials Research and Testing, Germany) for their valuable contributions and guidance during the preparation of this report. The IAEA officers responsible for this report were Joon-Ha Jin, A.A. Khan, B.P.C. Rao and P. Brisset of the Division of Physical and Chemical Sciences.

EDITORIAL NOTE

This report has been edited by the editorial staff of the IAEA to the extent considered necessary for the reader's assistance. It does not address questions of responsibility, legal or otherwise, for acts or omissions on the part of any person.

Although great care has been taken to maintain the accuracy of information contained in this publication, neither the IAEA nor its Member States assume any responsibility for consequences which may arise from its use.

The use of particular designations of countries or territories does not imply any judgement by the publisher, the IAEA, as to the legal status of such countries or territories, of their authorities and institutions or of the delimitation of their boundaries.

The mention of names of specific companies or products (whether or not indicated as registered) does not imply any intention to infringe proprietary rights, nor should it be construed as an endorsement or recommendation on the part of the IAEA.

The IAEA has no responsibility for the persistence or accuracy of URLs for external or third party Internet web sites referred to in this book and does not guarantee that any content on such web sites is, or will remain, accurate or appropriate.

CONTENTS

1.	INTRODUCTION	1
1.1.	The radiographic testing method	1
1.2.	Filmless radiographic testing methods	2
1.2.1.	Limitations of the conventional film RT method	2
1.2.2.	Film digitization	2
1.2.3.	Fluoroscopy and radioscopy	2
1.2.4.	Computed radiography with imaging plates	3
1.2.5.	Digital detector arrays or flat panel detectors	3
1.2.6.	Computed tomography	4
1.2.7.	Advantages of digital radiographic systems	5
1.3.	Essential concepts related to digital industrial radiography	5
1.3.1.	Radiation attenuation in materials	5
1.3.2.	Characteristics of film image	6
1.3.3.	Characteristics of digital image	7
2.	DESIGN AND CONSTRUCTION OF FLUOROSCOPIC SYSTEM FOR DIGITAL INDUSTRIAL RADIOLOGY	9
2.1.	BAM construction drawings for digital fluoroscope	9
2.2.	Selection of materials and components for construction of a digital fluoroscope	10
2.3.	Instructions for assembly of digital fluoroscope housing	10
2.4.	Problems encountered during implementation and their solutions	14
2.5.	Cost analysis of various digital industrial radiology systems	15
3.	EXPERIMENTAL PROCEDURES	16
3.1.	Introduction to ISee! software for image processing	16
3.2.	Data acquisition and image calibration procedure	16
3.2.1.	Software and hardware installation	16
3.2.2.	Software operation and image acquisition	16
3.2.3.	Calibration of fluoroscope	22
3.3.	Qualification procedures for fluoroscope qualification using Isee! According to ASTM E 2597 ..	22
3.3.1.	Measurement procedure for basic spatial resolution (SR_b)	24
3.3.2.	Measurement procedure for efficiency $dSNR_n$	25
3.3.3.	Measurement procedure for achievable contrast sensitivity and specific material thickness range	29
3.3.4.	Identification of radiographs	31
4.	ACQUISITION AND ANALYSIS OF RESULTS	32
4.1.	Measurements of basic spatial resolution	32
4.2.	Measurements of efficiency	32
4.3.	Measurements of achievable contrast sensitivity and specific material thickness range	34
4.4.	Comprehensive results	35
4.5.	Comparison of results with those obtained from other digital industrial radiology methods	36
4.6.	Experience with isotopic radiation sources	39
4.7.	Standards, image quality and compensation principles	40
4.7.1.	Introduction	40
4.7.2.	Requirements for image quality in digital industrial radiology	41
4.7.3.	Magnification technique	42

4.7.4.	Compensation principle I	43
4.7.5.	Compensation principle II	45
4.7.6.	Application of compensation principle II	47
4.7.7.	Selection of tube voltage	47
4.7.8.	Overall conclusion about image quality	48
5.	RADIATION PROTECTION IMPLICATIONS OF INDUSTRIAL RADIOGRAPHY	49
6.	CATALOGUE OF IMAGES	49
7.	SUMMARY	57
	REFERENCES	59
	BIBLIOGRAPHY	61
	ANNEX: BAM CONSTRUCTION DRAWINGS FOR PRODUCING A CASING FOR THE DIGITAL FLUOROSCOPE	67
	CONTRIBUTORS TO DRAFTING AND REVIEW	91

1. INTRODUCTION

1.1. THE RADIOGRAPHIC TESTING METHOD

Non-destructive testing (NDT) methods, including radiography, are largely used for detection, location and sizing of surface and internal defects (in welds, castings, forging, composite materials, concrete, etc.). The radiographic testing (RT) method consists in passing a beam of radiation from a source (X rays or gamma rays) through a test specimen and detecting it on the opposite side (Fig. 1).

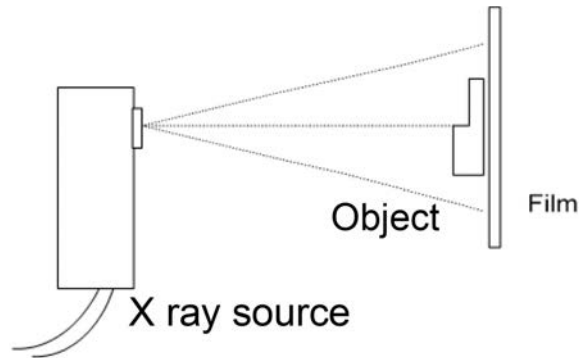


FIG. 1. Typical set-up for radiographic inspection with films.

RT still represents the largest NDT method on the market. At present, the amount of industrial NDT carried out using radiographic film sandwiched between lead intensifying screens as a detector is continuing to increase around the world, largely for the following reasons:

- RT is technically superior in detection ability for internal defects in many situations, e.g. inspection of complicated shapes and where non-contact techniques are required.
- RT is the only option for the majority of in-line factory production line testing, e.g. in-line testing of castings, electronic components such as printed circuit boards and food products. Here, any interruption of the process is unacceptable, and RT is the only testing method that can satisfy this constraint.
- RT can detect defects in structures where direct access is not possible, e.g. pipelines and other structures covered with thick paint or insulation, or having a rough surface finish. Here, other NDT methods require considerable preparation effort and time.
- RT shows good detection ability for defects in multi-layered structures, austenitic steels and composites where other NDT methods such as ultrasonic testing cannot be used due to attenuation and scattering problems.
- Results of inspections are easy to interpret.

The ability of this source–specimen–film system to detect flaws, usually referred to as sensitivity of flaw detection, depends on a number of factors. Most of these can be attributed to all three components of the system: the source, the specimen and the film. These factors can be briefly listed as:

- (1) Type of specimen, its geometry, shape, thickness, physical density, type, location and orientation of defects with respect to the direction of the beam;
- (2) Energy of radiation and source size;
- (3) Scattered radiation, filters if used, source to film and specimen to film distances;
- (4) Type of film (its definition, contrast and graininess), film processing and optical density, viewing conditions, intensifying screens;
- (5) Operator's eyesight, qualifications, skill and experience.

Sensitivity is a general term used to describe the ability of a radiograph to show details in the image. It is a reference to the amount of information or detail in the image. For example, if very small flaws can be seen in

the radiograph, it is said to have high or good sensitivity. Radiographic sensitivity depends on image contrast, definition and graininess.

Practically, sensitivity is determined through the use of image quality indicators (IQIs), of which there are several kinds. These include the wire type, step wedge type, and step and hole type. In the wire type there are two classifications, the single wire type and the duplex or wire pair type. The IQI, in principle, should be of the same material as the test specimen. It is placed on the surface of the test specimen facing the source, and then the exposure is made and the film is processed. The minimum diameter of the wire visible on the radiograph is noted. The sensitivity is then calculated as a percentage, for example, 1%, 2%, 4%, etc. The lower the percentage, the better is the sensitivity for flaw detection.

1.2. FILMLESS RADIOGRAPHIC TESTING METHODS

1.2.1. Limitations of the conventional film radiographic testing method

Although film radiography presents high resolution images, it suffers from several major disadvantages including the following:

- Low efficiency leads to longer exposure times;
- Radiographic films are not reusable;
- Considerable film processing facilities are required;
- Considerable time is required to develop the film and interpret the results;
- Workers are exposed to hazardous chemicals during film development;
- There are storage and retrieval costs for radiographs after inspection;
- X ray film deteriorates over time;
- Interpretation of radiographs is subjective;
- There is difficulty in full automation.

1.2.2. Film digitization

Film digitization is not a filmless technology, but it allows the use of all means of computer processing with traditional film exposures. There are several types of film digitization system, such as point by point digitization, line by line digitization and array digitization. The most commonly used is point by point digitization, in which the film is moved in front of a collection tube. A laser beam (with a wavelength of about 680 nm, red) with a fixed diameter (approximately 50 μm) passes the film. The diffuse transmitted light through the film is integrated by the collection tube and registered by a photo multiplier (PMT) on top of the collection tube. During the scan, the folding mirror moves the laser beam along a horizontal line on the film. The film is moved with a speed of 75 lines per second. The resulting voltage at the photo multiplier is proportional to the light intensity behind the film. After logarithmic amplification, 12 bit digitization yields grey values that are proportional to the optical density of the film.

Unlike in other digitization methods, the laser scanner illuminates with focused light and measures the diffuse light intensity behind the film. All other methods illuminate with diffuse light (the film is illuminated with a diffuser) and measure the light intensity that passes through film in one direction (camera objective or human eye in traditional film inspection) (see Section 3.2).

Because of a spatial resolution of better than 10 μm and optical density of up to 5, high end digitization yields several new possibilities for conventional RT. These include, for example, digital film archiving, quantitative evaluation, image processing, automatic image evaluation, remote image transfer and production of reference catalogues for flaw evaluation.

1.2.3. Fluoroscopy and radioscopy

In the typical source–specimen–film radiographic setup, the film is replaced with a fluorescent screen that emits visible light when exposed to radiation. The screen, which contains the image of the test specimen, can either be read by direct viewing or be photographed by a camera (fluoroscopy).

Alternatively, instead of a fluoroscopic screen, an image intensifier with a built-in scintillation screen can be used to enhance the brightness of the input image as compared with a fluorescent screen. The intensified light image at the exit screen of the image intensifier is coupled via mirror lenses to a charged coupled device (CCD) camera to photograph the image (radioscopy). This CCD camera converts visual signals to electrical signals that can be fed to a computer, where they can be processed and analysed. The light intensification of the image intensifier allows inspection of moving objects in real time (e.g. 30 images per second) (see also Section 3.2).

1.2.4. Computed radiography with imaging plates

Direct digitizing systems accelerate the application of intelligent procedures to facilitate and enhance image interpretation. For almost ten years, imaging plate systems have been available for NDT, and these can be used as a filmless radiography technique, also known as computed radiography with imaging plates.

In the 1980s, a step forward was made in medicine by using imaging plates able to store the image, eliminating the film and different chemicals, thus giving birth to computed radiography.

An imaging plate consists of a flexible polymer support coated with a sensitive layer. On top it is covered with a thin transparent protective layer. The sensitive layer of the most common systems consists of a mixture of BaFBr crystallites doped with europium and a binder. X ray or gamma ray quanta result in activation of F-centres in the crystallites, which result in the emission of blue light photons upon stimulation with red light photons through a process known as photo stimulated luminescence (see Fig. 2). After X ray exposure, imaging plates have to be scanned by a laser scanner to obtain a digital image radiograph. Finally, the residual information stored in the F-centres can be erased by exposure to bright white light and the imaging plate can be reused up to 1000 times. Different plate systems are commercially available with different thickness, unsharpness and sensitivity. Guidelines and standards that define good workmanship criteria for new digital detectors have been developed and remain under revision, aimed at avoiding a loss of information and reduced probability of flaw detection, which may occur by adoption of medical systems without adaptation to NDT requirements.

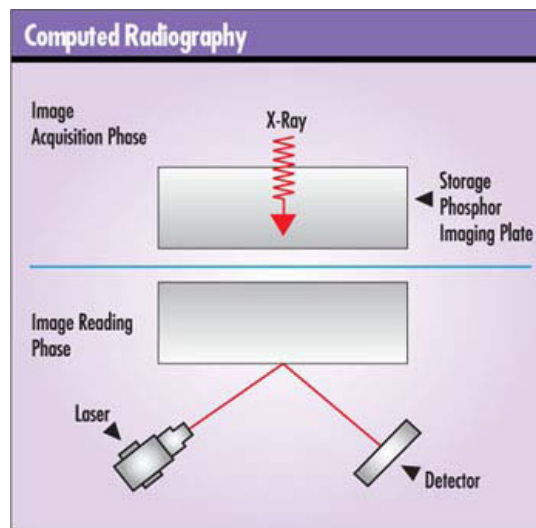


FIG. 2. Principle of computed radiography with imaging plates.

1.2.5. Digital detector arrays or flat panel detectors

1.2.5.1. Indirect X ray imaging

The intrinsic photon detection in photodiodes works fine for light photons and X ray photons up to 20 keV. Above that level, the absorption rate caused by the thin photodiode layer is too low for effective image generation.

For higher X ray energies, indirect detection is used based on a scintillation screen as used in a fluoroscope, but here it is in direct contact with the photodiode matrix for light detection. In this way, nearly all light photons

leaving the scintillator screen are collected by the photodiodes directly touching the screen. All losses connected with light imaging by a mirror and lens, as used in fluoroscopes, are omitted. The photodiode layer should not be degraded by X ray radiation and the light detection should not be degraded by the penetrating X ray photons. Because CCD elements are very sensitive to X rays and cannot be used in direct contact with the scintillator, photodiodes made on complementary metal oxide semiconductor (CMOS) or amorphous silicon panels are used for light detection.

In what is commonly called an amorphous silicon flat panel, X rays (or gamma rays) first strike a scintillation layer. This layer emits photons in the visible spectrum. These photons are picked up by the underlying amorphous silicon photodiode array, which converts them to an electric charge. This charge is then converted into digital values for each pixel.

The scintillation layer is commonly composed of either caesium iodide or gadolinium oxysulfide. This selection and the optimum scintillator thickness depend on the desired image unsharpness and radiation energies used.

1.2.5.2. Direct X ray imaging with photo conductors

Another way to record information regarding detection of electromagnetic waves is what is called direct imaging, using, for example, amorphous selenium technology or crystalline CdTe technology (Fig. 3). X rays (or gamma rays) strike a photo conductor made of amorphous selenium or a CdTe layer, which converts them directly into electric charge that is further converted to a digital value for each pixel. Pixelated metal contacts (pixel sizes down to 70 μm are available) and ball grid arrays are used to contact the photoconduction layer to the underlying CMOS or amorphous silicon readout electronics.

The transmitted X ray intensity at each detector element position in the detector array is converted to a digital output level and fed to a computer, where the images from the individual slices and/or projections are computed in a reconstruction process to form a three dimensional (3-D) image of the specimen.

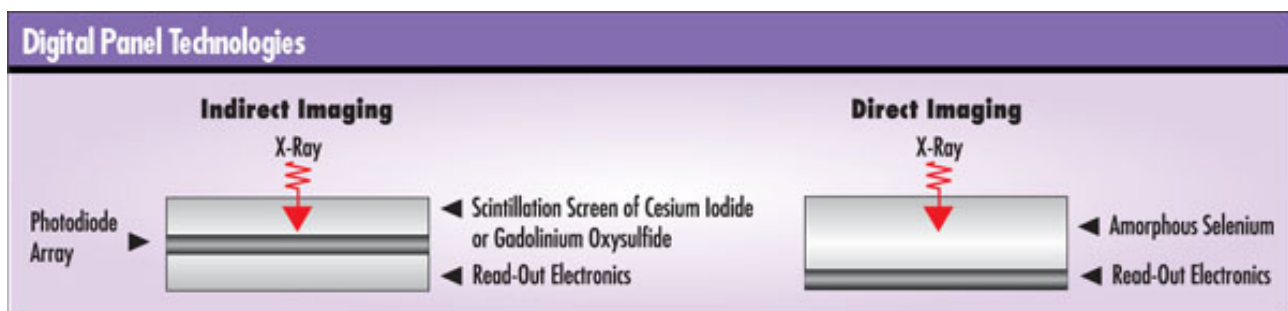


FIG. 3. Comparison of detection technologies for digital detector arrays.

1.2.6. Computed tomography

Computed tomography (CT) uses measurements of X ray transmission from many angles encircling the test specimen to compute the relative X ray linear attenuation coefficients of small volume elements (3-D voxels) and presents the data as a cross-sectional or 3-D attenuation map. The clear images of interior planes of an object are achieved without the confusion of superposition of features that is often found with conventional projection radiography. In the typical source–specimen–film radiographic set-up, the film is replaced with a one dimensional (1-D) or two dimensional (2-D) array of radiation detectors. For a 1-D detector array, the X ray beam and the detector elements are collimated to a narrow slit and highly aligned to each other to define a slice plane in the specimen. This slit collimation reduces scattered radiation from the inspected object and improves the reconstruction result of this fan beam CT (which is important for high X ray energies with increased X ray scatter by the inspected object).

Faster inspection times can be realized by using a 2-D image detector (digital detector array or flat panel) and a cone beam X ray beam. In this way, a 360° rotation provides projection images of a complete specimen volume. The disadvantage is the missing suppression of scattered radiation generated in the object, which introduces artefacts in the volume reconstruction and reduces the contrast in the projections.

Either the test specimen or the source–detector assembly can be translated and rotated to obtain projections from multiple angles. The 3-D cone beam CT, in particular, needs computer clusters for image reconstruction of data sets of gigabytes per inspected volume.

1.2.7. Advantages of digital radiographic systems

Digital industrial radiography (DIR) has the following benefits:

- It reduces radiation dosage and exposures, resulting in less risk to the operator and less disruption to other operations.
- It reduces radiographic inspection time and improves productivity.
- It eliminates film processing chemicals, chemical disposal and storage costs.
- Digital radiographs are not degradable.
- It is easily customized for field radiography in a portable package.
- It allows analysis using image processing and defect detection algorithms.
- Storage costs are minimized, as all images are stored on hard disks or optical media such as CD-ROMs or DVD-RAMs. Images can also be accessed via network and even emailed to experts for real time verification.
- Reusable imaging plates mean that savings can be generated, as one plate can be used many times.

Significant cost savings from the use of DIR systems have been reported by industry. With the advancement of image intensifier systems, imaging plates, flat panel detectors and fast multimedia computers, DIR is finding increased applications.

1.3. ESSENTIAL CONCEPTS RELATED TO DIGITAL INDUSTRIAL RADIOGRAPHY

1.3.1. Radiation attenuation in materials

Suppose we have a primary X ray intensity I_0 incident on the surface of a material. After passing through the material, with thickness x , we have intensity I , the relationship between I_0 and I being:

$$I(x) = I_0 e^{-\mu x} \quad (1)$$

where μ is the linear attenuation factor, or absorption factor. Intensity I has the usual meaning, being the average of the Poynting vector S , namely, the quantity of electromagnetic energy traversing a unit of surface in a unit of time. If monochromatic radiation is used, μ can be taken as constant. In practice it is better to use the effective attenuation coefficient μ_{eff} , which depends on the radiation energy, the test specimen thickness (because of radiation hardening and generation of scattered radiation in the object), tube filters, detector screens and the geometrical set-up used for inspection (this determines the scatter contribution). The coefficient μ_{eff} will always be smaller than the theoretical μ as obtained for the mono-energetic narrow beam energy.

The effective attenuation coefficient μ_{eff} can be calculated from the following formula (using NDT films with optical density proportional to the radiation dose):

$$\mu_{\text{eff}} = 1n \left[\frac{(D_{\text{object}} - D_{\text{fog}})}{(D_{\text{step}} - D_{\text{fog}})} \right] / \Delta w \quad (2)$$

where

- D_{fog} is the optical density of the film fog and base;
- D_{object} is the optical density inside the object investigated (hole, step, etc.);
- D_{step} is the optical density at base material;
- Δw is the wall thickness difference between base material and the imaged object.

1.3.2. Characteristics of film image

1.3.2.1. Optical film density

The process of film blackening can roughly be described as follows. The electromagnetic waves (or free electrons generated by lead intensifying screens under X ray exposure) impinge the film and set free electrons from negative Br ions. These electrons are captured by electron traps, so the free positive Ag ions are attracted by these negative centres, becoming neutral and blackening the film after development. The number of neutral Ag atoms formed on the film is directly proportional to the number of electromagnetic waves incident on it.

The optical film density achieved depends on the radiographic exposure or the radiation dose received by the film, measured by the tube current or source strength multiplied by the time of exposure. The optical density D is the degree of blackening of the film after development and fixing. It is also called the ‘film response’ to the dose of radiation and is expressed as:

$$D = \log(L_0/L) \quad (3)$$

where

L_o is the diffuse light intensity (luminance) measured on the image viewer;
 L is the diffuse light intensity (luminance) measured on the film on the viewer.

The IQI sensitivity achieved in the final radiograph depends on the value of achieved optical density D .

The number of photons incident on film is the number of photons that have traversed the material to be studied and according to Eq. (4) is exponentially decreased; as a result, the film’s blackening density can be written as:

$$D = D_{Max} e^{-\mu x} \quad (4)$$

where

D is the film blackening or optical density;
 D_{Max} is the quantity depending on the current of the X ray source, the film to source distance, exposure time t , and some constants which are characteristic of the film used.

1.3.2.2. Image contrast, definition and granularity

The quality of a radiographic image can be described in terms of three factors, namely contrast, definition (unsharpness) and image noise (granularity). All three of these important factors affect defect detectability. Radiographic contrast is the density difference between areas of a radiograph. Obviously, an image becomes more discernible when contrast is increased. Contrast depends on X ray energy, radiation scatter conditions, the type of film and film processing used, and film density.

Definition refers to the sharpness or unsharpness of the image. In general, one can assume that a sharp image is of higher quality than a less sharp image. Definition is dependent on the geometric condition of the radiographic set-up, focal spot size, radiographic energy, intensifying screens used, type of film used and its development, and/or radiation imaging system used.

The image noise, visible as granularity in the film image (e.g. by using a magnifying glass of 10×), depends on the film speed (film sensitivity given by the film grain size during film manufacturing or film system class), the development conditions and the exposure time (or optical density).

For linear NDT films, the normalized signal to noise ratio (SNR_{Norm}) at an optical density of 2 can be calculated from the following film system parameters:

$$SNR_{Norm} = \log(e)(G_2/\sigma_D) \quad (5)$$

where

G_2 is the film gradient at an optical density of 2;
 σ_D is the film granularity at an optical density of 2;
 G_2/σ_D is the gradient to noise ratio for films.

SNR_{Norm} can be calculated from the curves drawn between gradient to noise ratios and the square root of the dose (or exposure). However, at the limit of detection, the quality of the image depends on all three factors: contrast, unsharpness and granularity.

1.3.3. Characteristics of digital image

1.3.3.1. Signal to noise ratio

The optical film density and granularity are defined for films only. If film is replaced with other detectors, equivalent detector properties must be considered.

The image obtained by digital detectors is described in terms of ‘grey levels’, which is a kind of darkening or blackening depending on the visual presentation of an image display. The exposure to the digital detectors by the image-forming radiations produces a ‘grey level’ as digital pixel value numbers in the digital image. This can be defined as the signal of the detector. The ‘grey level’ variations produced by fluctuations of the signal intensities of the different detector elements due to quantum statistics of X ray radiation and/or electronic noise sources can be referred to as ‘noise’ or ‘grey level variations’. The detector response can then be measured in terms of the signal to noise ratio (SNR). Since imaging plates and digital detector arrays (DDAs) are linear detectors, their image quality can be characterized by this SNR. For quantum limited detection, the SNR will improve the square root of the X ray exposure, and the signal (grey level) is proportional to the exposure (mA·s). Thus, the requirement for a minimum SNR in the image of digital detectors is equivalent to the requirement for a minimum optical density of film. The SNR of a film can be derived from the film system class and the film density.

1.3.3.2. Contrast to noise ratio

The contrast C (in grey values) of IQIs and flaws is defined as the difference between the radiation intensities measured with a detector, which is given as:

$$C = I - I_{flaw} = \Delta I \quad (6)$$

The relative contrast, C_r , which is mainly used for digital systems, is normalized to the radiation intensity at a given area in the radiation image:

$$C_r = \Delta I / I \quad (7)$$

For very small thickness changes (differential), it can be derived from the attenuation law using μ_{eff} (in 1/mm):

$$C = I \Delta w \mu_{eff} \quad (8)$$

The specific contrast, C_s , is now defined as detector response, which is ΔI per thickness change (grey values per mm):

$$C_s = C / \Delta w = I \mu_{eff} \quad (9)$$

Here, I is the radiation intensity at a specific pixel area in a radiographic image. The grey values of linear detectors as well as the grey value difference increase with increasing exposure time (dose). Therefore, the detector

signal (S) for a given radiation intensity (linear to dose) determines the contrast of a flaw or IQI in any radiographic image as follows:

$$C_s = S\mu_{eff} \quad (10)$$

The perception of a certain flaw or IQI in an image depends not only on the C_s but also on the image noise. Flaws and IQIs are only discernable if the contrast is higher than the image noise. Wires and lines are visible if the contrast to noise ratio (CNR) is about one; pores and IT holes are visible if the CNR is greater than 2.5. Higher exposure dose increases the CNR proportionally to the square root of dose (or exposure), if the detector responds linearly to dose and no other noise sources contribute to the image.

The CNR, which is the essential parameter for the visibility or detectability of flaws and IQIs, can be calculated from the detector response, SNR, as a function of signal and dose as follows (small flaws):

$$CNR/\Delta w = (SNR)(\mu_{eff}) \quad (11)$$

Therefore, the image quality depends on the μ_{eff} and the detector response SNR. This applies to all linear X ray image detectors and NDT film systems. The CNR is inversely related to the contrast sensitivity, which is normally measured as a percentage of detectable wall thickness difference.

1.3.3.3. Basic spatial resolution

The detectability of fine flaws depends on the detector unsharpness, the geometrical unsharpness, and the SNR or CNR. If a magnification technique is applied, the total image unsharpness is the combined effect of geometrical unsharpness and detector unsharpness divided by the magnification.

Digital detectors are typically characterized by their detector pitch (also called the pixel size), which is equivalent to the distance between the centres of two neighbouring detector elements. To consider, in addition, unsharpness contributions by the sensitive detection layer of imaging plates, CR scanners and DDAs, the concept of the basic spatial resolution (SR_b , in μm), was introduced, which corresponds to an effective pixel size. Whereas the pixel size is determined by the construction or software settings (e.g. within CR scanners), the SR_b can be measured in the image in a number of ways. The most convenient and recommended method is to use the duplex wire method (see the IQI description in EN 462-5, ASTM E 2002 or ISO 19232-5). The measurement with the duplex wire IQI provides a total unsharpness value (u_T) in μm which is equivalent to the spatial resolution. The basic spatial resolution (SR_b) is calculated by:

$$SR_b = u_T/2 \quad (12)$$

1.3.3.4. Specific material thickness range

Considering the practical aspects of radiographic applications, an additional parameter used is the specific material thickness range (SMTR), which means the extent of material thicknesses covered in the same image without detector saturation and ensuring a minimum SNR in the image. Since this value is low for NDT film systems (limited by the usable optical density range of 2–4.5, corresponding to a radiation intensity ratio of only 3), it usually is not considered for film radiography in textbooks and standards. Since modern DDAs and CR can have a much wider dynamic range compared with even the double film technique, this parameter was introduced for manufacturer characterization of DDAs in ASTM E 2597.

2. DESIGN AND CONSTRUCTION OF FLUOROSCOPIC SYSTEM FOR DIGITAL INDUSTRIAL RADIOLOGY

2.1. BAM CONSTRUCTION DRAWINGS FOR DIGITAL FLUOROSCOPE

The construction drawings developed by Germany's Federal Institute for Materials Research and Testing (BAM) for producing a casing for the digital fluoroscope are provided in the Annex to this publication. These are available in German; Table 1 provides a translation into English. German terms used in the drawings and their translation into English are given in Table 2.

TABLE 1. PARTS OF THE HOUSING

Part No.	Quantity	Description	Material
			Stainless steel X5CrNi18-10 (ASTM Alloy Type 304, EN 1.4301, UNS S30400) or similar
1	1	Casing bottom plate	
2	1	Casing right plate	X5CrNi18
3	1	Casing left plate	X5CrNi18
4	1	Casing top plate	X5CrNi18
5	1	Casing front plate	X5CrNi18
6	1	Input window	Aluminium alloy
7	1	Casing rear plate	X5CrNi18
8, 9	2	Bolts (as part of handle)	X5CrNi18
10	1	Handle	X5CrNi18
11	1	Mirror holder	X5CrNi18
12	1	First surface mirror (purchased)	First surface mirror
13	1	Holder of inner (CCD camera) casing	X5CrNi18
14	1	Flat spring	X5CrNi18
15	1	Camera holder, part 1	Aluminium alloy
16	1	Camera holder, part 2	Aluminium alloy
17, 18	2	Lead glass holder, upper side	X5CrNi18
19	1	Lead glass holder, bottom side	X5CrNi18
20	1	CCD camera (purchased)	
21	1	Lead glass (purchased)	Lead glass (Pb glass)
22	2	Spring (diameter: 10 mm × 1 mm × 13 mm) (purchased)	X5CrNi18
23	1	Inner casing right plate	X5CrNi18
24	1	Inner casing left plate	X5CrNi18
25	1	Inner casing left shielding	Lead/Pb
26	1	Inner casing right shielding	Lead/Pb
27	1	Inner casing from (main beam) shielding	Lead/Pb
28	1	Inner casing top shielding	Lead/Pb
29	1	Inner casing bottom shielding	Lead/Pb
30	1	Inner casing rear shielding	Lead/Pb
BS 4168 - M4 x 10	4	Hexagon socket set screw with cone point	X5CrNi18
DIN 7991/M4 x 12	12	Hexagon socket countersunk head screw	X5CrNi18
DIN 7991/M4 x 16	12	Hexagon socket countersunk head screw	X5CrNi18
DIN 7991/M4 x 20	22	Hexagon socket countersunk head screw	X5CrNi18
DIN 7991/M5 x 16	2	Hexagon socket countersunk head screw	X5CrNi18
DIN 912/M4 x 20	17	Hexagon socket head cap screw	X5CrNi18
DIN 912/M4 x 25	1	Hexagon socket head cap screw	X5CrNi18
DIN 912/M5 x 16	8	Hexagon socket head cap screw	X5CrNi18
DIN 912/M5 x 20	12	Hexagon socket head cap screw	X5CrNi18

TABLE 2. TRANSLATION OF TERMS IN THE DRAWINGS

German Teil/Bauteil	English part
Gehäuse/Kameragehäuse/Detektorgehäuse	Casing/camera casing (fluoroscope casing)
Kameraabschirmung	Camera shielding
Spiegel	Mirror (first surface mirror)
Halter	Holder
Bolzen	Bolts
Platte	Plate
Blech	Thin plate (thin metal sheet)
Blei	Lead (Pb)

For details, see the drawings in the Annex to this publication.

2.2. SELECTION OF MATERIALS AND COMPONENTS FOR CONSTRUCTION OF A DIGITAL FLUOROSCOPE

In addition to the drawings used to construct the housing, including X ray and light shielding, some components have to be purchased commercially. The drawings are adapted to the selection of special parts as described in the following. If other parts are used, some of the construction details may need to be changed.

To assemble a digital fluoroscope, the items listed in Table 3 need to be purchased (one item per position). The total price of the components for one fluoroscope unit (excluding personal computer and FireWire hub) was about €2160 (excluding value added tax) in Europe in 2008.

2.3. INSTRUCTIONS FOR ASSEMBLY OF DIGITAL FLUOROSCOPE HOUSING

The manufactured digital fluoroscope housing and shielding components comprise 26 fabricated details, two springs (detail No. 22), a CCD camera with an objective, a first surface mirror, a fluorescent screen, lead protecting glass and number of connecting screws (Fig. 4). Detail numbers mentioned in this section correspond to those in the BAM drawings provided in the Annex to this publication.



FIG. 4. The fluoroscope housing and shielding details to be assembled.

For the assembling processes:

- (1) The housing must have black matt painting inside to avoid harmful reflection. Therefore, the corresponding parts must be painted before the beginning of assembly.
- (2) Start the assembly from the 'camera module' (Fig. 5). Leave the fixing of the lead glass and its supports (detail Nos 17 and 18) for the end of module assembly.
- (3) Using adjusting screws and springs (detail No. 22), fix the objective's optical axis in the middle of the circular hole of the steel plate (detail No. 19). During this adjustment, the screws may extend beyond the camera bearing plate (detail No. 13) (Fig. 6). In this case, shorter screws may be used or additional hollows in lead (detail No. 30) should be drilled.

TABLE 3. ADDITIONAL ITEMS TO BE PURCHASED FOR COMPLETION OF THE DIGITAL FLUOROSCOPE

Item No.	Name/description	Supplier	Price per item in euros (prices from 2008, excluding value added tax)
1	Kyokko DRZ-PLUS fluorescent screen	Kasei Optonix, Ltd., 1060 Naruta, Odawara City, Kanagawa, 250-0862, Japan, Phone: +81-465361027, Fax: +81-465361151, Email: KOX0197@cc.m-kagaku.co.jp , Web site: http://www.kasei-optonix.co.jp	185 (for one 197 mm × 294 mm sheet), one 115 mm × 155 mm sheet is needed as input area
2	FOculus FO442SB 2/3" CCD Camera	New Electronic Technology NET GmbH, Lerchenberg 7, D-86923 Finning, Germany, Phone: +49 (0)880692340, Fax: +49 (0)8806923477, Email: info@net-gmbh.com , Web site: http://www.net-gmbh.com	1810
3	EO Megapixel fixed FL lens 12 mm/1:1.8, Edmund Optics (Product ID NT58-001)	Edmund Optics GmbH, Schoenfeldstrasse 8, D-76131 Karlsruhe, Germany, Phone: +49 (0)721 6273730, Fax: +49 (0)721 6273750, Email: info@gmbh.edmundoptics.de , Web site: http://www.edmundoptics.com/	185
4	First Surface Mirror, 81 mm × 100 mm (1 mm support), Edmund Optics (Product ID Y41-621)	Edmund Optics GmbH (as above)	12
5	X ray protective Pb-Glas 65 mm × 65 mm, 10 mm thickness (2.5 mm Pb-equivalent @ 180 kV or similar)	Advanced Materials SCHOTT AG, Huetttenstraße 1, D- 31073 Gruenenplan, Germany, Phone: +49 (0) 5187 7710, Fax: +49 (0)5187 771300, Email: info.gruenenplan@schott.com Web site: www.schott.com	55
6	Personal computer running Windows XP and having active FireWire (IEEE-1394) interface ^a , minimum CPU frequency 2 GHz, minimum RAM 512 MB.	Various brands and models are possible; a supplier located at the site of the project partner is probably preferable	Not included, locally available

^a Active FireWire (IEEE-1394) means that the camera power is supplied via FireWire. Virtually all six pin connectors found on desktop motherboards have this. In laptops/notebooks, FireWire implementation is usually with a four pin connector; these have no power wires. In this case, an additional active FireWire hub having an external 12V power supply can solve the problem. It is also possible to use old external iPod (from Apple Inc.) FireWire adapter cables, which enables charging the iPod while connected to the Mac Powerbook.

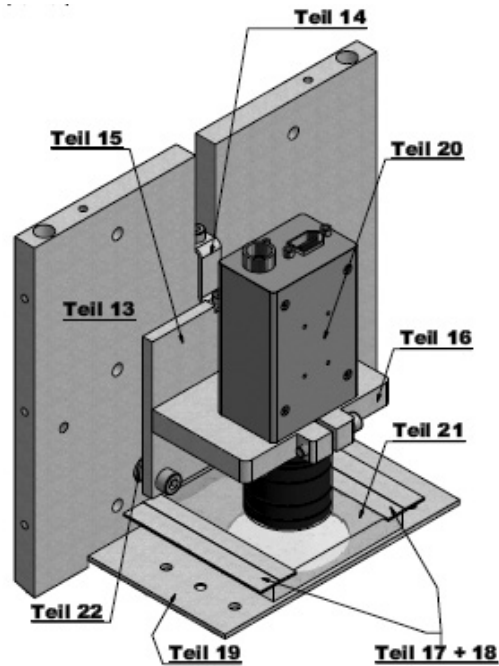


FIG. 5. The camera module (Teil means part).

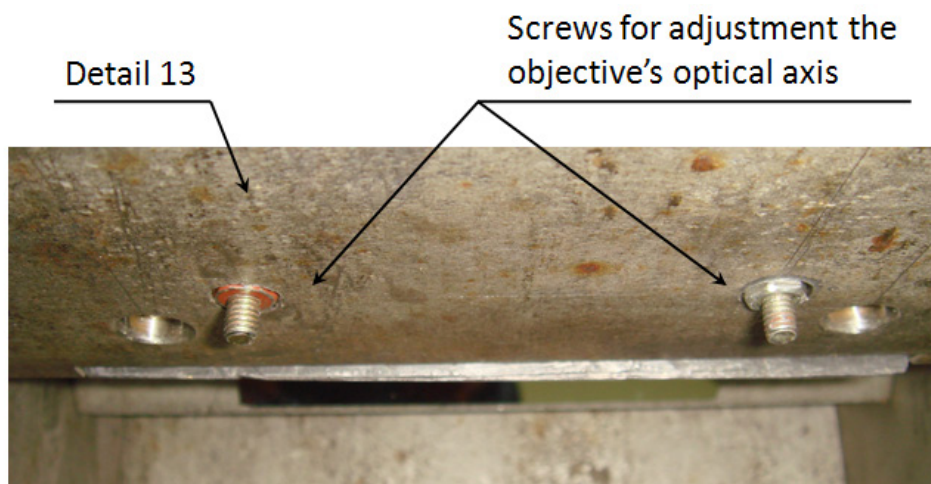


FIG. 6. Detail No. 13 with screws sticking out approximately 5 mm.

- (4) Continue assembling shielding and housing details according to the BAM drawings. Leave the installation of the mirror and the fluorescent screen until the end, to minimize the possibility of damage to them.
- (5) Carefully paste the first surface mirror (detail No. 12) on the pivot plate (detail No. 11). This can be done using two-sided sticky tape.
- (6) Fix the plate bearing mirror at a 45° angle to the optical axis of the objective directed by the reflecting side to the place where the fluorescent screen will be installed.
- (7) The aluminium plate (detail No. 6) must be clean and smooth to avoid artefacts on the radiographic pictures. If there are any scratches on any of its sides, the plate should be abraded and, if necessary, polished (possibly galvanically).
- (8) Carefully paste the fluorescent screen on the aluminium plate (detail No. 6). This can be done using two-sided sticky tape.

- (9) Before installing the fluorescent screen into the system, the positions of the mirror and the objective can be adjusted by the implementation of some tests in visible light. This can be done using a BAM adjustment target printed on thin paper and installed in place of the fluorescent screen (Fig. 7).

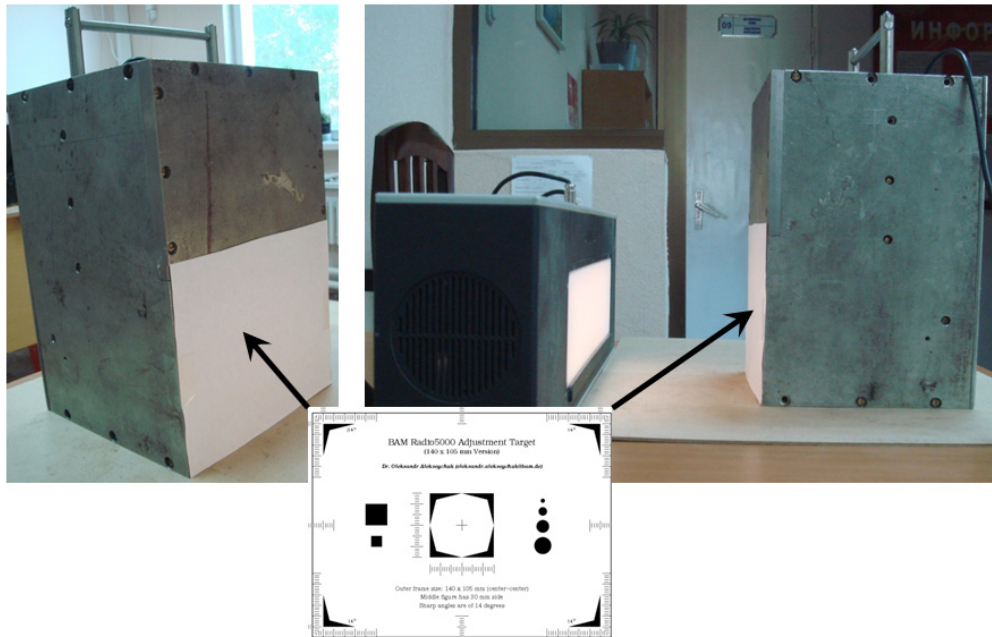


FIG. 7. Adjustment of mirror and objective positions in visible light.

The assembled fluoroscope and the fluorescent screen can be seen in Fig. 8. The overall dimensions of the assembly are 285 mm \times 195 mm \times 182 mm, and its approximate weight is 30 kg.

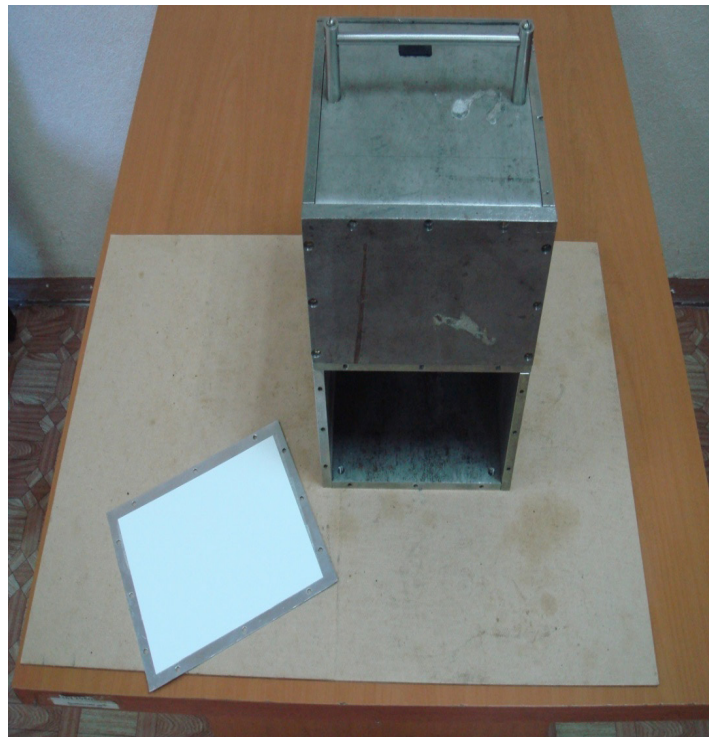


FIG. 8. Assembled fluoroscope and fluorescent screen.

2.4. PROBLEMS ENCOUNTERED DURING IMPLEMENTATION AND THEIR SOLUTIONS

Table 4 shows some of the problems observed during the case studies in participating laboratories as well as their solutions.

TABLE 4. PROBLEMS ENCOUNTERED AND THEIR SOLUTIONS

Problem encountered	Solution
Light reflection from the internal walls of the housing causes image artefacts	Use black matt painting inside the fluoroscope box along with firm and light-tight assembly
Increased background noise due to scattered radiation	Use masking and collimation of the X ray beam
Dark image, distortion, no image for thick specimens	Turn aperture of the objective to maximum Adjust brightness to obtain grey value between 2 and 10 for no radiation. Adjust shutter (exposure time per frame) to have a high grey value for the thinnest part of the specimen to be inspected (just below the red warning colour in the V2 window)
Unstable image from self-rectifying single tank X ray tubes	Try another tube with constant potential generator Use digital temporal filter in V2 software
Image distortion caused by improper geometry of the housing (smaller or large dimensions of the fluoroscope's optical system)	Assemble the housing strictly according to BAM drawings Field of view should be 100 mm × 150 mm To increase or decrease field of view, change the optical system (dimensions, magnification, etc.)
Image quality cannot be measured correctly, e.g. Duplex Wire IQI readout or wire number readout is too low	Use Duplex Wire IQI according to ISO 19232-5, ASTM E2002 or EN 462-5 and one of the following: — Single Wire IQI according to ISO 19232-1 and EN 462-1 or ASTM E 747 — Plate Hole Penetrameter according to ASTM E1025 — Step/Hole IQI according to EN 462-2 Use compensation principle for IQI sensitivity measurement as described in ISO/DIS 17636-2 Follow the requirements for minimal SNR values and exposure time as specified in ISO/DIS 17636-2 Increase exposure time if wire IQI readout is too low
Duplex Wire IQI procurement	IQI suppliers, for worldwide distribution: http://www.wilnos.de (request IQI manufactured by Kowotest, clear IQI) http://www.ie-ndt.co.uk/ (old version in yellow colour)
V2.exe software does not work on some computers at all. On others, it can only run in an unstable way, caused by a failing connection of V2 to the direct show library and resulting in no image data and a frame rate of 0 frames per second	This problem has not been solved yet. BAM is working on it. Only one V process can access the Direct Show library per device; more processes running on the same computer do not show any image data Check if the computer has the minimum specifications and operating system as recommended in the V2 manual. Reinstall the software and hardware according to manufacturer instructions Follow the guidelines of the V2 manual exactly Check Windows Direct Show version and try other ones As a final option, reformat the hard disk and reinstall Windows, e.g. WinXP SP2 (be aware of potential data loss)
FO control does not work on some computers (only 32 bit drivers available)	Incomplete driver installation by FO control software installation process or FireWire hardware issues Try another computer with 32 bit Windows version and working FireWire connection providing 12 V to the camera
FireWire connectors and adapters are not readily available in some countries	Select a camera of equivalent specifications with USB connection
Wrong exposure conditions, measurements of quantitative parameters, IQI values, etc.	Follow procedures or protocol for image analysis included in this publication

TABLE 4. PROBLEMS ENCOUNTERED AND THEIR SOLUTIONS (cont.)

Problem encountered	Solution
Difficulties in image analysis or lack of functions in software	Updates of ISee! software: http://www.kb.bam.de/~alex/ic/index.html Latest ISee! manual: http://www.kb.bam.de/~alex/ic/ic-manual_v1.10.pdf Updates of V2 software: http://www.kb.bam.de/~alex/v2/index.html
Problems with image acquisition and fluoroscope calibration	Select proper number of frames to be averaged (frame integration number): 50–500 is suggested. It should be high enough to meet the required minimum SNR value Frame integration number for calibration must be two to four times the frame number used for acquisition Follow the calibration procedure: http://www.kb.bam.de/~alex/ic/calibration-correction/index.html

2.5. COST ANALYSIS OF VARIOUS DIGITAL INDUSTRIAL RADIOLOGY SYSTEMS

The construction of the digital fluoroscopic system (DFS) consists of two parts, i.e. the casing (housing and shielding) and the optical components. Table 3 lists the components of the digital fluoroscope. These were directly purchased and provided by the IAEA at a total cost of €2882 per DFS. Table 5 shows the cost of DIR systems of different Member States. For the fabrication of the DFS casing, the cost ranges between €1900 and €3000, depending on the manufacturing costs in the Member States. The software developed by BAM was used and the other hardware items listed in the table were provided by the IAEA at a total cost of €2882 per DFS. Therefore, the total cost to fabricate the complete DFS was observed to range between about €4800 and €5900 without taking into consideration the cost of the computer and the shipping and transportation costs. The prices indicated exclude taxes and overhead. It can be observed that the overall cost of the DFS is quite comparable among the various Member States.

For purposes of comparison, the costs of commercial DIR technology such as film digitization, computed radiography, flat panel and image intensifier in selected Member States are also given in Table 5. It should be highlighted that a DFS can be built at a cost of about €5000. This is about 10–20% of the cost of comparable commercial DIR systems that provide similar image quality.

TABLE 5. COST OF DIGITAL INDUSTRIAL RADIOLOGY SYSTEMS (EUROS) IN SELECTED COUNTRIES AT THE TIME THE COORDINATED RESEARCH PROJECT WAS CARRIED OUT

Country	Fluoroscope (housing and shielding) as BAM design + optical components ^a	Film digitization system (manufacturer)	Computed radiography (manufacturer)	Flat panel (manufacturer)	Image intensifier
Argentina	2000 + 2882 = 4882	32 000 (GE)	77 000 (GE)		45 000 (Yxlon XRS 232)
India	2000 + 2882 = 4882	50 000 (Array 2905)	55 000 (HD-CR 35 NDT, Dürr NDT)	60 000 (Thales, France)	40 000 (Yxlon XRS 232)
Malaysia	3000 + 2882 = 5882	45 000 (Array 2905)	60 000 (HD-CR 35 NDT, Dürr NDT)	50 000 (FPDDigit13-127, Balteau NDT, USA)	
Pakistan	2000 + 2882 = 4882	33 000 (GE FS-50B)	40 000, (CR 35 NDT, Dürr NDT)		45 000 (GE system)
Romania	2000 + 2882 = 4882				
Syrian Arab Republic	200 + 2882 = 3082				
Uruguay	1900 + 2882 = 4782				
Uzbekistan	400 ^a + 2882 = 3282				

^a Internal costs.

3. EXPERIMENTAL PROCEDURES

3.1. INTRODUCTION TO ISEE! SOFTWARE FOR IMAGE PROCESSING

ISee! is software developed by BAM for the purpose of radiographic image analysis using the Microsoft Windows operating system. The demonstration and full versions of this software, along with the user manual, can be downloaded from the Internet (<http://www.kb.bam.de/ic>). There is no installation required. The entire file can be copied to a personal computer and run using the ic.exe or ic-demo.exe file, as applicable.

To process images, open the digital image in ISee! (just drop the image file via mouse on the ISee! program icon). The digital images can be raw data (without calibration) or can be captured including calibration. The image stored in the form of raw data is calibrated by using ISee! for optimum contrast sensitivity and better flaw detection with the digital fluoroscope.

The main purpose is analysis, i.e. adjustment for the human eye, of various tasks such as wall thickness measurement, profile based measurement, calculation of image statistics, SNR measurement in a defined window region, various types of filter for image enhancement and documentation of high resolution images with high bit depth usually arising in scientific and industrial digital imaging and in DIR in particular.

The details of functions and parameters for operation are available in the user manual. The manual also provides tips on useful image processing tools for better visualization of the digital radiographs on monitor screens and paper prints.

3.2. DATA ACQUISITION AND IMAGE CALIBRATION PROCEDURE

3.2.1. Software and hardware installation

The selected FireWire camera FOculus FO442SB requires special drivers to operate under Windows operating systems. The manufacturer (NET GmbH, Germany) provides the latest version on its web site (<http://www.net-gmbh.com>). The following files were available during the CRP for download concerning the FO442SB camera:

- (1) FOcontrol_Install_4.0.3.0.exe (the camera drivers and the demo application FOcontrol.exe);
- (2) FOcontrol_V3.0.7.0_manual.pdf (the user manual for the demo application FOcontrol.exe);
- (3) NET_FOculus_S_user_manual_v1.15_001.pdf (the detailed description of the FO442SB camera specifications and the software and driver installation).

The first file has to be started once on the computer to install all necessary drivers and the demonstration application "FOcontrol.exe". Finally, a link to this demonstration application is installed on the desktop. After the software installation, reconnect the camera to the hot pluggable FireWire interface. *Only then* will all necessary Windows drivers be installed and the camera become visible under the system -> hardware -> device manager as 'image processing device' with the name 'NET GmbH 1394 Digital Camera'. When the device is shown in the manager window without a yellow exclamation mark, the camera is ready for operation.

A beep should be heard from the computer when the camera is connected or disconnected on the running Windows system. The camera power has to be provided by the FireWire cable. A standard six pin IEEE 1394 cable and connector at the computer provide this power; the smaller four pin connectors found on laptops do not. Here, adapter cables from four pin to six pin with an additional power supply of 12 V should be used.

Caution: Be sure to connect the six pin cable only side correctly. With force the steel frame of the six pin connector can be expanded so that the cable, turned 180°, can be plugged in. If power is then provided to the camera, the exit circuit of the FireWire interface inside the camera will be destroyed and the camera will have to be sent for repair to the manufacturer (NET GmbH, Germany).

3.2.2. Software operation and image acquisition

As the next step, start the FOcontrol application from the desktop link. Select the set-ups as shown in Fig. 9. Clicking the 'start camera' button will show a live camera image; the 'stop camera' button will erase this image

from the window. If all works correctly, stop the camera and exit FOcontrol. For more information, see the manual (FOcontrol_V3.0.7.0_manual.pdf).

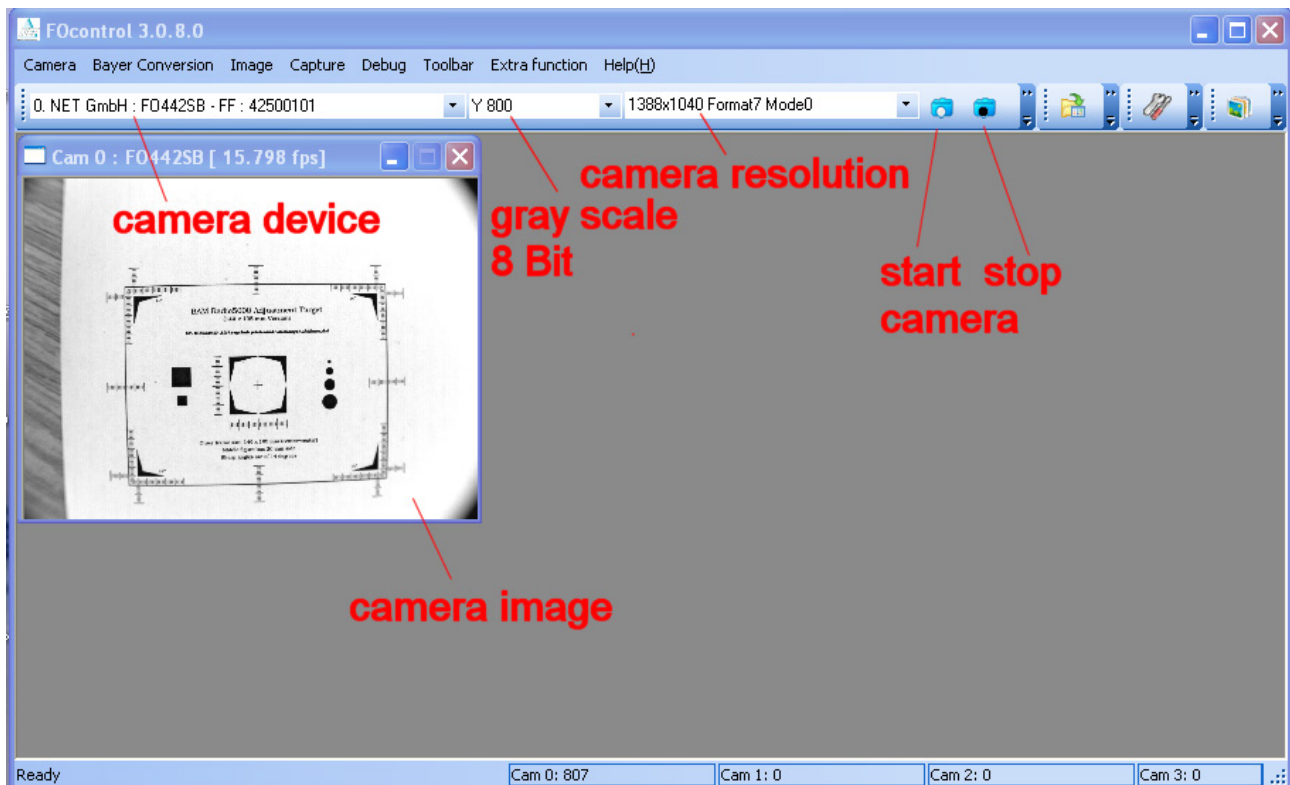


FIG. 9. FOcontrol.exe demonstration application of NET GmbH for basic camera tests.

The application V2.exe was developed especially for data acquisition with the Radio5000 fluoroscope at BAM and released under GNU public domain. This program does not require any installation; simply start V2.exe from a suitable directory. The V2.exe file requires some more dynamic link libraries (DLLs) to run, as shown in Fig. 10. There is no installation required; simply start V2.exe and keep all four files in the same directory.



 V2.exe	691 KB	18.07.2009 13:51
 QtCore4.dll	2.031 KB	27.03.2008 18:38
 QtGui4.dll	8.935 KB	19.02.2008 21:29
 mingwm10.dll	16 KB	27.12.2007 17:23

FIG. 10. V2 acquisition program and its components.

The main window, as shown in Fig. 11, appears on the desktop after starting the application V2.exe. Clicking the 'About' button opens the window pictured in Fig. 12.

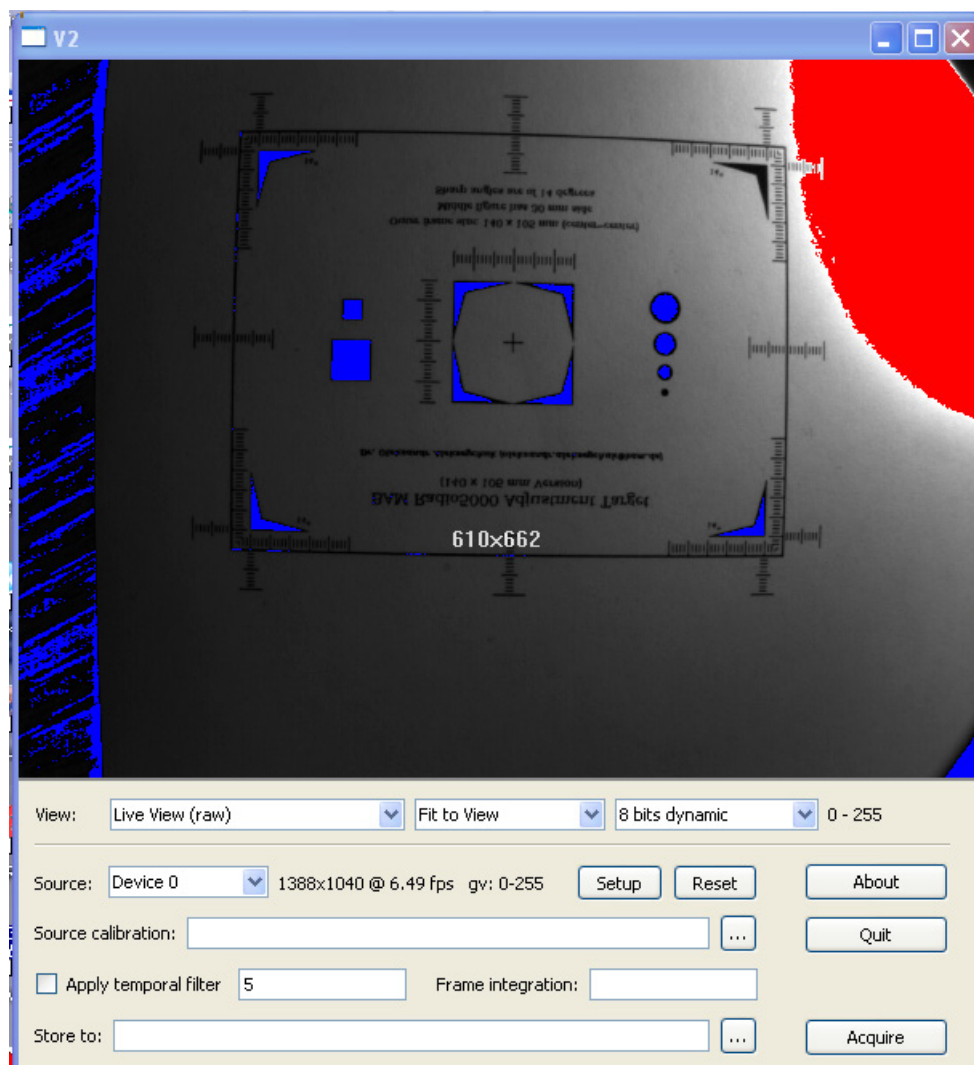


FIG. 11. Main window of the V2.exe application with live camera image (camera recognized as 'Device 0', image size 1388 pixels \times 1040 pixels, 8 bit grey values 0–255 in the live image, frame rate 6.49 frames per second).

The V2.exe application uses standard Windows video streams via DirectShow and ActiveX. In this way, a wide range of video devices with live data streams are supported, at the moment only with 8 bit colour or greyscale images. The basic functions of V2 are as follows:

- (1) Display of live video in the main window with markers on information clipping (grey values of 0 are displayed in blue, grey values of 255 in red; see Fig. 11).
- (2) Control of camera settings via 'Setup' button.
- (3) Integration of multiple frames to 16 bit greyscale images by averaging of 8 bit frames and scaling to 16 bits for increased dynamic range and SNR.
- (4) Temporal median filtering prior to averaging for suppression of directly converted X ray photons reaching the CCD chip despite the lead shielding.
- (5) Selection of file name for storage of integrated images as standard 16 bit TIFF image.
- (6) Calibration of the integrated raw images via calibration set-up file (see Section 3.2.3) for reduction of electronic background (so-called dark image) and inhomogeneities between single pixels via additional multiple gain images ('bright images' with flat field X ray exposure of different intensities). V2 allows also replacement of 'bad pixels'.
- (7) The calibration procedure, file and functionality are the same as used in ISee! via the menu Image -> Adjust pixels ...

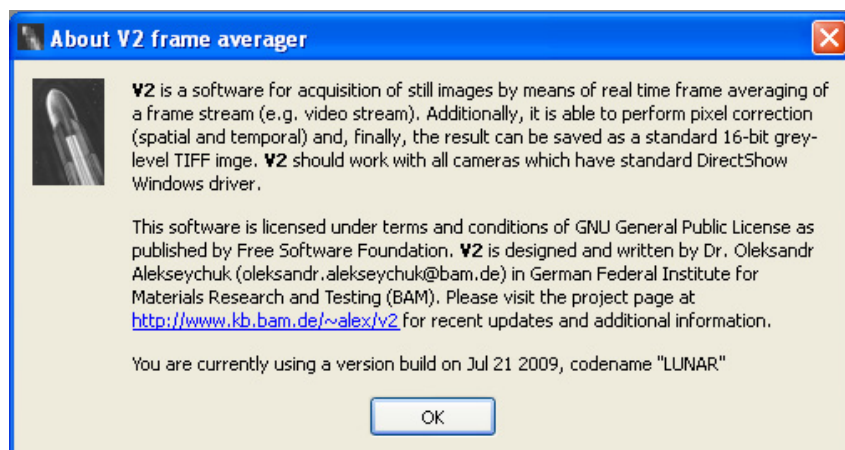


FIG. 12. 'About' window for the BAM V2.exe software, with information on licence and availability.

There can be several circumstances in which the V2.exe program simply crashes. This can be caused by software bugs between the public domain library used for Video-I/O and the DLLs provided by the camera manufacturer. This is outside the V2.exe program and cannot be prevented completely. It can also happen that the camera is recognized but no data are transferred (0 frames per second and a black image window). This occurs mostly after reconnection of the camera to the system. In this case, start the FOcontrol.exe application and start and stop the camera as shown in Fig. 10. After exiting the FOcontrol.exe, the program V2.exe should start smoothly and display the correct camera live data as shown in Fig. 11.

The first line 'View' in V2.exe allows configuration of the image display in the main window. All possible choices are shown in Fig. 13.

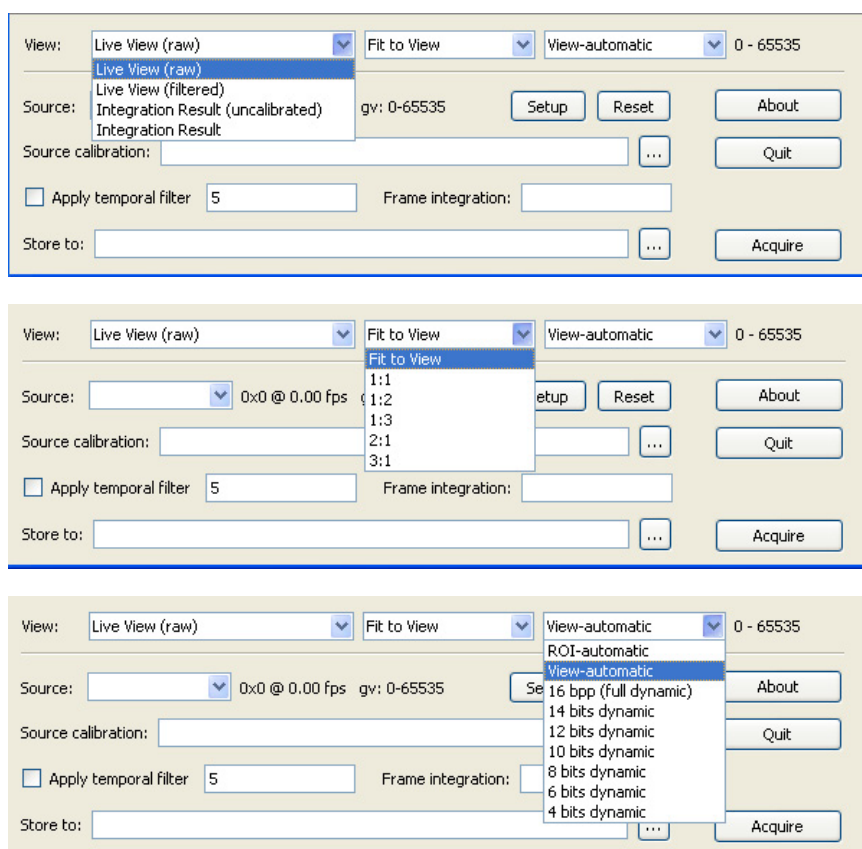


FIG. 13. All possibilities to control the image display in the V2 main window.

The right most bottom menu shown in Fig. 13 requires some explanation. ‘View-automatic’ is the default greyscale presentation, i.e. scaling of the maximum 16 bit grey values in the image data to the 8 bit dynamic range of the display. Here, the complete image (View) is automatically scaled, i.e. the minimum grey value is scaled to black and the maximum grey value in the image is scaled to white. The scaled grey value range is displayed on the right most side of the ‘View:’ line.

The top option ‘ROI-automatic’ is selected when a red rectangle is drawn by the mouse (left mouse button pressed) inside the main image window. Then only the grey values inside this red rectangle are considered for automatic histogram scaling to full 8 bit of the display. By pressing the right mouse button and moving the mouse, the position of this red region of interest (ROI) rectangle can be moved inside the image window.

The other settings shown in Fig. 13 (bottom image), from ‘16 bpp (full dynamic)’ up to ‘4 bits dynamic’, fix the look-up table for image display to the indicated number of bits considered in the image grey values. The image at the top of the figure shows the selection of different data streams. That in the middle shows the image display with different zooming factors, also adjustable via the scroll wheel on the mouse. At the bottom are different settings for grey value stretching. The numbers on the right hand side show the grey value range displayed between black and white.

The ‘Reset’ button in the V2 window resets the used IO library, the ‘Setup’ button calls the camera configuration window. The layout of the set-up window depends on the camera functionality and the implemented features of the ActiveX video components by the manufacturer of the camera driver. For the FOculus camera, this is shown in Fig. 14.

There are only two parameters that have to be adjusted and checked every time the camera is reconnected with the FireWire interface: ‘Brightness’ (grey value of dark image without exposure) and ‘Shutter’ (which determines the light exposure time of each camera frame). None of the other parameters should be changed. The correct settings are shown here for the BAM camera working at 200 ms exposure time (shutter = 1829) and a dark level of 1–2 grey values (brightness = 555). For details see the camera manual at: NET_FOculus_S_user_manual_v1.15_001.pdf.

If ‘Brightness’ and ‘Shutter’ are not set correctly, images as shown in Fig. 14 are acquired with clipped grey values (zero value in blue, maximum value of 255 in red). Information kept in the image and cannot be enhanced by any frame integration, so it is important to set the ‘Brightness’ level correctly. This will avoid any blue coloured pixels showing grey values of zero. The optimum setting is also shown in Fig. 14. At ‘Brightness’ equal to 555, the electronic background of the camera without light is between 1 and 2 grey values. The exact ‘Brightness’ value depends on the individual camera and its actual temperature.

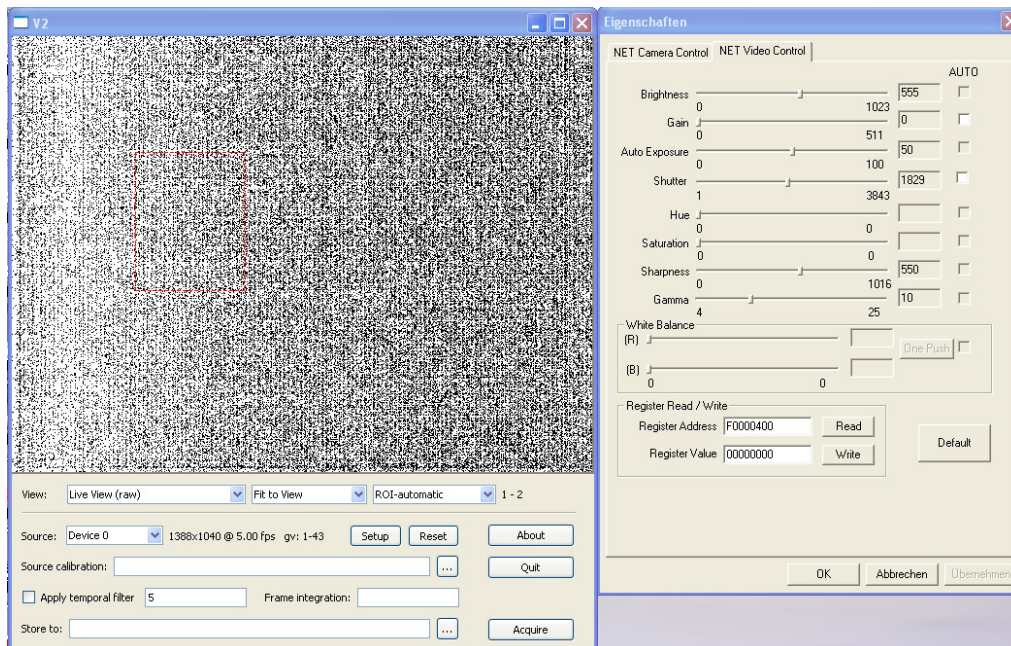


FIG. 14. Typical image with clipped grey level values as result of incorrect selection of brightness and shutter (left), and optimum settings of the camera FOculus FO 442SB (right).

On the right hand side of Fig. 14 is the camera control Windows shown for the FOculus FO 442SB camera after pressing the ‘Setup’ button in the V2 main window. Only the ‘Net Video Control’ tab is of importance; the ‘NET Camera Control’ tab should not be changed.

The other important setting parameter, electronic ‘Shutter’, will set the exposure time for the single camera frame. This value is an encrypted value derived from the frame time in ms. Depending on the selected frame time, the correct ‘Brightness’ setting will change, because the dark signal of the CCD chip will increase with increasing frame exposure time. So it is useful to operate the fluoroscope only with a very limited number of different shutter settings, because the fluoroscope calibration also depends on this setting. Depending on the available X ray power and distances, the frame exposure time should be long enough to have enough signal in the middle of the image. At BAM, an X ray tube up to 225 kV and 1.8 kW at a distance of 700 mm is used. For this source, a frame exposure time of 200 ms (five frames per second unprocessed raw data) was always the optimum (shutter = 1829).

Table 6 provides typical shutter values and the corresponding frame exposure times calculated from the formula given in the user manual (NET_FOculus_S_user_manual_v1.15_001.pdf).

TABLE 6. FRAME EXPOSURE TIME OF THE CCD CHIP AND CORRESPONDING SHUTTER VALUE SETTING IN THE CAMERA SOFTWARE CONTROL TAB

1394 Shutter value	Frame exposure time	1394 Shutter value	Frame exposure time
1	1 μ s	1729	0.1 ms
10	10 μ s	1829	0.2 ms
100	100 μ s	2129	0.5 ms
500	500 μ s	2422	1 ms
550	1 ms	2522	2 ms
650	2 ms	2822	5 ms
950	5 ms	2944	10 ms
1045	10 ms	3044	20 ms
1145	20 ms	3318	60 ms
1445	50 ms	3323	65 ms

Figure 15 shows a snapshot of an ongoing flat field exposure. This is an example of ongoing integration with V2 (9 frames of 50 are already done) using all features including calibration. The acquired grey values of a single frame are between 14 and 129, so no clipping is shown and the source calibration should also work. The computer load by the applied temporal filtering of five frames and image integration decreases the frame rate from five to two frames per second. So an overall exposure time of $50 \times 0.2 \text{ s} = 10 \text{ s}$ is integrated, but the time needed for this integration is $50 \times 0.5 \text{ s} = 25 \text{ s}$. So a faster computer will save some overall exposure time.



FIG. 15. Snapshot of an ongoing flat field exposure.

3.2.3. Calibration of fluoroscope

As shown in Fig. 16, the calibration is controlled via a simple text file. The content of the file used here is given as highlighted text in Fig. 16.

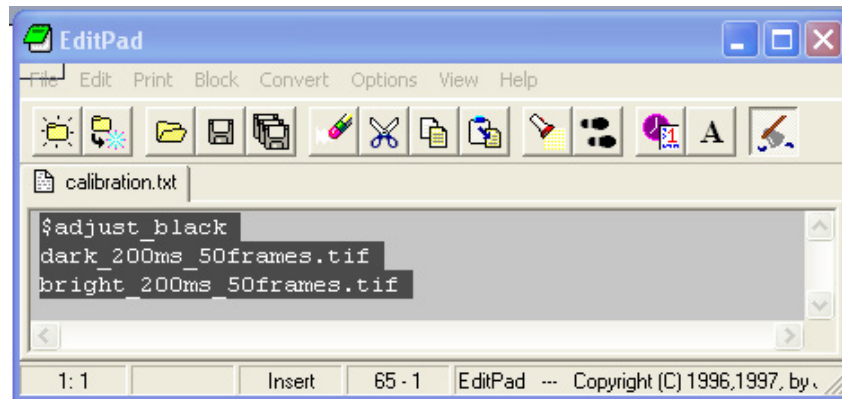


FIG. 16. Principle of fluoroscope calibration via text file containing keywords and image names used for grey value correction.

The keyword 'adjust_black' controls that the first image (dark_200ms_50frames.tif) is used to subtract any dark offset from each of the following white images. All the following images (here, only one image, "bright_200ms_50frames.tif", with a homogeneous exposure at the screen) are used for pixel-wise linear interpolation of the image to be calibrated for equalization of the individual pixel responses to provide the same median grey value of the calibration image. More details on image calibration can be found in the documentation included in the ISee! package (see <http://www.kb.bam.de/ic>). There, identical functions can be used via Image -> Adjust pixels.

A typical calibration text file for the BAM fluoroscope is given here:

```
$adjust_black
Dark2-200ms-240s.tif
Fe5mm-220kV-1mA-700mm-200ms-180s.tif
Fe5mm-220kV-2mA-700mm-200ms-120s.tif
Fe5mm-220kV-4mA-700mm-200ms-120s.tif
Fe5mm-220kV-8mA-700mm-200ms-60s.tif
```

A 5 mm thick steel plate was used for calibration. Besides the dark image, four white images were generated for calibration of the full dynamic range. With 8 mA at a 700 mm distance, no detector saturation was obtained. The other, darker images should have grey values linearly increasing from the darkest to the brightest image.

It is useful to have at least double the integration time for detector calibration as used later for image acquisition. If the source to detector distance changes, some artefacts in the detector calibration will appear, because of the changes in X ray source shading overlying the internal detector shading (mainly from objective).

In Fig. 17 the improvement of image quality is shown before and after calibration for an Inconel step wedge. Of course, during acquisition of images for fluoroscope calibration, the calibration function in V2 has to be deactivated (e.g. no source calibration text file as in Fig. 16). Exposure conditions are given in the displayed file name.

3.3. QUALIFICATION PROCEDURES FOR FLUOROSCOPE QUALIFICATION USING ISEE! ACCORDING TO ASTM E 2597

Procedures for image processing and data evaluation using ISee! version 1.10 are described in detail in the user manual. This manual, with procedures and examples for image processing, is available at <http://www.kb.bam.de/ic>.

The purpose of the following guidelines is to demonstrate and to assist in the application of the ASTM E 2597 standard for digital fluoroscope qualification. For full information and understanding of the concepts, it is necessary to read the full standard text of ASTM E 2597.

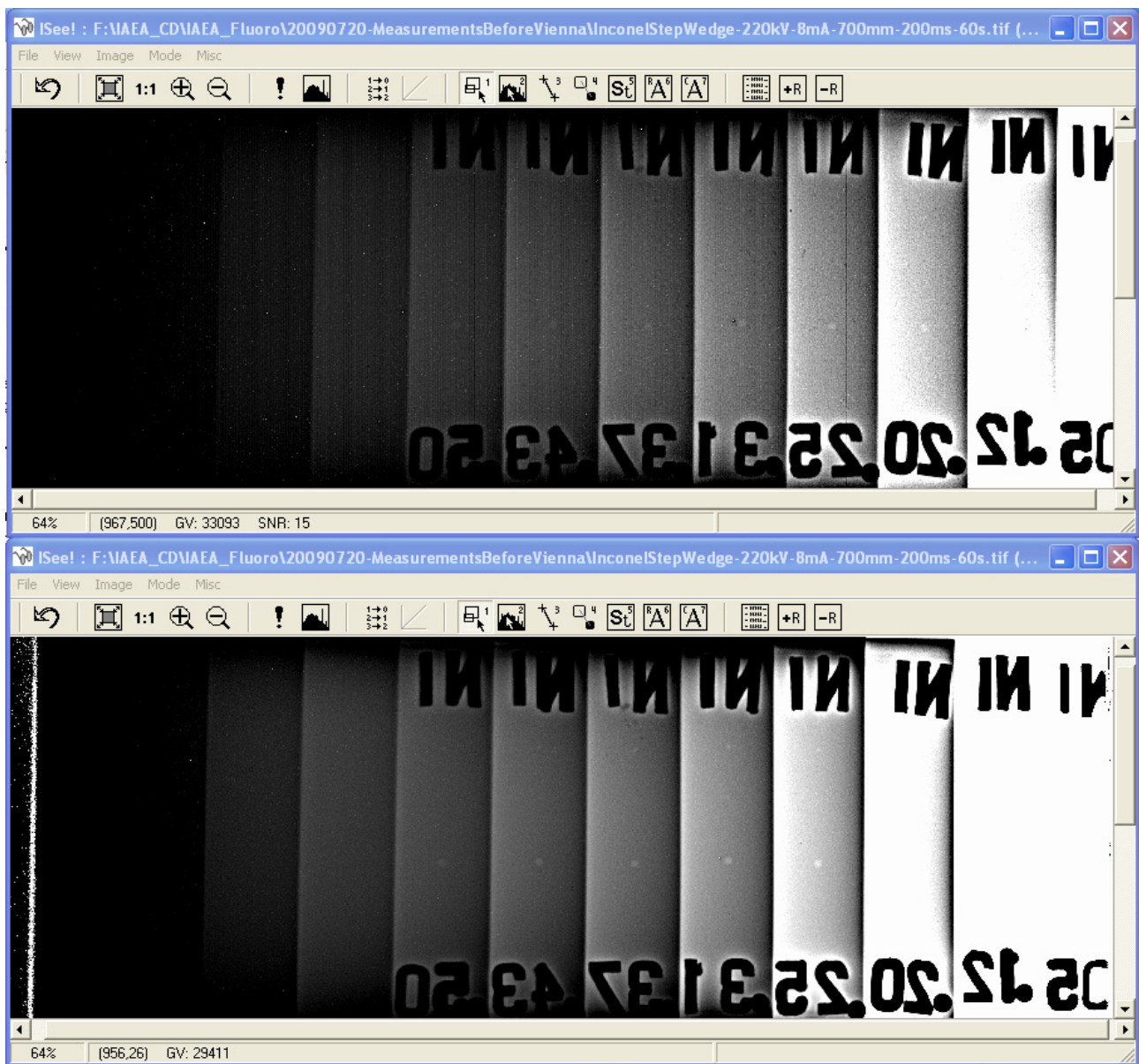


FIG. 17. Images of an Inconel step wedge with ASTM 2-2T penetrometers (after digital high pass filtering 'Enhance details'). Top: image without calibration, only 2-4T holes are visible. Bottom: after application of fluoroscope calibration to the raw data. Vertical banding is removed, the steps are more homogeneous and 2-2T holes are visible between 0.2 (5 mm) and 0.5 (12.5 mm) inch thickness.

The following equipment was used for the qualification example:

- X ray equipment: YXLON MCF-160 (constant potential, focal spot of 5.5 mm, 160 KV, 0.5–40 mA (depending on the voltage);
- Duplex Wire IQI (EN 462-5, ASTM E 2002);
- Aluminium (Al) and stainless steel (SS) step wedges (point 5.2 in ASTM E 2597 – 07);
- Dose rate meter and video camera to register the values remotely;
- Filters: 20 mm Al, 38 mm Al and 4 mm SS used at tube port.

3.3.1. Measurement procedure for basic spatial resolution (SR_b)

- (1) Place the duplex wire IQI directly on the detector (fluoroscope) with an angle between 2 and 5° to the rows/columns of the detector to avoid that wire pairs are in the same pixel lines.
- (2) Choose a source to detector distance of >1000 mm.
- (3) Define conditions such as focal spot size, no filters, etc.
- (4) Select the radiation energy (e.g. 90 kV). The current of the X ray tube is to be selected such that the grey value of the duplex wire IQI is 80% ($\pm 5\%$) of full saturation for the fluoroscope. In the example here, the acquisition parameters of V2 using the FO442SB CCD camera in the fluoroscope were:
 - (a) Shutter — 1829 (corresponds to 200 ms frame time);
 - (b) Brightness — 555;
 - (c) Number of frames — 500;
 - (d) Temporal filter — 5.
- (5) Use Fig. 18 and Eq. (13) to calculate the SR_b .
- (6) The measurement is to be carried out using a profile plot in ISee! on an area of 60% of the lines of the duplex wires for profile integration averaged to avoid variability along the length of the wires (Fig. 18). Use the mouse cursor within Isee! Version 1.10.2 to read the dip separation in per cent after marking of the 100% position at the dip maximum and the 0% position at the background between the wire pairs.
- (7) The SR_b is calculated as the linear interpolation of the wire pair distances between the last wire pair with more than 20% dip between the wires in the pair and the first wire pair with less than 20% dip between the wires (Fig. 18):

$$SR_b = D_1 - \frac{(D_1 - D_2)(R_1 - 20)}{(R_1 - R_2)} \quad (13)$$

where

- D_1 is the size of the smallest wire pair with >20% resolution of the gap;
 D_2 is the size of the largest wire pair with <20% resolution of the gap;
 R_1 and R_2 are the modulation of the corresponding wire pair (dip %value) of D_1 and D_2 , respectively.

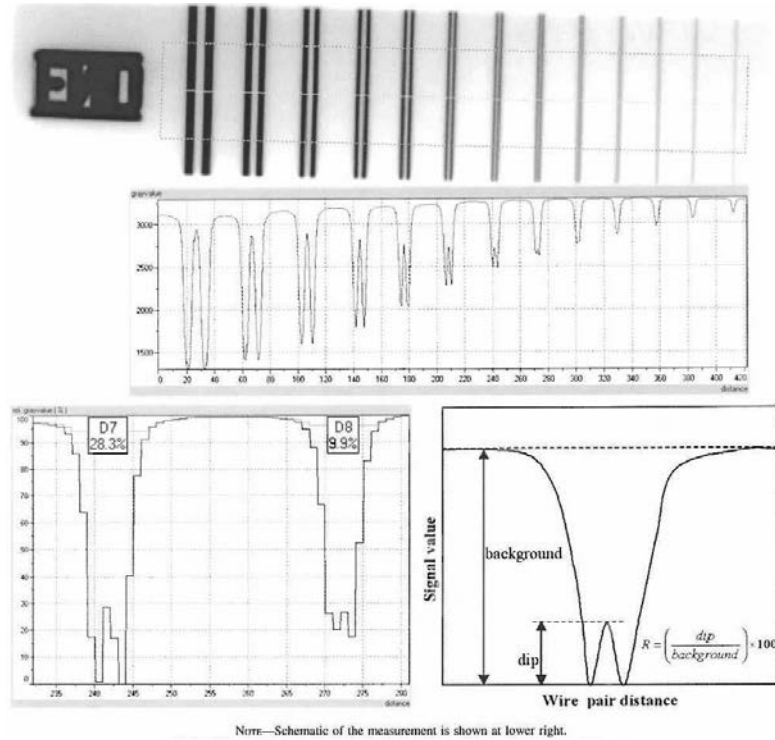


FIG. 18. Evaluation of the duplex wire IQI for determination of SR_b .

3.3.2. Measurement procedure for efficiency dSNRn

- (1) The efficiency of the digital fluoroscope is measured in the free beam without an object in front of the digital fluoroscope. For comparison between participants and between other detectors such as film, CR or DDAs, a typical dose of 1 mGy at the detector is used. The measurement is to be performed at a few points where the dose is above and below 1 mGy. The efficiency at 1 mGy can then be computed from the series of measured points. The series of points measured during the tests and a linear interpolation function including the point 0 dose/0 dSNRn verifies that the measurements are reliable and without artefacts. For simple verification, a dose of 1 mGy is reached if a D7 film (including 0.025 mm Pb screens) shows a density of about 0.6 above fog.
- (2) Obtain an offset image (black image, without radiation) with the digital fluoroscope using the same frame time (shutter and brightness setting in V2) as will be used later for the dose exposures. It is essential that for all digital fluoroscope settings used during acquisition of exposures, a corresponding offset image without any exposure dose is available. It is important, too, that for all measurements done for dSNRn, only the raw data of the digital fluoroscope without calibration are used. For an example of a correct offset image, see Fig. 19.

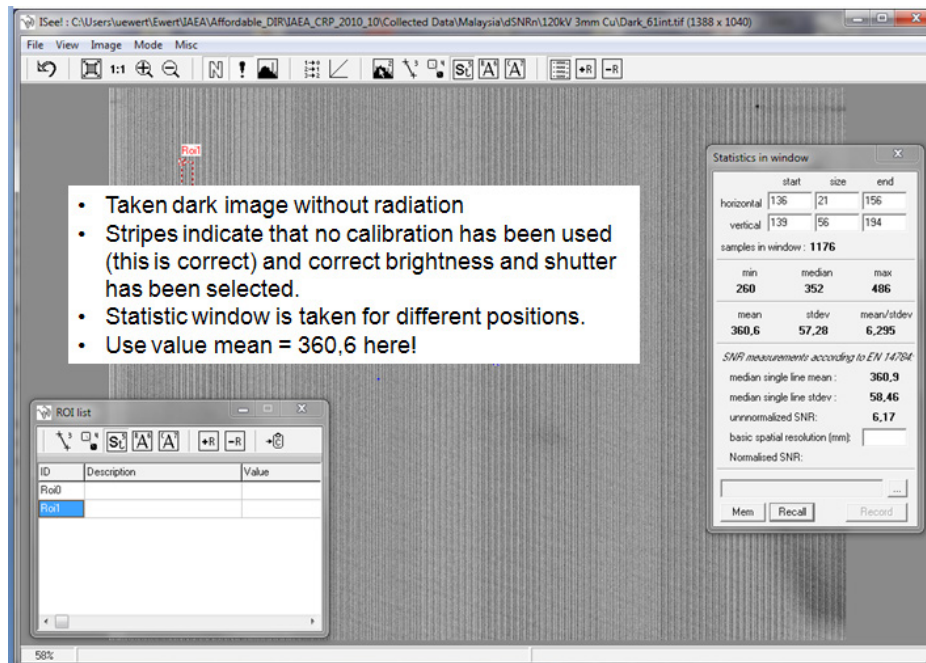


FIG. 19. Acquisition of a correct offset image with the digital fluoroscope.

- (3) The beam current and/or time of exposure needs to be adjusted such that a certain known dose rate is obtained at the location of the digital fluoroscope as measured with an ionization gauge (dose rate meter). Such a dose measurement may be made without any interference from scatter, so it is best to complete this measurement prior to placing the digital fluoroscope. The dose is obtained by multiplying the dose rate by the exposure time in seconds (or fractions thereof). To arrive at the 1 mGy dose, it is recommended to measure all of the data points (a few points below and above the 1 mGy dose) and record the mA·s values required to achieve these dose levels prior to placing the digital fluoroscope. The radiation qualities to be used for this measurement may be selected and documented. The radiation quality used for the example measurements was as follows: 60 kV (the standard requires 50 kV), 90 kV (20 mm Al), 120 kV (38 mm Al; the standard requires 40 mm) and 135 kV (4 mm SSt; the standard requires 120 kV and a 3 mm Cu plate). The material required to adjust the radiation quality has to be placed at the tube port of the radiation source. The ionization gauge used for measuring the dose rate is to be calibrated as per the manufacturer's recommendation.

- (4) Two images are collected (for each dose and each filter) under identical conditions immediately after one another. A correct example showing the attached dose meter is shown in Fig. 20. The two images are used to calculate the noise without any fixed pattern noise or other potential anomalies through a difference image (only the quantum noise is retained in this difference image). The difference image can be obtained with ISee! (v.1.10.2) applying the subtract function from 'pixel arithmetics' (see Fig. 21). An offset of 1000 should be added to this difference to avoid any clipping of noise values below 0. An example of what cannot be used as a difference image is shown in Fig. 22(a) (something was changed in the data acquisition of the two images); only an image as shown in Fig. 22(b) is useful for further analysis.

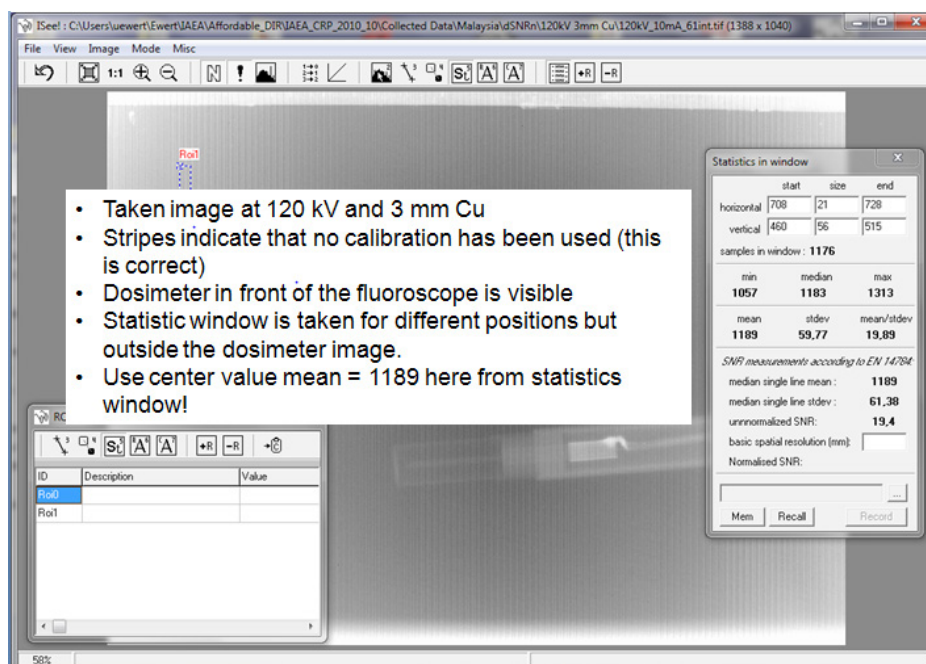


FIG. 20. One of the two raw images for $dSNRn$ measurement and its characteristics.

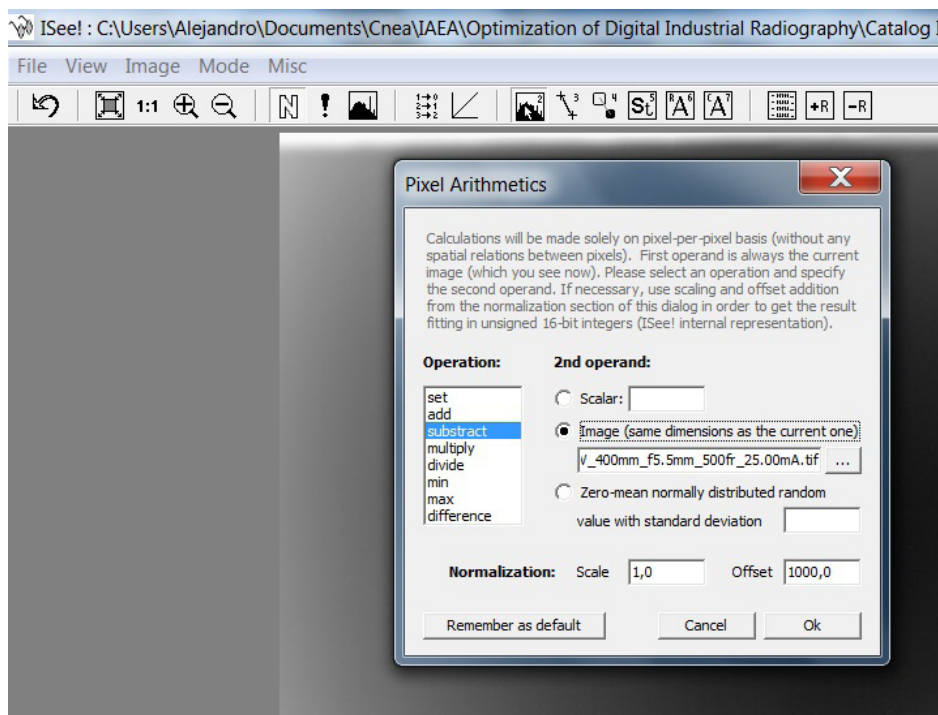


FIG. 21. 'Pixel arithmetics' in the ISee! software for calculation of the difference image.

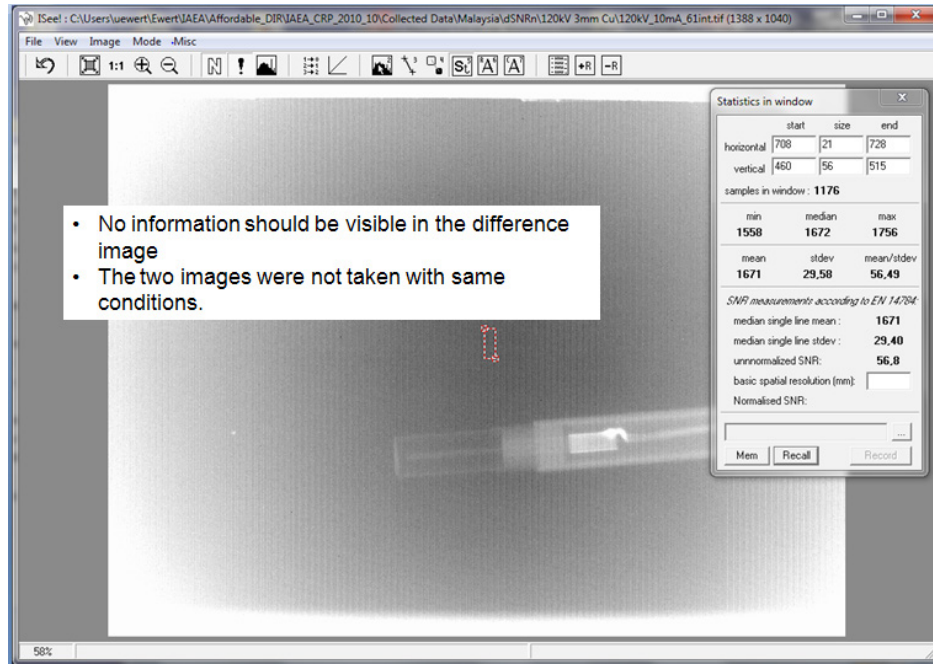


FIG. 22(a). Incorrect difference image showing details.

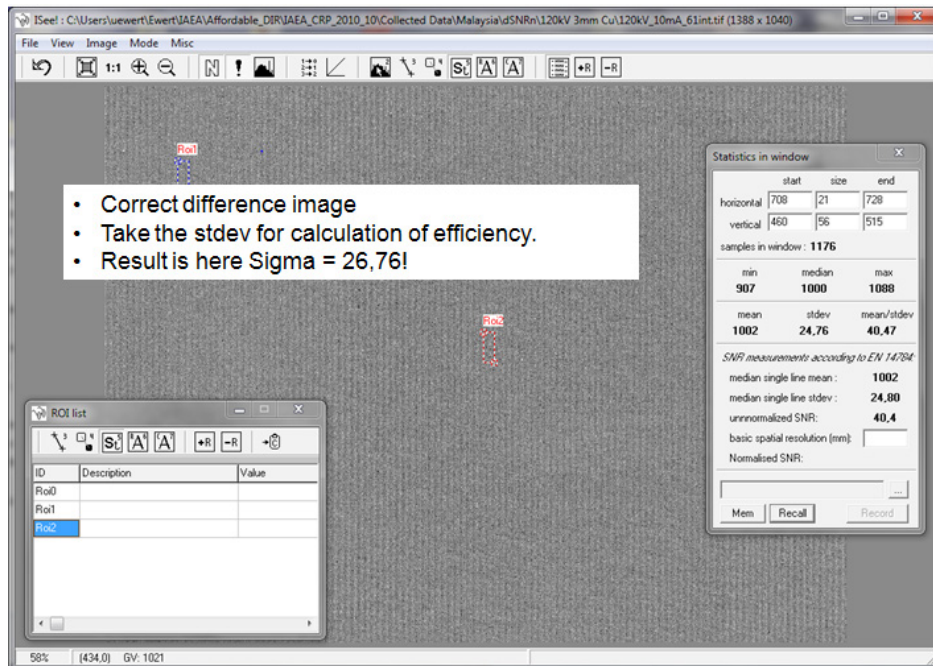


FIG. 22(b). Correct difference image showing constant background without any details and homogeneous noise from the X ray photons.

- (5) Compute the noise (standard deviation) in a 20 pixel \times 55 pixel area over five regions of the difference image. The mean value of these five standard deviations will be called the ' σ [difference image]'. The five 20 pixel \times 55 pixel areas are to be placed on the image such that one is at the centre of the image and four are at the corners with a distance to the edge of 10% of the effective digital fluoroscope range (Fig. 23).

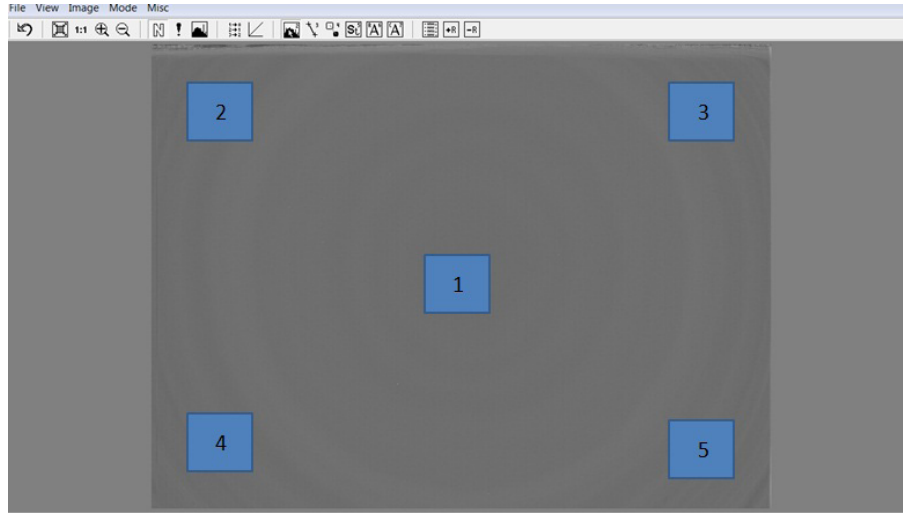


FIG. 23. Areas to be measured.

- (6) Calculate the mean signal of the 20 pixel \times 55 pixel averaged areas over the same five locations in one of the ‘non-difference’ images. This will be called the ‘Mean GV [first image]’ (no calibration is needed).
- (7) Calculate the average, in the same areas, of an offset image (without radiation). This is called the ‘Mean OV’ (see Fig. 19).
- (8) Calculate the dSNRn value using the following equation:

$$dSNR_n = \frac{(\text{Mean GV [first image]} - \text{Mean OV})}{\sigma[\text{difference image}]} \times \frac{(\sqrt{2} \times 88.6)}{SR_b} \quad (14)$$

V2.exe is used without any pixel calibration because a ‘difference’ image is used for calculation. The basic spatial resolution SR_b from Section 3.3.1 is used for normalization.

- (9) The dSNRn value obtained for the five different regions is averaged to obtain the final dSNRn value.
- (10) A plot may be drawn between various values of dSNRn (Y axis) and the square root of dose (X axis). Straight lines showing linear behaviour of dSNRn with the square root of dose should be obtained for different radiation energies. A typical plot is shown in Fig. 24 from ASTM E 2597, and the one from the example is shown in Fig. 25. The slopes of these straight lines define the efficiency of the detector. The value to be reported is the dSNRn at 1 mGy dose, depending on the radiation quality.

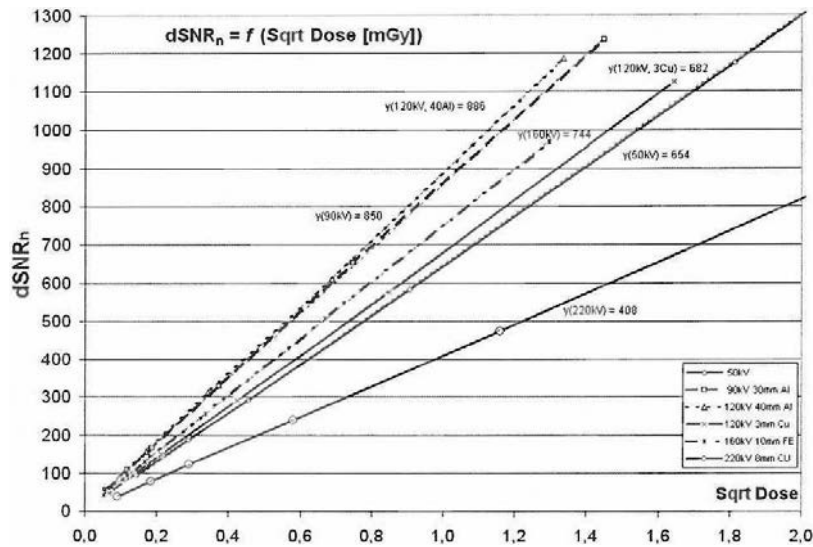


FIG. 24. Plot of dSNRn for efficiency measurements at different radiation qualities from ASTM E 2597.

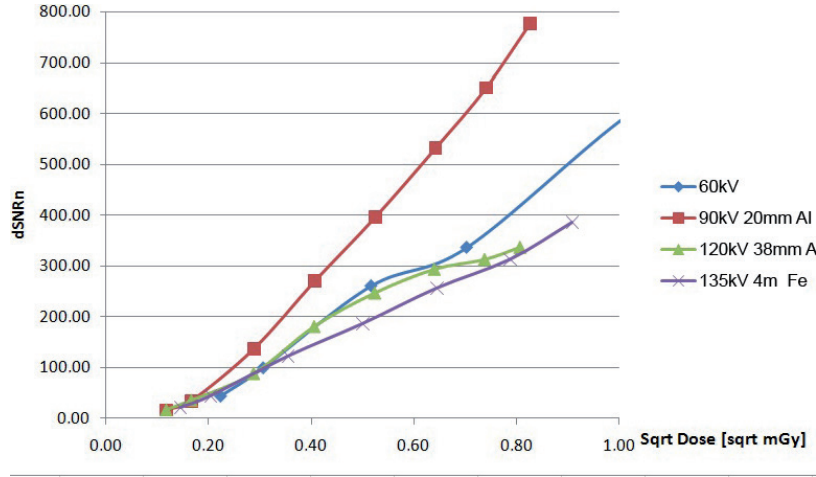


FIG. 25. Plot of $dSNR_n$ for efficiency measurements with the fluoroscope.

3.3.3. Measurement procedure for achievable contrast sensitivity and specific material thickness range

- (1) These measurements will be made using the two step wedge test blocks (Al and SS).
- (2) Place the step wedge for all these tests in front of the detector, with a source to detector distance of 1000 mm.
- (3) Collimate the beam to an area where only the step wedge is exposed.
- (4) If the area of the detector is too small to capture the complete step wedge in one image, two or more images with identical X ray and detector settings may be captured to cover the complete step wedge.
- (5) 'Setup' for this measurement should be set to 160 kV, with a 0.5 mm Cu filter placed directly in front of the tube.
- (6) The X ray tube current (mA) under this beam spectrum needs to be determined such that the detector is not saturated under the thinnest step for the integration time selected for all tests. Images are to be generated by averaging frames to obtain, as a minimum, 16, 64 and 256 s effective exposure times. These times should be calculated by multiplying the number of frames by the time of one frame (as set by the shutter value in the camera set-up of V2.exe).
- (7) The images should be calibrated for this test.
- (8) The signal (mean grey value) and noise (standard deviation) of each step should be computed in three rectangular regions, as shown in Figs 26 and 27. The minimum size of the rectangular ROI for evaluation is 20 pixels \times 55 pixels. The noise should be computed in the same rectangular region using the median of the single line standard deviations as listed in ASTM E 2446 and used in ISee!.
- (9) CNR (5%) should be computed as the ratio of the contrast (difference in signal between the region on the groove and those off the groove) to the noise of those regions off the groove, using Eq. (15) as follows:

$$CNR(5\%) = \frac{0.5 \times (signal(area\ 1) + signal(area\ 3) - signal(area\ 2))}{0.5 \times (noise(area\ 1) + noise(area\ 3))} \quad (15)$$

- (10) This is computed for each step of the step wedge images.
- (11) With a groove thickness of 5% of the base step thickness, the specific contrast (CSa) can be calculated from Eq. (16) as follows:

$$CSa = \left[\frac{5}{CNR(5\%)} \right] \quad (16)$$

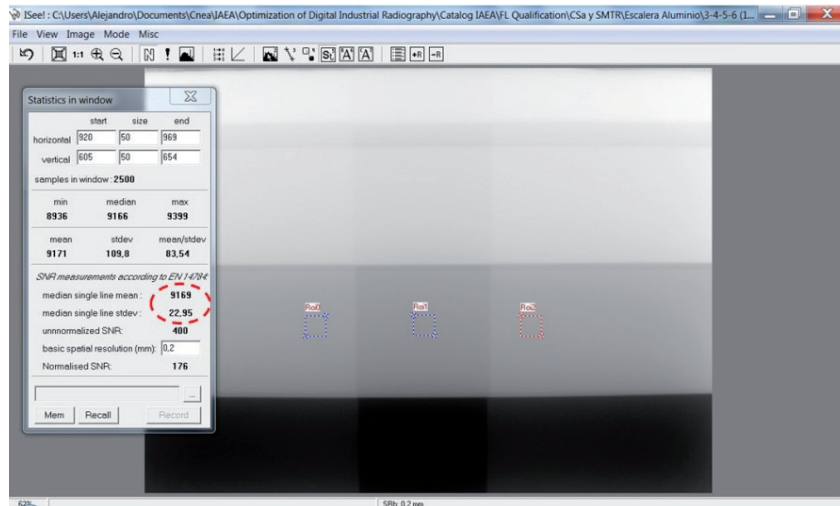


FIG. 26. Step wedge evaluation for specific contrast (CSa) calculation.

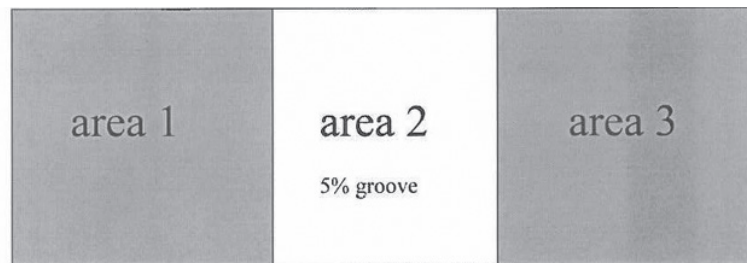


FIG. 27. Measurement areas for determination of the specific contrast (CSa).

- (12) Obtain values of CSa for different image acquisition times, say, 16, 64 and 256 s.
- (13) Draw a curve between CSa [% of penetrated wall thickness] and wall thickness for each material and exposure time (see Fig. 28).
- (14) For calculations of SMTR, first compute the normalized SNR for each step with ISee! (read the normalized SNR value).
- (15) Draw a curve between SNR and wall thickness for each material and exposure time.

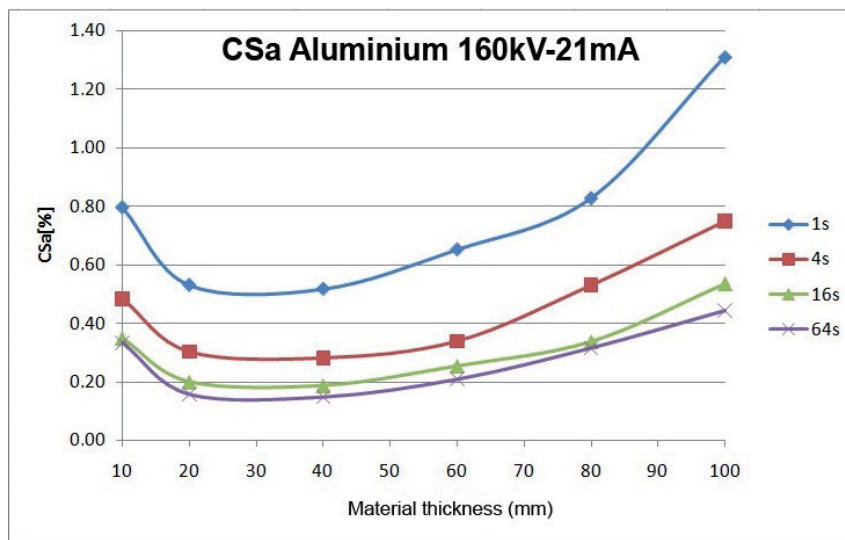


FIG. 28. Example of a CSa measurement for fluoroscope according to ASTM E 2597.

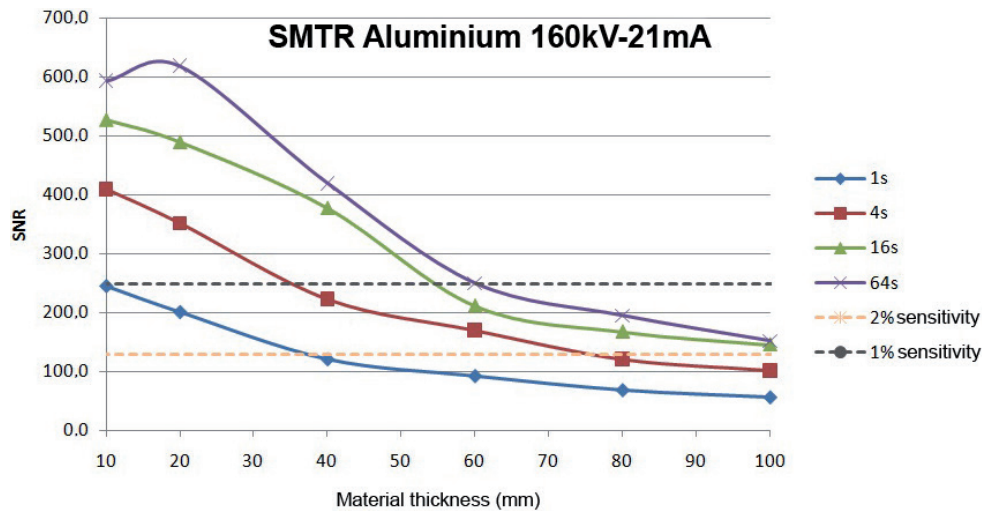


FIG. 29. Example of an SMRT measurement for fluoroscope according to ASTM E 2597.

- (16) For 2% sensitivity it should come out to be $\text{SNR} \geq 130$. In the example in Fig. 29, the specific material thickness range for 2% sensitivity is from 10 to 77 mm Al with 4 s exposure time.
- (17) For 1% sensitivity applications a $\text{SNR} \geq 250$ should be achieved. In the example in Fig. 29, the SMTR for 1% sensitivity would be 10–56 mm at 16 s exposure time.

A summary of all results of the participating countries is given in Section 4.

3.3.4. Identification of radiographs

The following naming and indexing system is to be used for providing digital radiographs:

- (1) Country name XXX (e.g. ARG, PAK, etc.);
- (2) Method (digital fluoroscope (FL), computed radiography (CR); image intensifier II, film digitization (FD));
- (3) Material (e.g. SSt or Al);
- (4) Type of specimen (e.g. weld (W) or casting (C));
- (5) Thickness in mm (e.g. 50);
- (6) Serial number of specimen;
- (7) Exposure conditions, kV, mA, source to detector distance, integration time (e.g. 200kV_50mAs_700mm_60s).

4. ACQUISITION AND ANALYSIS OF RESULTS

4.1. MEASUREMENTS OF BASIC SPATIAL RESOLUTION

All participating countries provided SR_b values based on the measurement procedure described in Section 3.3.1. The results are shown in Table 7.

TABLE 7. BASIC SPATIAL RESOLUTION (SR_b) OBTAINED WITH THE DIGITAL FLUOROSCOPES

Country	Test specimen ^a	Exposure conditions					Measurements		Basic spatial resolution ^b , SR_b (μm)
		Source to detector distance (mm)	Nominal focal spot (mm)	Pre-filter, if any	kV	mA	Smallest wire No. (>20% dip)	Largest wire No. (<20% dip)	
Argentina	Duplex IQI	1000	5.5	No	100	30	D6	D7	200
Germany	Duplex IQI	1000	3.5	No	90	1	D6	D7	190
India	Duplex IQI	1000	1.5	No	90	1	D6	D7	200
Malaysia	Duplex IQI	700	3	No	225	3	D6	D7	200
Pakistan	Duplex IQI	1000	1.6	No	100	4	D7	D8	190
Romania	Duplex IQI	700	3	No	200	4.5	D6	D7	200
Syrian Arab Republic	Duplex IQI	700	1.5	No	200	4	D7	D8	180
Uruguay	Duplex IQI	700	2.3	No	120	8	D6	D7	200
Uzbekistan	Duplex IQI	1000	3	No	160	4.5	D6	D7	200

^a IQI at detector front surface.

^b Averaged and rounded.

The average SR_b of all manufactured fluoroscopes was 200 μm. This corresponds to the expected value from the fluorescence screen manufacturer. Thus the optics and data acquisition hardware have an adequate fit to the screen unsharpness.

4.2. MEASUREMENTS OF EFFICIENCY

The measurement of the $dSNR_n$ is required to evaluate the efficiency of the developed fluoroscope and to compare it with the commercially available digital detectors (fluoroscope, computed radiography, DDAs and digitized film). The measurement procedure is described in Section 3.3.2. Table 8 summarizes the measurement results obtained by the Member States that took part in the CRP.

The results are very similar, despite the fact that the Syrian Arab Republic used only 8 bit data acquisition and Pakistan also reported problems. For these reasons, neither was able to reach the values of the other countries.

TABLE 8. EFFICIENCY MEASUREMENTS FOR DIFFERENT RADIATION QUALITIES
($dSNR_n$ at 1 mGy dose at detector entrance window)

Country	Condition for 1 mGy			Ionization gauge or dose meter (manufacturer, model)	Noise of (standard deviation) difference image at 1 mGy	Mean grey value (first image)	Mean offset value (first image)	Efficiency (dSNRn, averaged value) at 1 mGy
	Distance (mm)	Tube current (mA)	Integration time (s)					
Efficiency (dSNRn) at 50 kV, no material								
Argentina	1000	27	0.2	Berthold TOL-F	388.20	14 406	403.00	22.6
Germany	1000	6	4	PTW Unidos	962	52 352	6 400	22.0
Malaysia	1100	10	7	PTW Unidos (TW23331-0841)	29.1	1 740	358.2	29.7

TABLE 8. EFFICIENCY MEASUREMENTS FOR DIFFERENT RADIATION QUALITIES
(*dSNRn at 1 mGy dose at detector entrance window*) (cont.)

Country	Condition for 1 mGy			Ionization gauge or dose meter (manufacturer, model)	Noise of (standard deviation) difference image at 1 mGy	Mean grey value (first image)	Mean offset value (first image)	Efficiency (<i>dSNRn</i> , averaged value) at 1 mGy
	Distance (mm)	Tube current (mA)	Integration time (s)					
Syrian Arab Republic	1000	4	40	Babyline 81, Eurisys measures, France	5	110	50	12.0
<i>Efficiency (dSNRn) at 90 kV, 30 mm Al</i>								
Argentina	1000	20.3	0.85	Berthold TOL-F	301.4	19 417	397	39.5
Germany	1000	10	24	PTW Unidos	387	51 840	6392	52
Pakistan	1000	4	55					10.0
Uruguay	1000	8	52	Inovision, 451B	51	3 450	370	37.5
<i>Efficiency (dSNRn) at 120 kV, 40 mm Al</i>								
Argentina	1000	3.95	1.2	Berthold TOL-F	540.4	33 624	446	38.5
Uruguay	1000	8	38	Inovision, 451B	71	4 432	369	35.9
<i>Efficiency (dSNRn) at 120 kV, 3 mm Cu</i>								
Argentina	1000	14.95	1.2	Berthold TOL-F	494.5	28 016	435	34.9
Germany	1000	7.7	22	PTW Unidos	402	52 102	6385	50.4
Malaysia	1100	10	10	PTW Unidos (TW23331-0841)	26.94	2 670	373	53.4
Pakistan	1000	4	33					13.0
Uruguay	1000	8	44	Inovision, 451B	55	3 612	366	36.4
<i>Efficiency (dSNRn) at 160 kV, 10 mm Fe</i>								
Argentina	1000	11.65	1.6	Berthold TOL-F	412.3	17 137	407	25.4
Malaysia	1100	10	10	PTW Unidos (TW23331-0841)	27.32	2 510	380	48.8
Pakistan	1000	4	33					9.5
Uruguay	1000	8	54	Inovision, 451B	44	2 163	368	25.6
<i>Efficiency (dSNRn) at 100 kV, no material</i>								
Argentina	1000	6.05	0.2	Berthold TOL-F	470.4	24 761	420	32.4
Malaysia	1100	10	10	PTW Unidos (TW23331-0841)	31.29	2 410	364.2	40.9
Syrian Arab Republic	1000	4	11	Babyline 81, Eurisys measures, France	3.9	93	50	11
Uzbekistan	1000	4.5	8	Polimaster, ДКГ-PM1621	54	6 580	300	64.6
<i>Efficiency (dSNRn) at 220 kV, 8 mm Cu</i>								
Germany	1000	4.8	6	PTW Unidos	789	53 845	6405	26.6
Uruguay	1000	8	18	Inovision, 451B	101	4 261	367	24.1

The efficiency of the digital fluoroscope depends on the X ray energy. Figure 30 shows the measured dependence of the efficiency (*dSNRn*) in the centre of the fluoroscopic screen from the radiation energy.

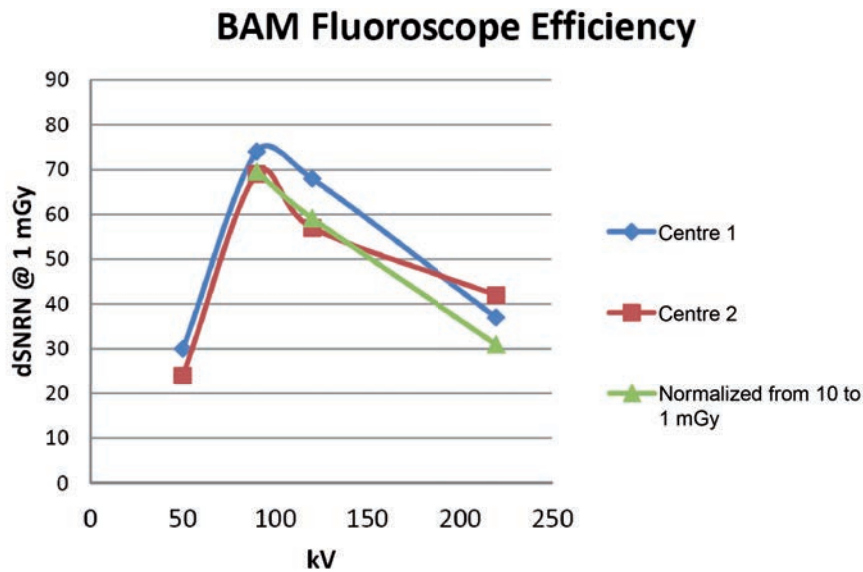


FIG. 30. BAM measured centre efficiency at different radiation energies.

Data in Fig. 30 were taken with 2 s frame time and 2 frames (centre 1), and with 0.2 s and 20 frames (centre 2) for exposure with 1 mGy. A third exposure was taken with 2 s frame time and 20 frames with a total exposure of 10 mGy. This curve was normalized by $1/\sqrt{10}$ and included in this figure.

The developed fluoroscope has the highest sensitivity at about 100 kV tube voltage. At lower energies the protecting input screen of 1 mm Al limits the efficiency, and at higher energies the efficiency declines because of the reduced attenuation of the fluorescence screen.

4.3. MEASUREMENTS OF ACHIEVABLE CONTRAST SENSITIVITY AND SPECIFIC MATERIAL THICKNESS RANGE

These measurements according to Section 3.3.3 and ASTM E 2597 allow the contrast sensitivity of the digital fluoroscope to be evaluated, depending on the material and its wall thickness. For aluminium, a wall thickness of up to 100 mm was investigated; for steel up to 12.5 mm. The radiation quality is fixed to 160 kV and 0.5 mm Cu at the tube port in accordance with ASTM E 2597.

Tables 9 and 10 give measurement results for aluminium and steel step wedges with six steps.

TABLE 9. MEASUREMENT RESULTS FOR ACHIEVABLE CONTRAST SENSITIVITY (CSa, %) FOR ALUMINIUM STEP WEDGE WITH SIX STEPS (10, 20, 40, 60, 80 AND 100 mm THICKNESS) ($SDD = 1000$ mm; $SOD = 600$ mm; pre-filter = 0.5 mm Cu; voltage = 160 kV)

Country	Tube current (mA)	CSa (%) at step No.:																	
		1			2			3			4			5			6		
		Exp. time (s)			Exp. time (s)			Exp. time (s)			Exp. time (s)			Exp. time (s)			Exp. time (s)		
		16	64	256	16	64	256	16	64	256	16	64	256	16	64	256	16	64	256
Argentina	14	0.5	0.4	0.4	0.3	0.2	0.2	0.3	0.3	0.3	0.4	0.4	0.3	0.4	0.3	0.3	0.6	0.4	0.3
Germany	3.5	1.9	1	0.8	1.6	1	0.5	2.1	1.3	0.9			1.5			3.5			7
Pakistan	4	3.2	0.2	5.5	0.3	0.2	0.2	0.9	0.5	0.4	1.7	1.3	1.3	2.1	1.8	1.6	2.5	1.8	1.6
Romania	1	1.6	1.3	1.4	1.5	1.3	1.1	1.9	2.1	1.4	2	2.6	1.9	2.1	2.2	1.7	3.2	3.6	3
Syrian Arab Republic	4	1.2	0.9	0.6	0.9	0.7	0.4	1.2	0.8	0.4	1.8	1.1	0.6	2.9	2.2	1.2	5	3.8	2.8
Uruguay	8	1.1	0.6	0.3	0.8	0.4	0.3	1	0.5	0.3	1.3	0.7	0.4	2.7	1.4	1.1	5	3.2	2.5

TABLE 10. MEASUREMENT RESULTS FOR ACHIEVABLE CONTRAST SENSITIVITY (CSa, %) FOR STAINLESS STEEL STEP WEDGE WITH SIX STEPS (1.3, 2.5, 5, 7.5, 10 AND 12.5 mm THICKNESS) (*SDD = 1000 mm; SOD = 600 mm; pre-filter = 0.5 mm Cu; voltage = 160 kV*)

Country	Tube current (mA)	CSa (%) at step No.:																	
		1			2			3			4			5			6		
		Exp. time (s)			Exp. time (s)			Exp. time (s)			Exp. time (s)			Exp. time (s)			Exp. time (s)		
		16	64	256	16	64	256	16	64	256	16	64	256	16	64	256	16	64	256
Argentina	12.3	1	0.6	0.5	2.6	1.6	1.2	0.4	0.2	0.2	0.4	0.2	0.2	0.6	0.3	0.2	0.6	0.3	0.2
India	2	1.7	1	0.7	1.5	1	0.5	1.5	1.3	0.4	2.6	1.4	0.8	3.6	3.2	1	5.5	0.7	1.3
Malaysia	8	1.3	0.7	0.4	1.2	0.6	0.3	1.2	0.6	0.4	2.4	0.9	0.7	5.6	1.2	0.8	4.6	2.1	1.4
Pakistan	4	0.3	0.2	0.2	0.4	0.3	0.2	1.1	0.7	0.6	1.3	1	1	1.9	1.5	1.5	2.4	1.7	1.6
Romania	1.8	3.3	3.2	2.3	2.2	1.8	1.4	2.9	2	1.7	5.7	3.6	3.2	8.6	4.4	4.5	12	7.3	7.2
Syrian Arab Republic	4	1.5	0.9	0.5	1.5	0.9	0.5	1.5	0.8	0.5	1.6	1.1	0.6	2.3	1.5	0.8	3.1	2.2	1.4
Uruguay	8	1.2	0.6	0.4	1	0.6	0.3	1.2	0.6	0.4	1.4	0.7	0.5	2.6	1	0.9	3.8	1.6	1.3
Uzbekistan	4.5	2.1	2.1	2.1	1.4	1.4	1.4	2.5	1.6	1	2.4	1.5	1.1	5.2	4.1	3.4	13	7.3	6.5

The specific contrast CSa as reported in Tables 9 and 10 increases with the exposure time, but decreases for a fixed exposure condition with increasing wall thickness.

Finally, the achieved SMTR was reported by the different countries as presented in Table 11.

TABLE 11. SNR VALUES FOR EACH STEP OF THE ABOVE STEP WEDGES AND THE RESULTING SPECIFIC MATERIAL THICKNESS RANGE (SMTR, mm) FOR SNR >130 or SNR >250

Country	Step Wedge	Tube current [mA]	SNR at Step No																		SMTR [mm]					
			1			2			3			4			5			6			for SNR > 130			for SNR > 250		
			Exp. Time [s]			Exp. Time [s]			Exp. Time [s]			Exp. Time [s]			Exp. Time [s]			Exp. Time [s]			Exp. Time [s]			Exp. Time [s]		
			16	64	256	16	64	256	16	64	256	16	64	256	16	64	256	16	64	256	16	64	256	16	64	256
Argentina	Al	14	200	269	299	179	253	313	112	133	145	63	73	77	56	71	75	61	96	120	34	41	43	0	21	28
	Steel	12,3	183	272	322	147	245	313	127	208	321	84	135	196	54	100	137	41	72	108	4,8	7,5	10,5	0	2,5	6,5
India	Al	2	476	551	632	386	495	573	312	398	471	206	290	380	118	163	215	96	142	186	73	100	100	53	74	81
	Steel	2	582	641	701	415	526	612	380	476	545	231	315	446	137	191	276	115	163	207	9,7	12	12	7,3	8,8	11
Malaysia	Al																									
	Steel	8	93	184	268	112	194	303	43	79	134	40	86	101	21	43	49	8	19	28	0	2,1	4,8	0	0	2,5
Pakistan	Al	4	132	148	170	109	95	104	49	40	43	32	19	19	24	16	16	17	11	11	10	10	10	0	0	0
	Steel	4	116	194	265	103	284	298	55	111	181	34	65	91	30	56	81	20	38	67	0	4	6	0	0	4
Romania	Al	1	65	68	70	55	61	59	49	52	57	58	45	51	42	52	53	33	40	46	0	0	0	0	0	0
	Steel	1,8	87	129	150	69	101	127	32	46	53	18	30	35	11	19	23	7	12	14	0	1,3	2,5	0	0	0
Syrian Arab Republic	Al	4	69	156	256	61	103	178	44	57	102	22	40	47	12	19	26	7	16	21	0	16	35	0	0	12
	Steel	4	72	138	208	46	102	165	30	61	96	26	41	62	15	18	44	9	16	21	0	2	4	0	0	0
Uruguay	Al	8	94	178	295	67	122	217	31	61	108	15	46	40	6	12	16	3	5	7	0	19	36	0	0	16
	Steel	8	80	149	267	57	110	198	32	64	115	19	37	62	10	26	53	6	13	31	0	2	4,5	0	0	1,5
Uzbekistan	Al																									
	Steel	4,5	32	32	32	41	44	43	51	77	122	28	49	60	14	19	21	9,4	13	14	0	0	0	0	0	0

The results obtained are highly dependent on the calibration procedure and the SNR reached at the single steps of the set wedges. As expected, the SMTR of the less absorbing aluminium material is higher than that of steel. If the SNR measured at a specific step did not reach the minimum SNR value of 130, the corresponding wall thickness is outside the SMTR.

4.4. COMPREHENSIVE RESULTS

All Member States that participated in the CRP were able to construct, assemble and operate the DFS as described in this report. The DFSs of all participants achieved a similar basic spatial resolution of about 200 μm .

The efficiency of the DFS measured in normalized SNR per mGy radiation dose is dependent on the radiation energy and had a maximum at 100 kV. The maximum SNR at this energy is between 40 and 80 as measured by the participating Member States for a dose of 1 mGy at the DFS screen, neglecting the measurement artefacts.

The results of measurements of achievable contrast sensitivity varied much more between the different countries. This is a result of differences in detector operation and especially in detector calibration. This showed that experience and knowledge are necessary for optimum DFS operation.

The results for SMTR were the most different between the countries. India reported extremely good results, Argentina was also able to report reasonable material ranges. The other countries had problems reaching the requested SNR values of 130 or even 250, and were able to achieve only low SMTR values. The limitations in SR_b and SNR are the application limits of the DFS for NDT inspections. The following subsections highlight these limits in more detail.

Besides the measurement results reported in this section, a catalogue of images was prepared and collected from a variety of test samples acquired with the DFS as well as from other digital radiological detectors. Some examples from this catalogue are provided in Section 5.

4.5. COMPARISON OF RESULTS WITH THOSE OBTAINED FROM OTHER DIGITAL INDUSTRIAL RADIOLOGY METHODS

Several measurements using CR systems were carried out by BAM to measure the normalized SNR_n of imaging plate scanner systems at 220 kV. A DDA was also evaluated for comparison. Figure 31 shows the efficiencies of different digital systems in comparison with those of selected digitized X ray films. Differential dSNR_n values can be measured for the digital fluoroscope and DDAs only, because only these can be calibrated. Differential comparison cannot be applied accurately with other CR systems. Therefore, the uncalibrated SNR_n values were compared.

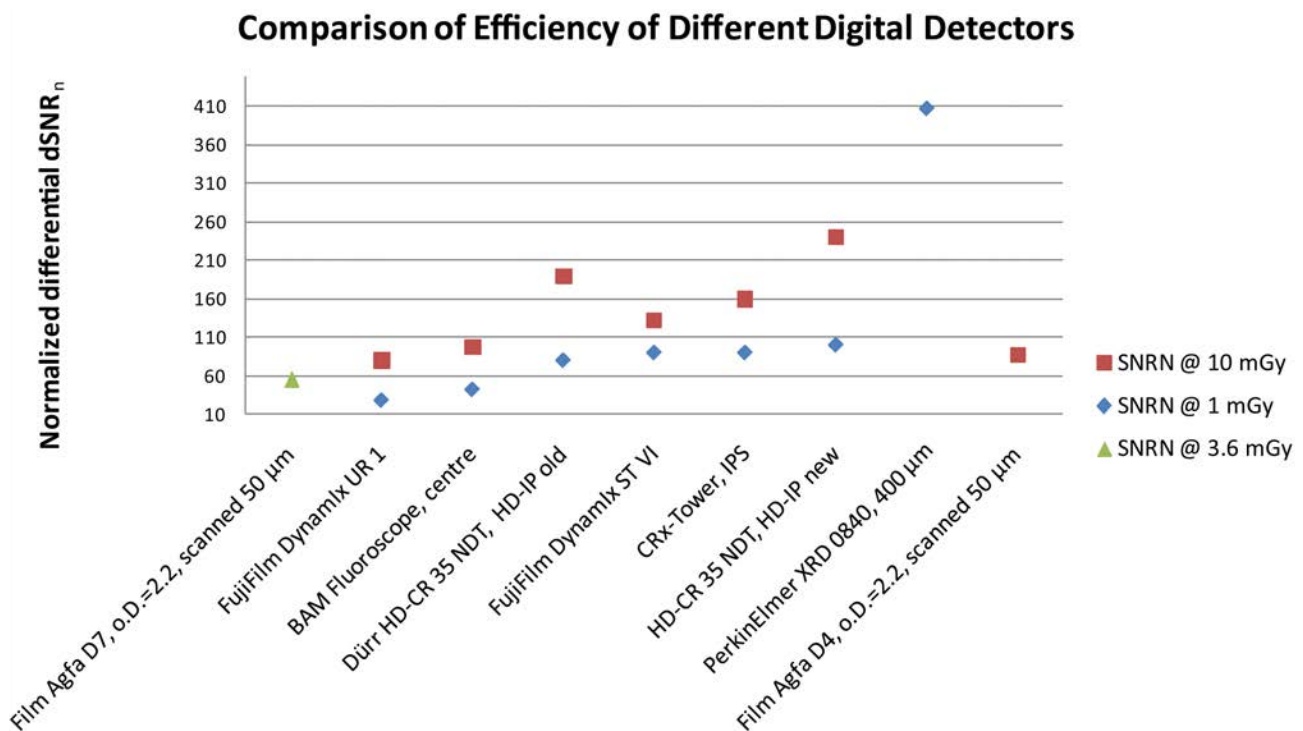


FIG. 31 Comparison of dSNR_n and SNR_n values obtained with CR systems of different detectors and films.

It can be concluded that the DFS has a sensitivity comparable to that of C5 film systems (ISO 11699-2) and high resolution CR systems. The advantage of the DFS is its applicability to a wide variety of inspections with different required sensitivities. Basically, the operator has to decide which dose is required for the exposure.

Exposures with a higher dose provide significantly better contrast sensitivity than do short exposures. A typical exposure (220 kV, 8 mm Cu) of an X ray film system C5 (e.g. Agfa D7, Kodak AA400) requires about 3.6 mGy at the film. The DFS at 220 kV and 10 mGy provides a dSNRn of about 80 (in screen centre). The C5 film system (AGFA D7) provides a dSNRn of only 56. From this number it can be derived that the fluoroscope (centre part of the input screen) can provide the same contrast sensitivity as the C5 film system in half the exposure time. Due to the significant reduction of the DFS sensitivity at the outer rim of the fluorescence screen, it is recommended to use the DFS with the exposure conditions as given in exposure charts for C5 film systems (at 220 kV) to achieve comparable image quality. This was experimentally verified for aluminium and steel. DFS exposures after proper calibration provided radiographs with the same or even more visible wires than those from digitized C5 films.

Experiments were carried out to compare the quality of CR and DFS radiographs with the BAM test weld BAM 5 (8 mm mild steel). Figure 32 shows the DFS exposure of BAM 5. It can be seen that the radiograph shows more wire and step hole IQI values than is required for class B testing of ISO 17636, EN 462-3, EN 1435 and ASTM 1742 (2%). The new ISO/DIS 17636-2 proposal requires achieving some minimum IQI values for wires or step hole IQIs and the duplex wire IQI, depending on the material thickness. Taking this into account, the DFS provides only the testing class A, due to the limitation of image sharpness. The missing sharpness (proven by duplex IQI) is compensated for by the additional wires seen, as required in ISO/DIS 17636-2.

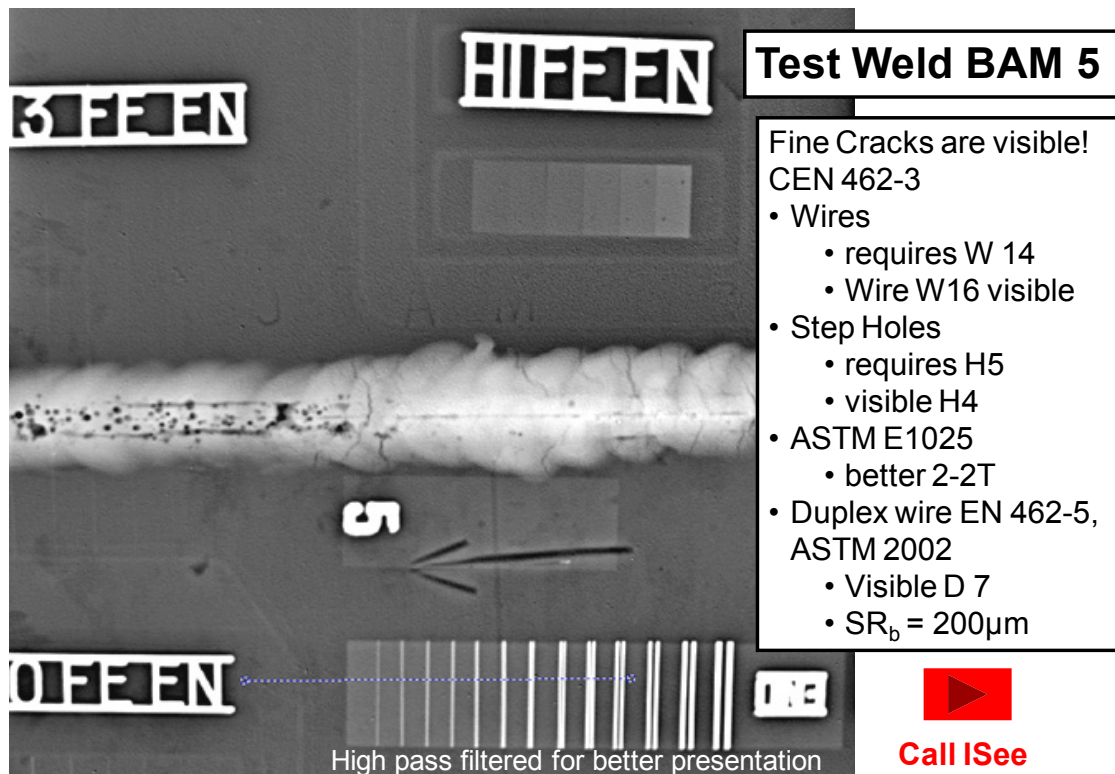
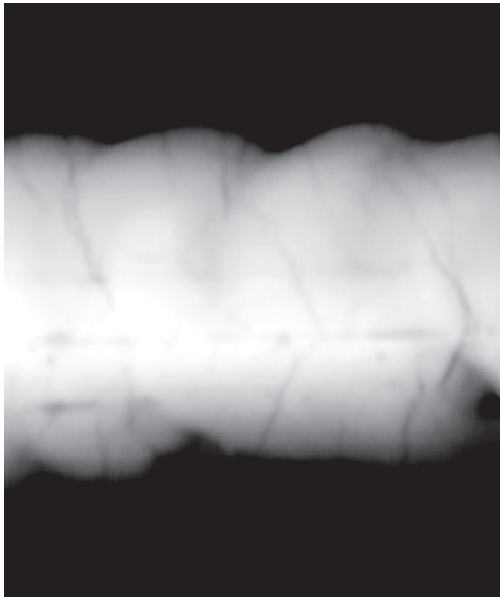


FIG. 32. DFS exposure of test weld BAM 5 (8 mm mild steel weld) after high pass filtering.

Figure 33 shows the radiographs taken with the DFS and the CR system of Dürr (HD-CR35 NDT and HD-IP). Both of the exposures were carried out at 130 kV with 100 mA. Figure 33 also shows the two digital radiographs in detail. No major differences can be observed. For better image evaluation, a high pass filter of ISee! (enhanced details) was applied. The visual image evaluation shows that the CR image is noisier and the contrast to noise ratio enables a significantly better visualization of cracks in the DFS image despite the higher unsharpness.

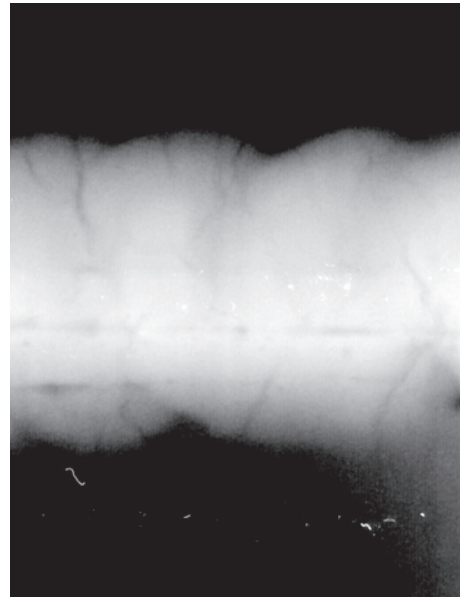
BAM Low Cost Fluoroscope vs. Computed Radiography

BAM5 test weld (8mm Fe), 130 kV, 0.5 m FOD, ~100 mAs



BAM fluoroscope 17 mA. 6 sec

(a)

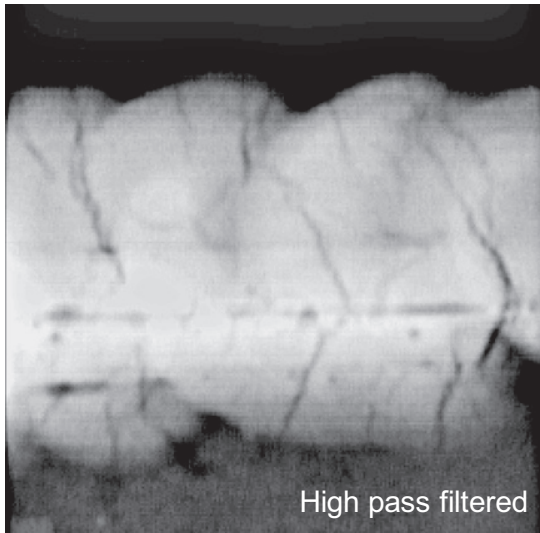


ST-VI IP. Dürr CR35V. 10 mA. 10 sec

(b)

BAM Low Cost Fluoroscope vs. Computed Radiography

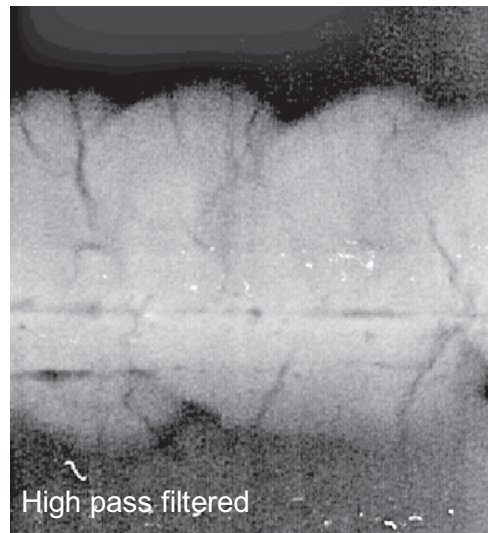
BAM5 test weld (8mm Fe), 130 kV, 0.5 m FOD, ~100 mAs



High pass filtered

BAM fluoroscope 17 mA. 6 sec

(c)



High pass filtered

ST-VI IP. Dürr CR35V. 10 mA. 10 sec

(d)

FIG. 33. Comparison of (a) DFS and (b) CR radiography. The radiographs were taken under the same exposure conditions. After high pass filtering, it can clearly be seen that (c) the DFS image is less noisy and shows better the crack details despite the higher unsharpness than (d) the CR image.

4.6. EXPERIENCE WITH ISOTOPIC RADIATION SOURCES

A successful attempt was made by India to use the digital fluoroscopic system with gamma rays (^{192}Ir). It is pertinent here to point out that in industrial radiography, isotopic sources are widely preferred for field applications, and a wide variety of sources such as ^{75}Se , ^{169}Yb and ^{192}Ir are in use. Experiments using ^{192}Ir were quite encouraging. Images could be obtained with suitable collimation of the radiation beam focused primarily on the ROI and additional shielding around the casing to prevent scattered radiation from reducing the SNR.

The DFS was used for the examination of welds using ^{192}Ir . The objects chosen were 8 and 10 mm thick stainless steel welds. Since these were preliminary trials, the choice of the thickness was based on the source activity ($\sim 18\text{ Ci}$) and the source–detector distance, which was fixed at 400 mm to ensure a higher dose rate at the detector face. A slightly longer integration time was also used. Figure 34(a) shows the gamma ray image of the weld with the DFS. The radiographic film image is also given for comparison purposes (Fig. 34(b)). It should be highlighted here that, compared with X ray imaging, gamma ray imaging necessitated the use of additional shielding. The gamma ray beam was collimated with the conventional tungsten collimator and additional shielding of lead of about 3 mm was provided around the DFS to ensure that radiation did not impinge on the CCD camera. In addition, lead bricks were placed on the front side to provide a window so that radiation was restricted to the ROI alone.

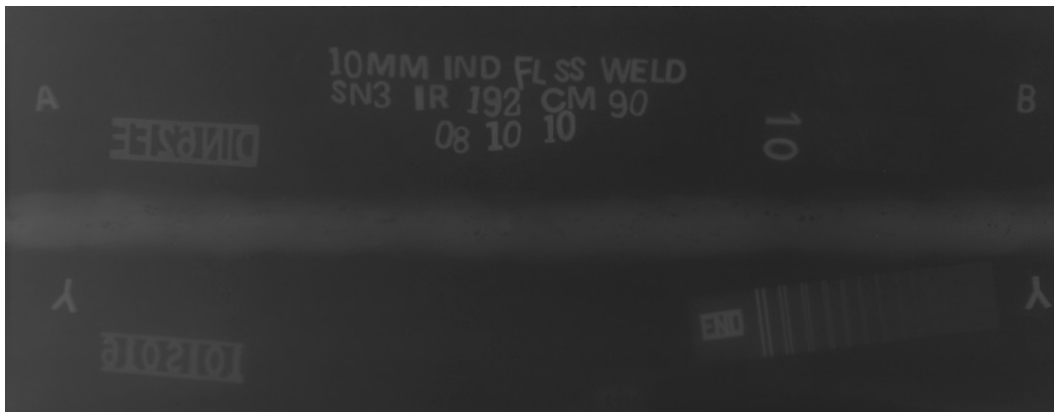


FIG. 34(a). Exposure of a 10 mm thick steel weld with ^{192}Ir and a digital fluoroscope.

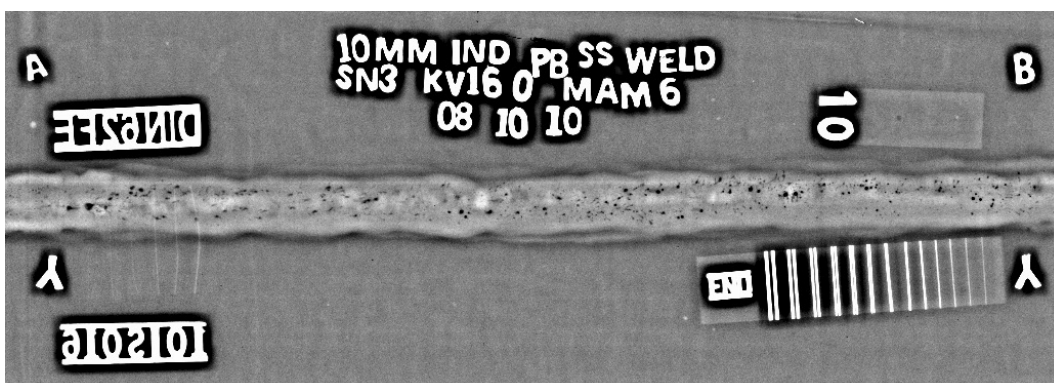


FIG. 34(b). Exposure of the same 10 mm thick steel weld with 160 kV X rays and film.

The gamma ray image using the DFS was contrast stretched, while the film image using X rays was subjected to high pass filtering to effectively show the defects in the specimen. It can be observed from Fig. 34 that porosity can be detected in the gamma ray image (though not all could be detected). A comparison of the image quality indicates that, in the case of the DFS, the duplex wire IQI of the 6D wire could be resolved, indicating a larger

unsharpness of 0.25 mm compared with film. While 1T could be resolved in the film, the 10-4T can be resolved in the DFS image, although with difficulty and processing. However, this is a major achievement, as it clearly reveals the potential of the DFS for use with gamma rays. This would be a real benefit to field personnel, as it would provide a low cost system with comparable sensitivity.

A spin-off from this CRP was a study of the dependence of the attenuation coefficient μ of the ^{192}Ir gamma rays in steel. ^{192}Ir has many gamma lines (130, 270, 296, 310, 320, 468, 485, 590, 610 and 890 keV) and is considered to be equivalent to a 600 kV X ray generator. It is well known that μ depends on energy (E) and penetrated material thickness (x):

$$\mu = \mu(E, x) \quad (17)$$

During the course of the experimental measurements, it was observed that μ , as a function of the thickness traversed by gamma rays, is best described by the following two nonlinear functions for non-collimated and collimated beams. Here, x is the thickness of the traversed steel and is measured in cm, coefficients a and b have the units of μ to be cm^{-1} . The fits have been made in the range of $0.1 \text{ cm} < x < 8 \text{ cm}$.

In the case of a non-collimated beam using ^{192}Ir and radiographic films, the following was obtained:

$$\mu_{\text{noncollimated}} = (0.4787 \pm 0.0016) + \frac{0.090 \pm 0.003}{\sqrt{x}} \quad (18)$$

For a collimated beam the following was obtained:

$$\mu_{\text{collimated}} = (0.6838 \pm 0.0024) + \frac{0.129 \pm 0.004}{\sqrt{x}} \quad (19)$$

These enhance the accuracy of results and can be used to derive a wall thickness difference from intensity differences using the ‘Penetrameter’ function of the ISee! software.

4.7. STANDARDS, IMAGE QUALITY AND COMPENSATION PRINCIPLES

4.7.1. Introduction

Since 2005, different standards for DIR have been developed and published. The international standards committees started with computed radiography. Most of these standards are now under revision. In 2010, the first practice on radiography with DDAs was published by ASTM International (ASTM). Similar standards are now under development at the European Committee for Standardization (CEN) and International Organization for Standardization (ISO). Table 12 provides an overview of present applicable RT and CT standards and the proposals that can be used for radiography with the developed digital fluoroscope.

TABLE 12. STANDARDS FOR RADIOGRAPHY WITH THE DIGITAL FLUOROSCOPE

Standard	Application
CEN: EN 13068	Radioscopy
CEN: prEN 16016 parts 1–4	NDT radiation methods CT
ASTM: Digital Detector Arrays	Manufacturing Characterization (E 2597), Practice (E 2698), Guide (E 2736), Performance Evaluation and Long-Term Stability (E 2737)
ASTM: E 2422	Digital catalogue of light alloy casting, digitized from ASTM E 155 films
ISO: ISO/FDIS 10893-7	NDT of steel tubes: Digital RT for inspection of longitudinal and spiral welded seams
ISO: ISO/DIS 17636-2	NDT of welds: Digital RT for film replacement
ISO: ISO 15708 parts 1–2	NDT radiation methods CT

Table 13 provides guidance on how digital detectors can be used for film replacement. All film standards worldwide require that a minimum optical film density be exceeded. The equivalent value in digital radiography is the linearized SNR. Also, in digital radiography IQIs are to be used. These are basically wire, step hole or plate hole IQIs. The image quality values achieved should be the same as or better than those with film radiography.

Contrast to noise ratio management by increase of radiation dose and the specific DDA or digital fluoroscope calibration allows an extraordinary increase of contrast sensitivity. It is obvious that a higher CNR permits the visualization of smaller defects, which inherently have a smaller contrast (see also Section 1.3.3). The high contrast sensitivity technique has been developed to improve the testing quality and to prove the compensation principles.

TABLE 13. BASIC STANDARD REQUIREMENTS FOR FILM AND DIGITAL RADIOLOGY IN COMPARISON

Film	Digital detector (CR)
Achieve minimum optical density	Achieve minimum SNR _n or calibrated minimum pixel value
Do not exceed maximum unsharpness	Correct geometry and detector selection
Prove minimum IQI perception with: – Wires; – Step holes; or – Plate holes	Achieve minimum CNR _n , use same IQIs to prove quality, use optional unsharpness IQI

4.7.2. Requirements for image quality in digital industrial radiology

After qualification of the digital fluoroscope, it is to be used with a sufficient frame time and frame integration number for providing digital radiographs with an SNR_n ≥ 100 in the heat affected zone of the weld radiographs and SNR_n ≥ 70 in the image region of the thickest section of the casting. The measurement of SNR_n is to be carried out after calibration but before image processing with any digital filter. For measurement of SNR and SNR_n, a 20 pixel × 55 pixel window is to be used. For higher accuracy, a 20 pixel × 200 pixel window can be used.

The IQIs listed in the following subsections are to be used.

4.7.2.1. Wire IQI in accordance with ISO 19232-1

The requirement of the visibility of wires is to be selected in accordance with ISO 19232-3 or ISO 17636, or EN 1435 testing class A (see Table 14). The wires to recognize are to be selected in agreement with the nominal wall thickness for weld inspection. The wire IQIs are to be placed nearest to, but not crossing, the weld. The wires are to be positioned 90° to the weld. The visibility of the wires is to be read nearest to the weld, and the smallest visible wire is to be at least two thirds visible over its full length. For best presentation in the catalogue, the single wire IQI is to be placed above the weld and the duplex wire IQI is to be placed below the weld, but both on the source side.

The IQIs for casting inspection are to be placed at the thickest and thinnest area of the specimen.

4.7.2.2. Plate hole IQI of ASTM E 1025

A 2% wall thickness is to be used for thickness selection (ASTM E 1742). The required radiographic sensitivity is 2–2T. These IQI are to be used with shims for wall thickness compensation to the real thickness of the weld, if the thickness of the weld exceeds the nominal thickness by more than 20%.

TABLE 14. MINIMUM REQUIREMENTS OF ISO/DIS 17636-2 (TESTING CLASS A) ON IQI REQUIREMENTS FOR DIGITAL RADIOGRAPHY (cont.)

Specified wall thickness, <i>t</i> (mm)	Wire number, diameter (mm)	Specified wall thickness, <i>t</i> (mm)	Hole number, diameter (mm)	Specified wall thickness, <i>t</i> (mm)	Duplex IQI	
					Unsharpness	Wire diameter and spacing (mm)
$t \leq 1,2$	W18, 0.063	$t \leq 2$	H3, 0.20	$t \leq 2$	D11 0.16	0.080
$1,2 < t \leq 2$	W17, 0.08	$2 < t \leq 3,5$	H4, 0.25	$2 < t \leq 5$	D10 0.20	0.100

TABLE 14. MINIMUM REQUIREMENTS OF ISO/DIS 17636-2 (TESTING CLASS A) ON IQI REQUIREMENTS FOR DIGITAL RADIOGRAPHY (cont.)

Specified wall thickness, t (mm)	Wire number, diameter (mm)	Specified wall thickness, t (mm)	Hole number, diameter (mm)	Specified wall thickness, t (mm)	Duplex IQI	
					Unsharpness	Wire diameter and spacing (mm)
$2 < t \leq 3.5$	W16, 0.10	$3.5 < t \leq 6$	H5, 0.32	$5 < t \leq 10$	D9 0.26	0.130
$3.5 < t \leq 5$	W15, 0.13	$6 < t \leq 10$	H6, 0.40	$10 < t \leq 25$	D8 0.32	0.160
$5 < t \leq 7$	W14, 0.16	$10 < t \leq 15$	H7, 0.50	$25 < t \leq 55$	D7 0.40	0.200
$7 < t \leq 10$	W13, 0.20	$15 < t \leq 24$	H8, 0.64	$55 < t$	D6 0.50	0.250
$10 < t \leq 15$	W12, 0.25	$24 < t \leq 30$	H9, 0.80			
$15 < t \leq 25$	W11, 0.32	$30 < t \leq 40$	H10, 1.00			
$25 < t \leq 32$	W10, 0.40	$40 < t \leq 60$	H11, 1.25			
$32 < t \leq 40$	W9, 0.50	$60 < t$	H12, 1.60			a
$40 < t \leq 55$	W8, 0.63					b
$55 < t$	W7, 0.80					b

^a Duplex IQI should be used in conjunction with either a wire or step/hole IQI.

^b Duplex IQI should be examined using a profile display; the largest wires which have a dip separation below 20% between the wire pair determine the unsharpness.

4.7.2.3. Duplex wire IQI in accordance with ASTM E 2002 or ISO 19232-5 or EN 462-5

The first unresolved wire pair is to be achieved in accordance with Table 14. The IQI (Fig. 35) is to be positioned nearest to the weld but slightly tilted by about 2–5° to the horizontal or vertical detector orientation.

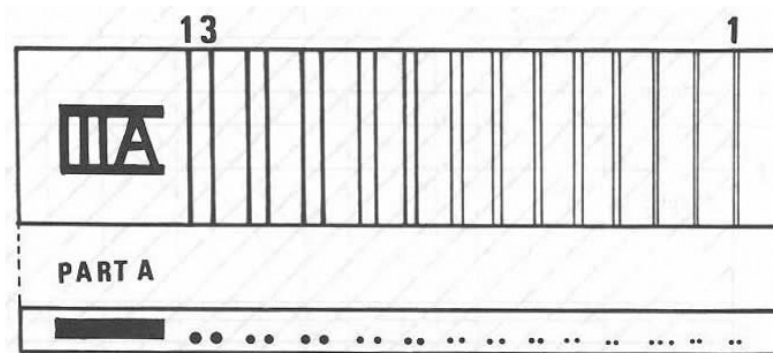


FIG. 35. Duplex wire type image quality indicator.

4.7.3. Magnification technique

If the required duplex wire indicated in Table 14 cannot be achieved and the compensation cannot be applied, a magnification technique is recommended. Before this is used, it is to be determined whether the focal spot and distance cause additional unsharpness. A larger source to detector distance and a smaller focal spot will reduce the unsharpness.

4.7.4. Compensation principle I

4.7.4.1. Compensation of reduced contrast (μ_{eff}) by increased SNR

The image quality in DIR depends on the product of effective attenuation coefficient μ_{eff} , also called specific contrast, and the SNR. This applies for CR, DDAs, DFs and X ray film. Figure 36 illustrates the effect of noise on flaw detection.

The specific contrast to noise ratio per wall thickness difference, Δw , which is the essential parameter for the visibility of flaws and IQIs of a given size, can be calculated from the detector response (SNR) as a function of exposure dose as follows (small flaws only; see Fig. 36 and Section 1.3.3):

$$CNR / \Delta w = SNR \cdot \mu_{eff} \quad (20)$$

Typical IQIs as plate holes (ASTM E 1025), step holes (ISO 19232-2) or wires (ISO 19232-1) change the hole diameters or wire diameters with their thickness. Therefore, the hole or wire visibility depends on the image unsharpness and the achieved CNR. If the hole diameter is much larger than the unsharpness, the equivalent IQI sensitivity (EPS, defined by IQI thickness in % of the penetrated material thickness for 2T hole visibility) changes proportionally to about $1 / \sqrt{SNR \cdot \mu_{eff}}$.

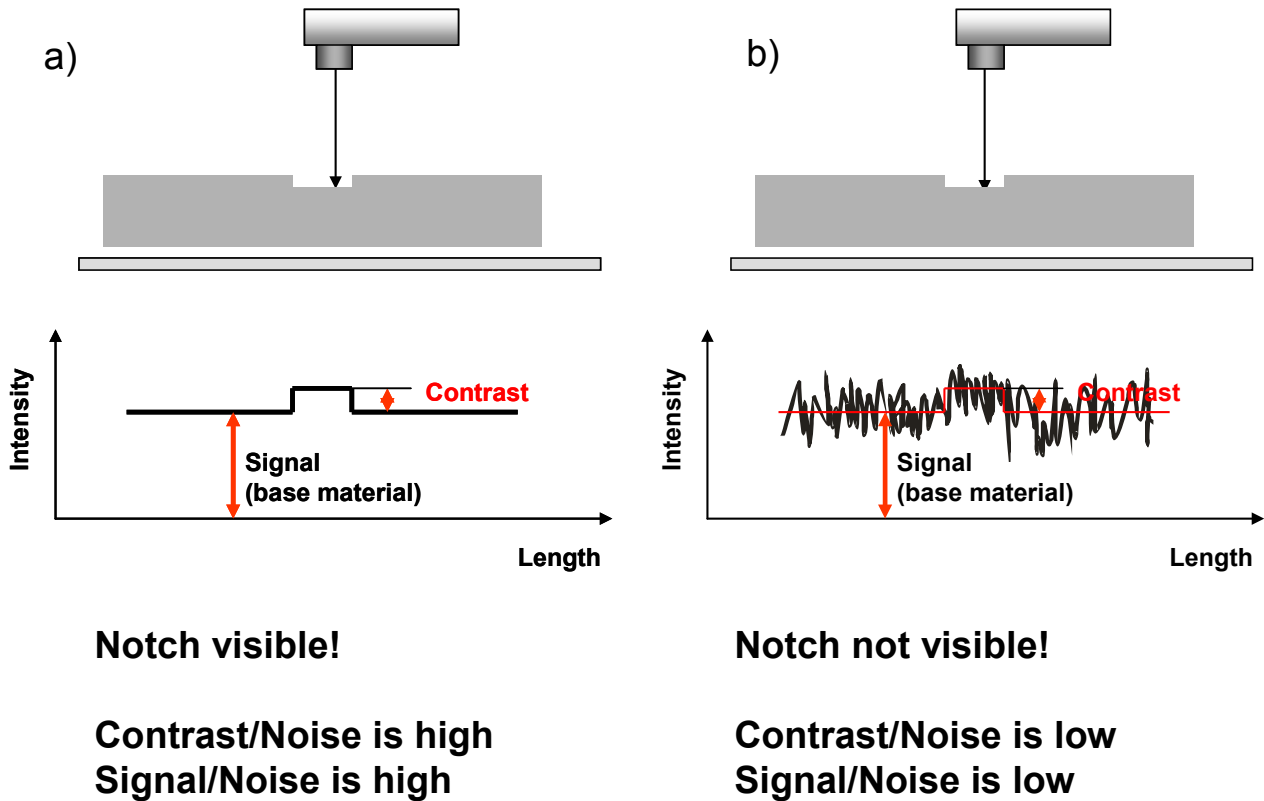


FIG. 36. The influence of noise on the visibility of a notch in radiography: (a) the notch is visible if the noise contribution can be neglected; (b) the notch is not visible if the noise is just higher than the contrast.

Since the grey values of the pixels in the digital images (assuming the signal is linear to dose) depend on noise and signal intensity independent of the contrast and brightness processing for image viewing, the SNR has been proposed and accepted as a value equivalent to the optical density and a certain film system in film radiography (EN 14784-1, EN 14784-2 and ASTM E 2445, E 2446). Visibility details of flaws can be increased by the SNR of the DDA image in comparison with a digitized film image (Fig. 37).

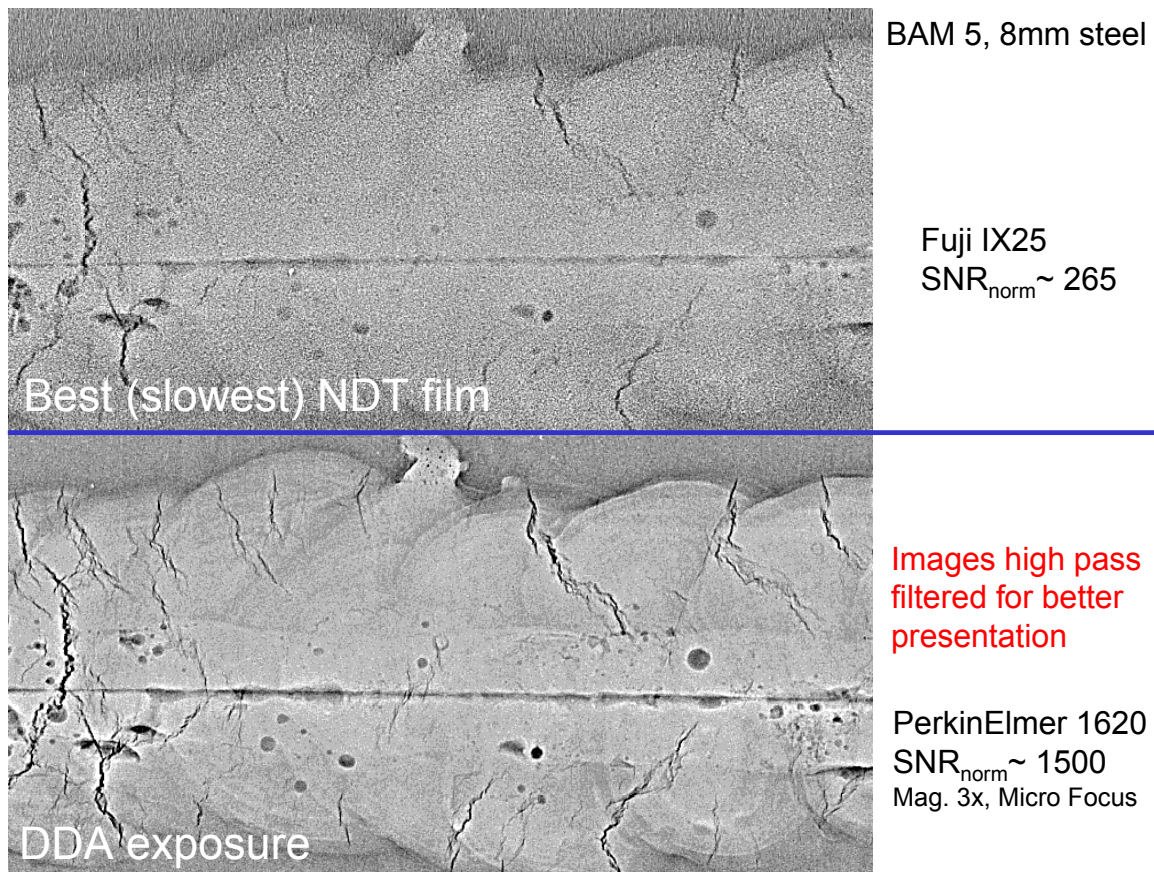


FIG. 37. Effect of increased signal to noise ratio of digital detector array image in comparison with digitized film image.

4.7.4.2. High contrast sensitivity technique

Four typical noise sources arise in radiography:

- Photon noise depending on exposure dose (e.g. mA·s or GBq·min);
- Structure noise of detector (fixed pattern noise);
- Crystalline structure of material (e.g. nickel based steel, mottling);
- Surface roughness of test object.

The first two noise sources can be influenced by the exposure conditions and detector selection. The SNR of images achieved depends on the exposure dose (low dose application). The SNR increases with the square root of mA·min or GBq·min, due to the improved photon quantum statistics. The structure noise of films and imaging plates depends on the manufacturing process and can be influenced by the selection of the specific detector type (e.g. fine or coarse grained film). Film development and imaging plate scanner properties also contribute to the final noise value. The structure noise of detectors and all noise sources depending on the object properties determine the maximum achievable SNR and, therefore, limit the image quality independent of the exposure dose (high dose application). Only with DDAs and a DFS can the structure noise (due to different properties of the detector or camera elements and fluorescent screen) be corrected by a calibration procedure, since the characteristic of each element can be measured quite accurately. Figure 37 shows the effect of an SNR increase (equivalent to a CNR increase) on the visibility of fine flaw indication. The digitized fine grained film provides an SNR of 265 in the base material region. The DDA image was measured with an SNR of about 1500. It shows significantly finer flaw indications. Digital fluoroscopes achieve SNR values between those of digitized films and DDAs.

In film radiography, it is well understood that the image quality increases if the tube voltage is reduced. In DIR, it can also be observed that the image quality increases in a certain range if the tube voltage is increased.

The higher photon flow (X ray intensity behind the object) increases the SNR in the detected image faster than the reduction of the contrast by the decreased transmission contrast (also known as specific contrast or effective attenuation coefficient, μ_{eff}). This effect depends on the ratio of attenuation decrease to SNR increase (see also Eq. (20)), since the product of SNR and μ_{eff} controls the contrast sensitivity in the digital radiograph. The effect has been observed if DDAs and a DFS are used for film replacement. Well calibrated DDAs and DFSs typically can be exposed at higher tube voltages than can films. However, too high a tube voltage may even reduce the attenuation faster than the SNR increases. The maximum achievable SNR is the limiting parameter for the described compensation. It depends on the detector efficiency and the detector calibration of DDAs or the structure noise of the imaging plates. It also depends on the noise of the material's structure and the material's roughness. Therefore, the compensation by increase of the tube voltage is restricted depending on the detector and material properties and especially on the maximum achievable SNR in the radiograph.

Figure 38(a) shows a typical example for the compensation of decreased contrast (μ_{eff}) by increased SNR. A step wedge with ASTM E 1025 IQIs (2%) was exposed at different X ray energies and mA·min with a constant source to detector distance. The visibility of the 2T hole (denoted by 2 in Fig. 38(b)) was achieved with increasing kV of the tube at shorter exposure times. This cannot be achieved with X ray films, since they will always be exposed to an optical density between 2 and 4. In this case, the films of a given class always have the same SNR in a small range owing to its specific manufacturing process. The increase of the tube voltage from 80 to 150 kV allows the reduction of exposure time down to 20% for DIR in the example shown in Fig. 38. All thickness steps of the test object can be inspected with one exposure at 150 kV. The steps with the smallest thickness are even radiographed with 2–1T quality. Here, the tube voltage increase yields a higher efficiency and an increased thickness range based on the digital ‘high CNR’ technique.

4.7.5. Compensation principle II

4.7.5.1. Compensation of insufficient detector sharpness (high unsharpness) by increased SNR

The EN 14784-2 standard requires the application of high definition CR systems for X ray inspection with pixel sizes of less than 50 μm for class B inspection (for wall thickness <12 mm and tube voltages <150 kV). Most available digital systems do not allow a resolution below 50 μm pixel size and are excluded for industrial X ray applications in Europe. The recent trials have shown that DDAs and DFSs provide better image quality and IQI visibility than do industrial X ray films. In a high contrast sensitivity mode, the DDAs achieve significantly better IQI readings than do film exposures. This effect is observed when sub-pixel contrast resolution is achieved. This is the case if the SNR at the detector is increased considerably. If a wire or crack is smaller than a pixel, it still influences the contrast and can be seen in the image if the contrast is sufficiently higher than the noise. Therefore, systems with insufficient spatial resolution can be applied if their high unsharpness is compensated for by an increased SNR.

The improved SNR of the DDA allows wire W19 (50 μm diameter) to be detected at a detector pixel size of 200 μm without a magnification technique.

It is proposed to permit the application of unsharp systems, if the visibility of the required wire or step hole IQI is increased by compensation for missing duplex wire resolution through SNR enhancement (see EN 462-5, ASTM E 2002 and the requirements of EN 14784-2). Several new standards define minimum duplex wire values for specific applications (e.g. ISO/DIS 10893-7, ISO/DIS 17636-2). Typically, one higher (smaller diameter, see EN 462-1) single wire (resulting in higher contrast sensitivity) is to be seen through adjustment of parameters that increase the SNR if an additional duplex wire of spatial resolution is required in the system qualification for a given material thickness and application. It was proposed in CEN TC 138 WG 1 that the compensation should allow a maximum 2 wires versus wire pair compensations. The compensation should be applicable to plate hole IQIs as well. This is still under discussion.

This effect has been proven with a PE XRD 1620 detector in combination with YXLON's Image.3500 software. Even at a magnification of 1 and a basic spatial resolution of 200 μm (pixel size), the significantly higher SNR of the DDA allows the detection of crack indications that are hidden by noise in the film image with its much better basic spatial resolution SR_b of 40 μm . Figure 39 shows the radiograph of a No. 13 wire IQI on an 8 mm steel plate. The radiographs were high pass filtered for better graphical presentation. The digitized film shows wire No. 16 and the DDA image shows wire No. 19 as being visible, with wire No. 19 having a diameter of 50 μm .

Therefore, the detector shows the wire 19 indication with a sub-pixel resolution. The DFS investigations also show improved wire visibility, even if the wire diameter is smaller than the basic spatial resolution of the DFS.

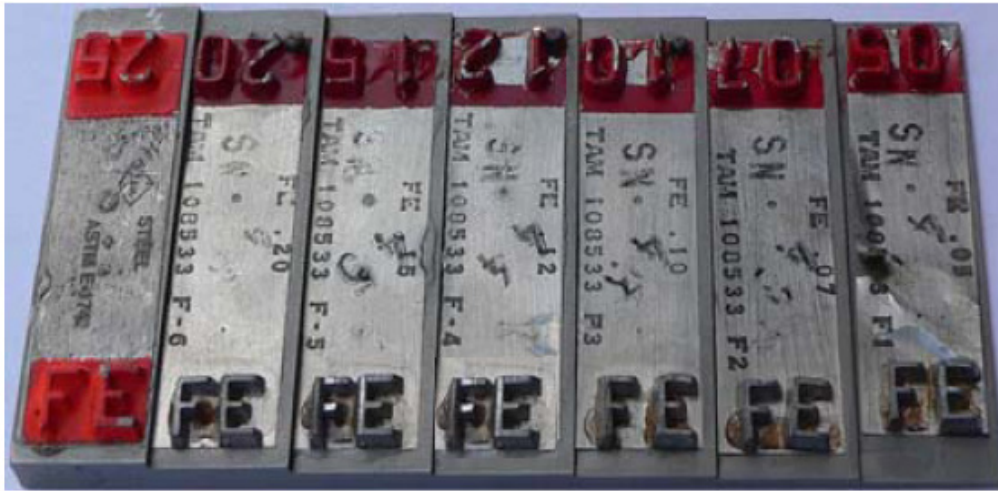


FIG. 38(a). Step wedge of steel with ASTM E 1025 IQIs for determination of image quality.

80kV	1 mA min	2 mA min	5 mA min	10 mA min	20 mA min
0,05 in	1	2	1	1	1
0,07 in	4	2	2	2	1
0,10 in	-	2	2	2	1
0,12 in	4	4	2	2	1
0,15 in	-	-	2	2	2
0,20 in	-	-	-	2	2
0,25 in	-	-	-	-	4

100kV	1 mA min	2 mA min	5 mA min	10 mA min	20 mA min
0,05 in	2	1	1	1	1
0,07 in	2	2	1	1	1
0,10 in	2	2	1	1	1
0,12 in	2	2	1	1	1
0,15 in	4	2	2	1	1
0,20 in	-	4	2	1	1
0,25 in	-	-	1	?	1

150kV	1 mA min	2 mA min	5 mA min	10 mA min	20 mA min
0,05 in	2	1	1	?	?
0,07 in	2	1	1	?	?
0,10 in	2	2	1	?	?
0,12 in	2	2	2	1	?
0,15 in	2	2	2	1	1
0,20 in	4	2	2	1	1
0,25 in	4	2	2	1	2

FIG. 38(b). Achieved IQI quality (smallest visible hole of 2% IQI; 1 — 1T hole; 2 — 2T hole; 4 — 4T hole) as a function of kV, mA·min and wall thickness in inches for test object shown in FIG. 38(a).

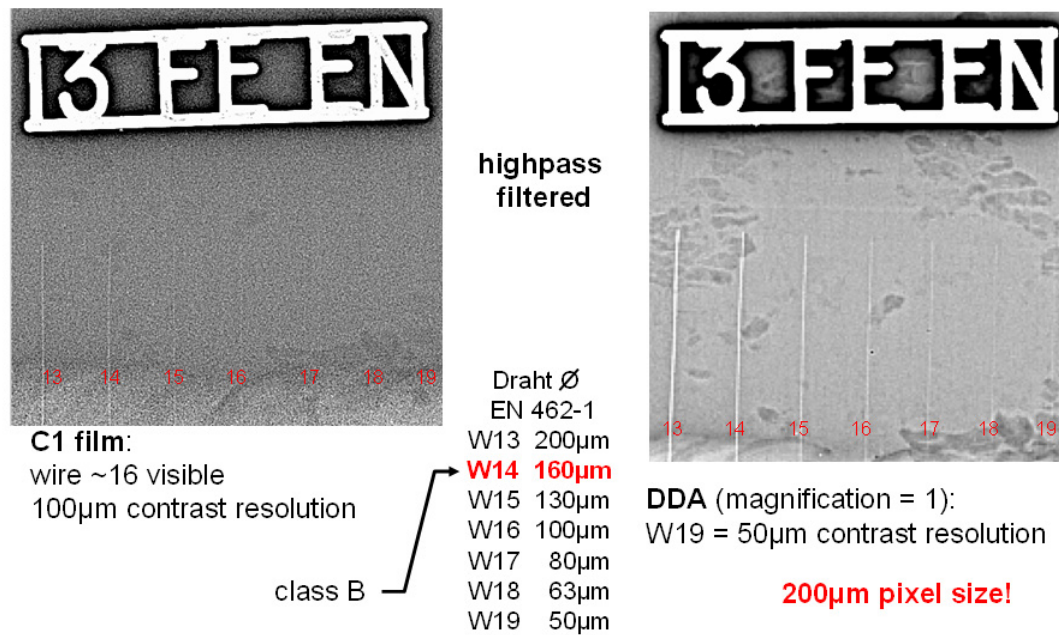


FIG. 39. Comparison of visibility of wire type IQIs according to EN 462-1 for film (left) and DDA (right) at 8 mm wall thickness (images high pass filtered for better visualization).

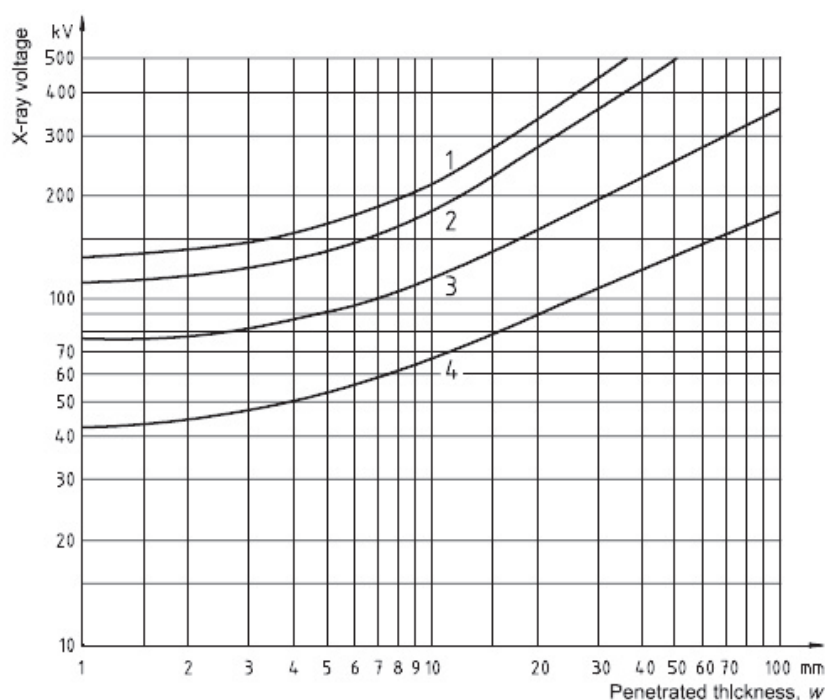
4.7.6. Application of compensation principle II

If both IQI sensitivities (contrast sensitivity by single wires (W) and spatial resolution by duplex wires (D)) indicated in Table 14 cannot be achieved by the detector system used, an increase in single wire visibility is to compensate for too high unsharpness values (i.e. if the required D 8 and W 12 are not achieved at the same time for a specific detector set-up, D 7 and W 13 provide an equivalent detection sensitivity). The compensation is to be limited to a maximum compensation of two wires and wire pairs.

For DDAs, the contrast sensitivity depends on the integration time and mA (tube current) used for acquisition of the radiographic images for a given distance and tube voltage. Thus the single wire or step hole visibility can be increased by increasing the frame integration time and/or frame number and mA setting. This also applies for CR, but with limitations associated with the maximum achievable SNR due to the structure noise of the sensitive crystalline photostimulable luminescence layer.

4.7.7. Selection of tube voltage

The tube voltage for film exposure is to be selected according to curve 2 of Fig. 40 for steel and according to curve 4 for aluminium. The voltage is not to exceed these values for the radiographic technique. For digital radiography, it is recommended to reduce the kV by 20%, especially for radiography with an image intensifier and CR. The suitable kV for the digital fluoroscope may be different and should be found by test exposures.



Key

- 1 copper/nickel and alloys
- 2 steel
- 3 titanium and alloys
- 4 aluminium and alloys

Figure 20 — Maximum X-ray voltage for X-ray devices up to 500 kV as a function of penetrated thickness and material

FIG. 40. Recommended energy for exposure according to ISO 17636-1.

4.7.8. Overall conclusion about image quality

- The image quality in digital radiography is predominantly determined by the CNR.
- Optimizing the contrast without considering the noise in digital radiography is not useful.
- The maximum permitted X ray voltage for film radiography (EN 444, EN 1435, ISO 5579, ISO 17636) can be exceeded in digital radiography. The increase of X ray tube voltage above the limit of EN 444 improves the image quality of digital radiographs, taken with very well calibrated DDAs and a DFS, above the quality level of the best NDT films because of the increase of SNR (compensation principle I).
- The image unsharpness limits the perception of small and linear structures only partially and can be compensated for by increased SNR (compensation principle II). Wires can also be seen in digital radiography at a high SNR, if the basic spatial resolution of the detector or the geometrical unsharpness is greater than the wire diameter.

5. RADIATION PROTECTION IMPLICATIONS OF INDUSTRIAL RADIOGRAPHY

Industrial radiography is routinely used for the detection of defects in welds in engineering structures and components. It is one of the major non-destructive methods for imaging defects in material structures using X ray or gamma ray emitting radionuclides such as ^{192}Ir and ^{60}Co . Exposure of any part of the human body to X rays or gamma rays may be harmful, and this necessitates appropriate regulatory controls over the use of ionizing radiation for industrial radiography.

General requirements for protection and safety are given in the Radiation Protection and Safety of Radiation Sources: International Basic Safety Standards (BSS) [1], with more specific guidance in the IAEA Safety Guide on Radiation Safety in Industrial Radiography [2].

The low cost DIR system described in this report reduces the typical exposures needed to produce an acceptable radiographic image to about 10–50% of that needed for film based industrial radiography. This should result in lower occupational doses per image, all other factors being the same. Whether this translates into lower occupational doses overall (such as per year) will depend, for example, on whether the lower exposures needed to produce an image lead to an increase in the number of images being taken per day. In any case, the requirements given in the BSS [1] and elaborated in the Safety Guide [2] are still applicable.

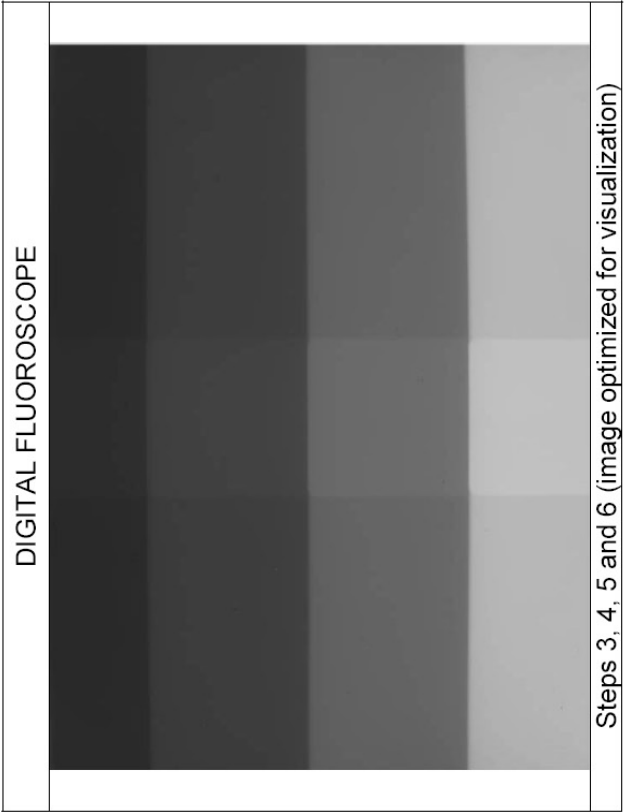
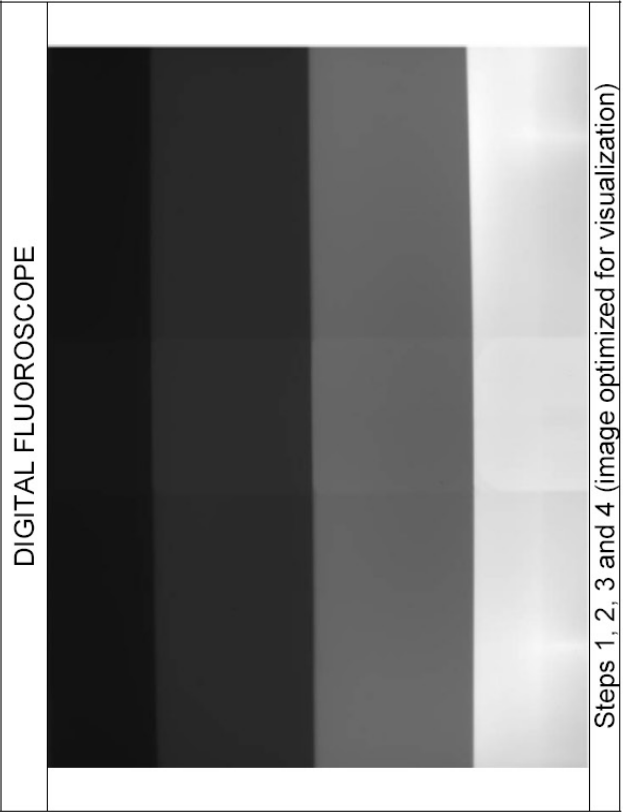
The radiation protection regulatory body in a Member State where the use of DIR is being proposed will need to ensure that the DIR system and its use will meet all the radiation protection requirements of the Member State.

6. CATALOGUE OF IMAGES

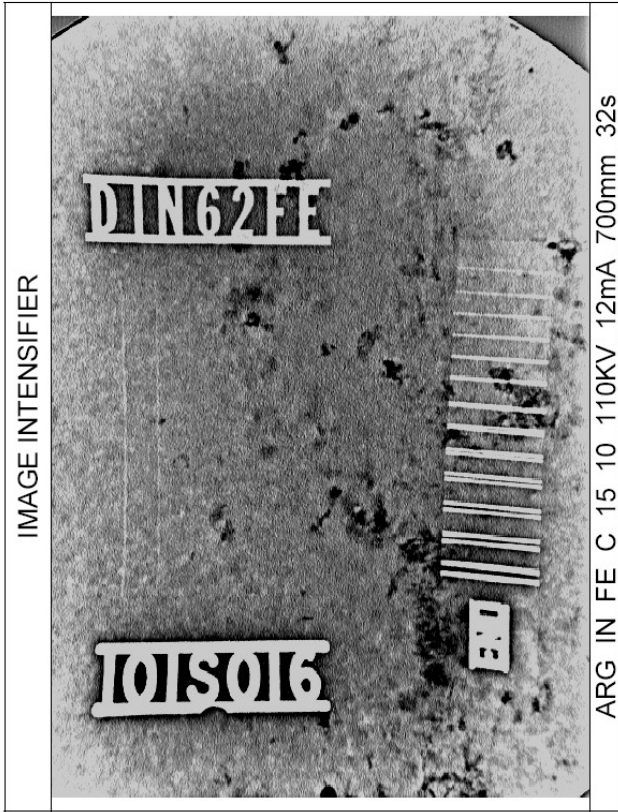
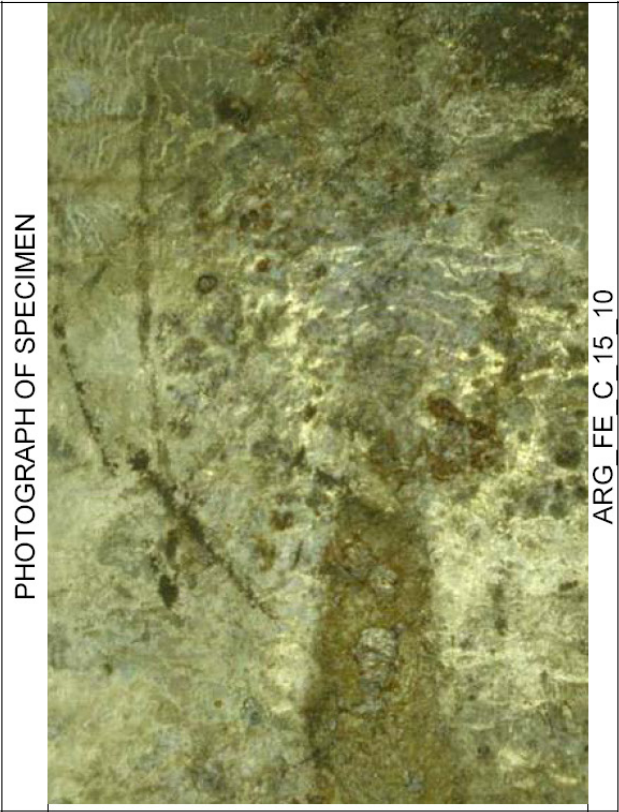
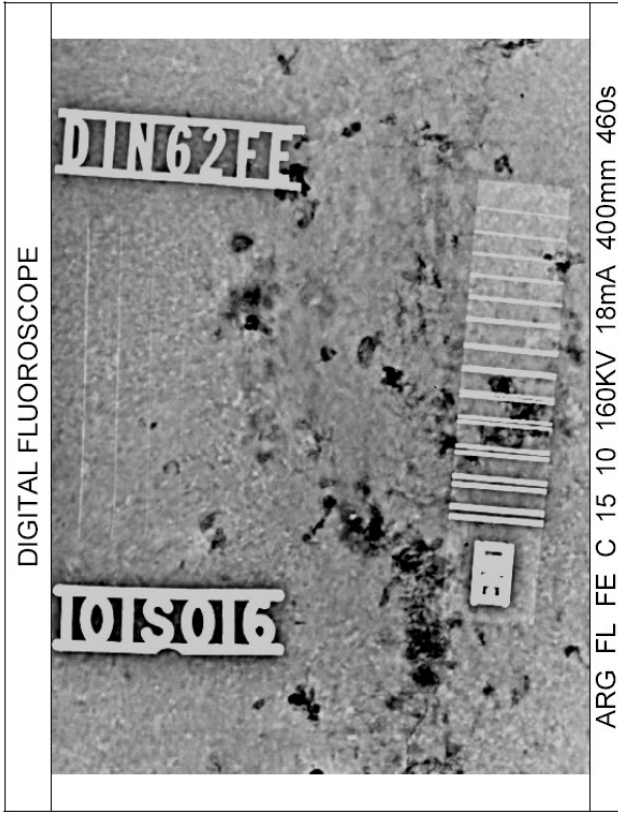
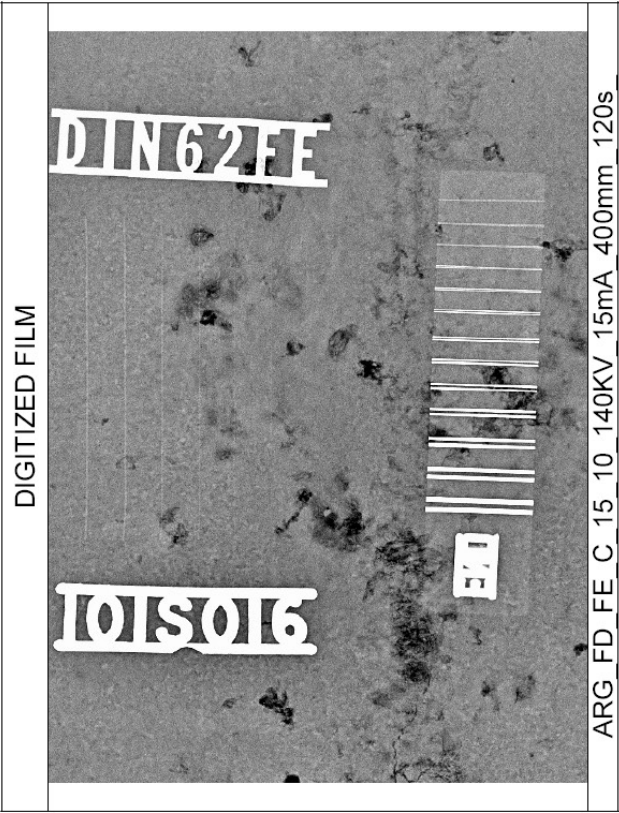
Catalogues were prepared during the CRP to allow a comparison of the image quality obtainable from the DFSs with that of images from digitized films and from CR systems using imaging plates and image intensifiers. Each catalogue comprises four images: one image obtained from a photograph of the test specimen, one from its fluoroscopic image, one image using digitized films, and one image from image intensifiers and CR systems. The images were identified according to the details set out in Section 3.3.4.

Many test specimens were fabricated by the participants. These include welding and casting samples of steel and aluminium with real flaws. Some examples of the collected catalogue images are provided in this section.

Catalogue Test Sample STAINLESS STEEL STEP WEDGE		
Specimen: Reference block	Welding Process: —	Joint Preparation: —
Material: Stainless Steel	Nominal Thickness: 1.2 to 12.5 mm	Source: X - Ray

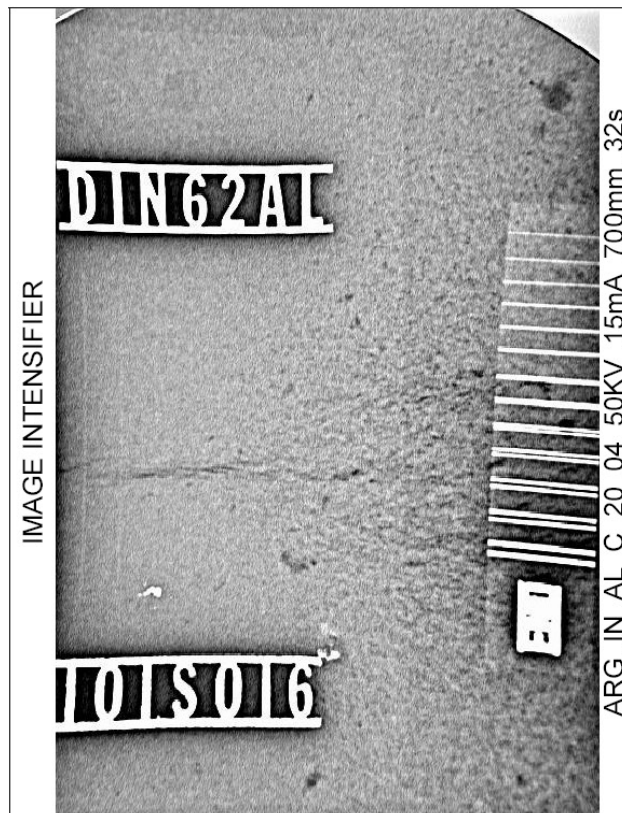
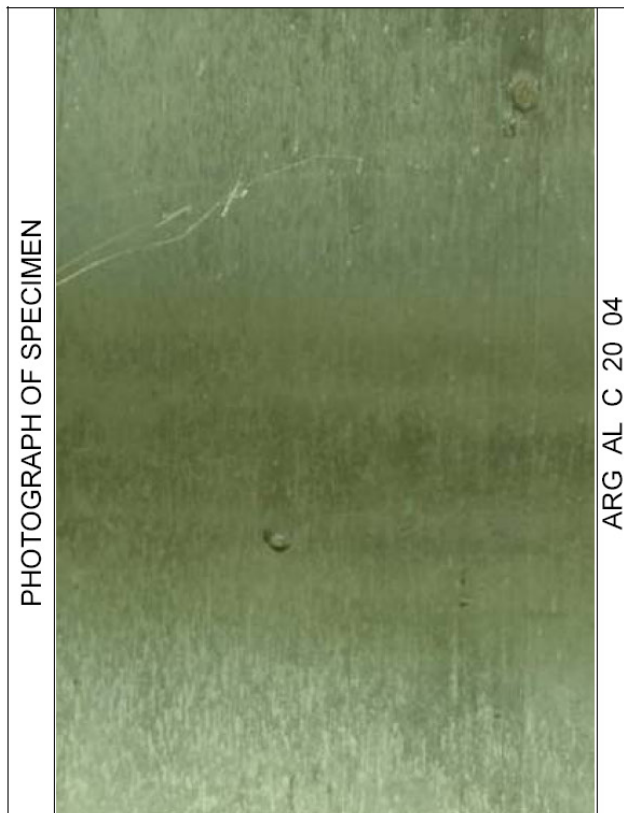
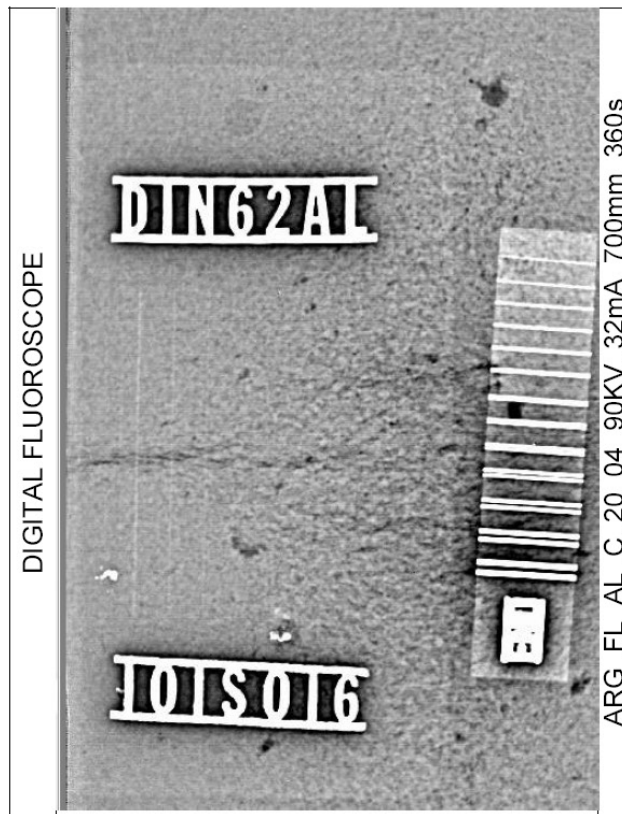
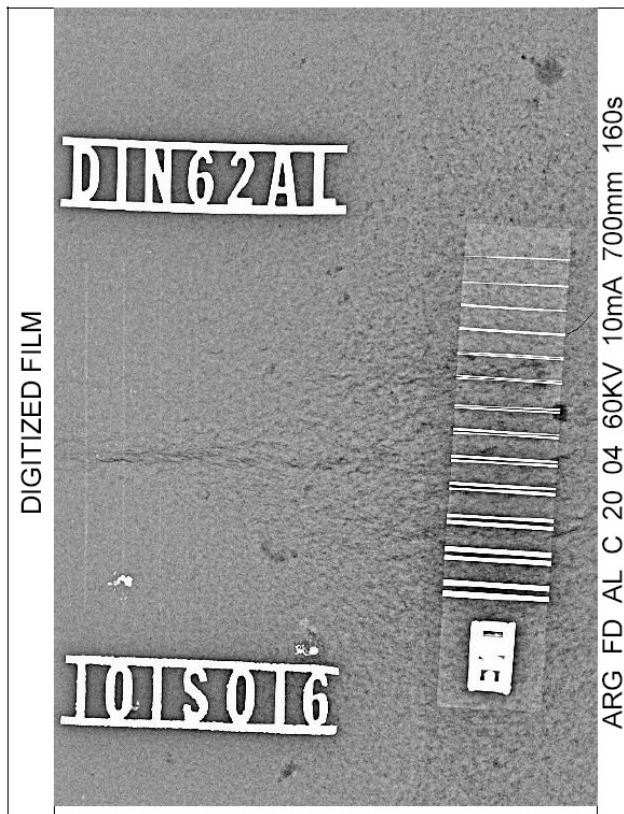


Catalogue Test Sample IAEA - 001		
Specimen: Casting	Welding Process: —	Joint Preparation: —
Material: Carbon Steel	Nominal Thickness: 15 mm	Source: X - Ray



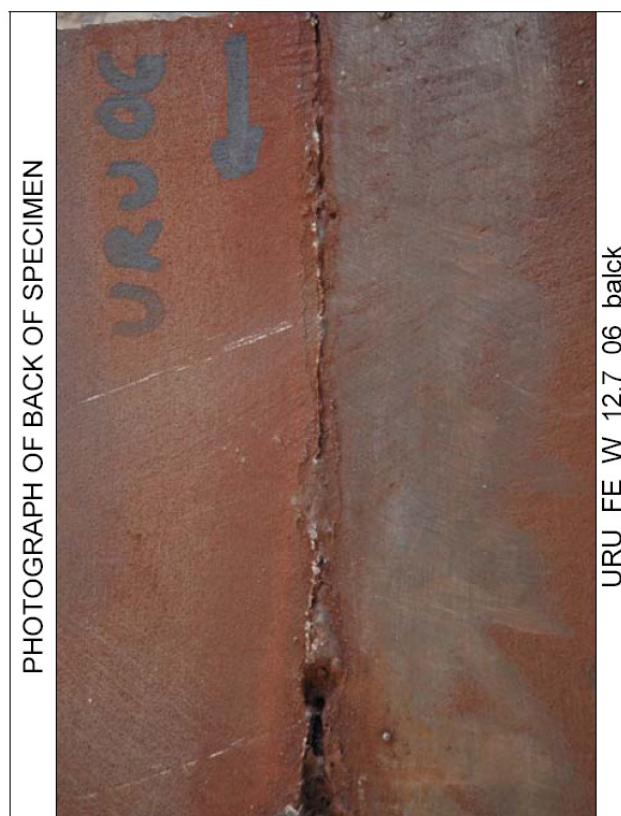
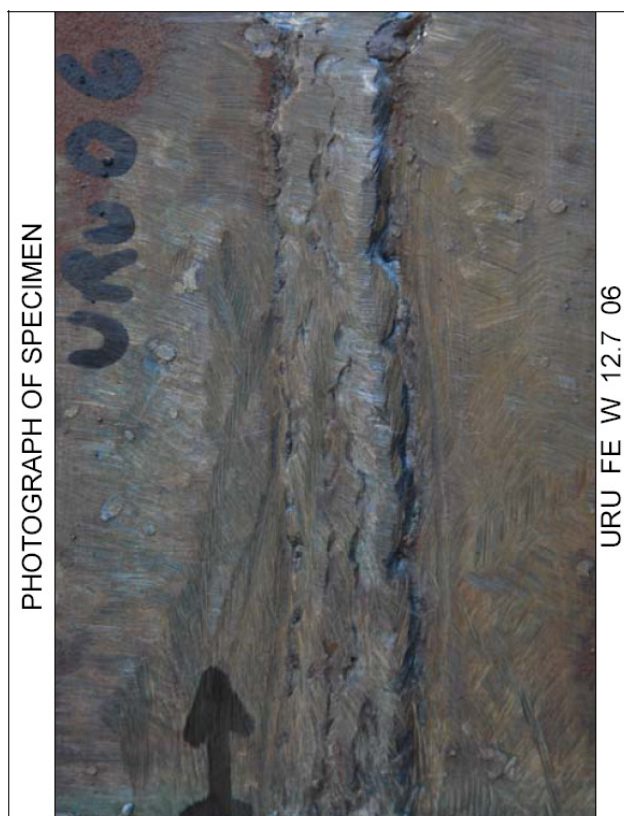
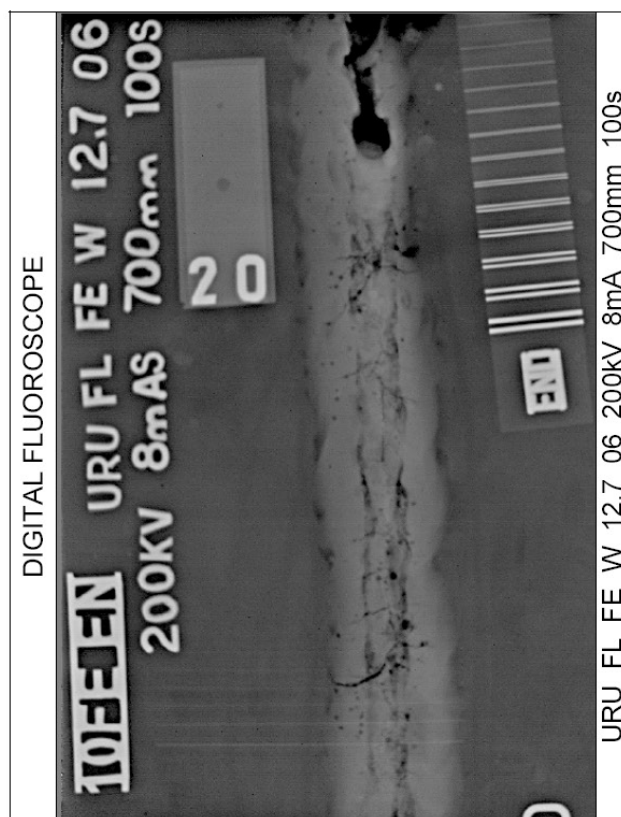
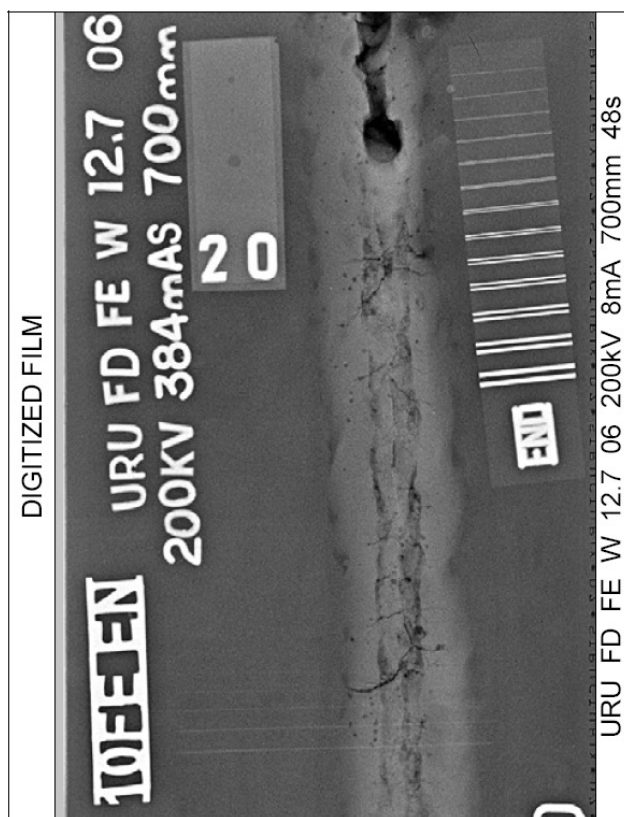
Discontinuities: Porosity category A, shrinkage (sponge), cracks

Catalogue Test Sample IAEA - 002		
Specimen: Casting	Welding Process: —	Joint Preparation: —
Material: Aluminum	Nominal Thickness: 20mm	Source: X - Ray



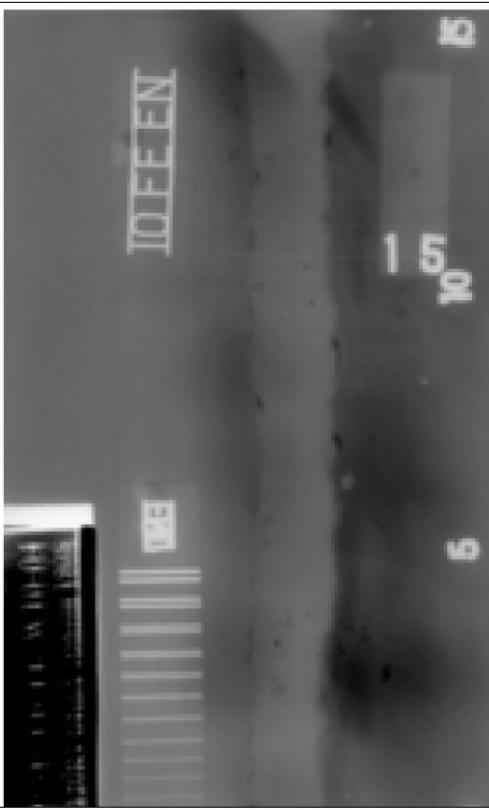
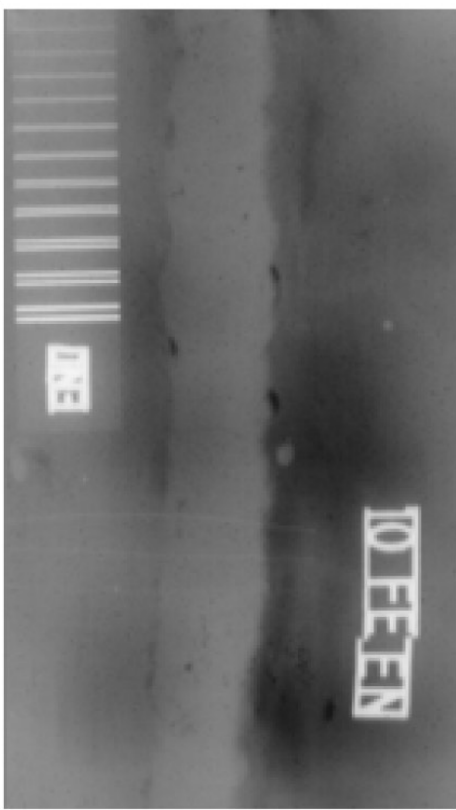
Discontinuities: Foreign Material, shrinkage (sponge)

Catalogue Test Sample IAEA - 003		
Specimen: Weld	Welding Process: GTAW	Joint Preparation: Single V
Material: Carbon Steel	Nominal Thickness: 12.7 mm	Source: X - Ray



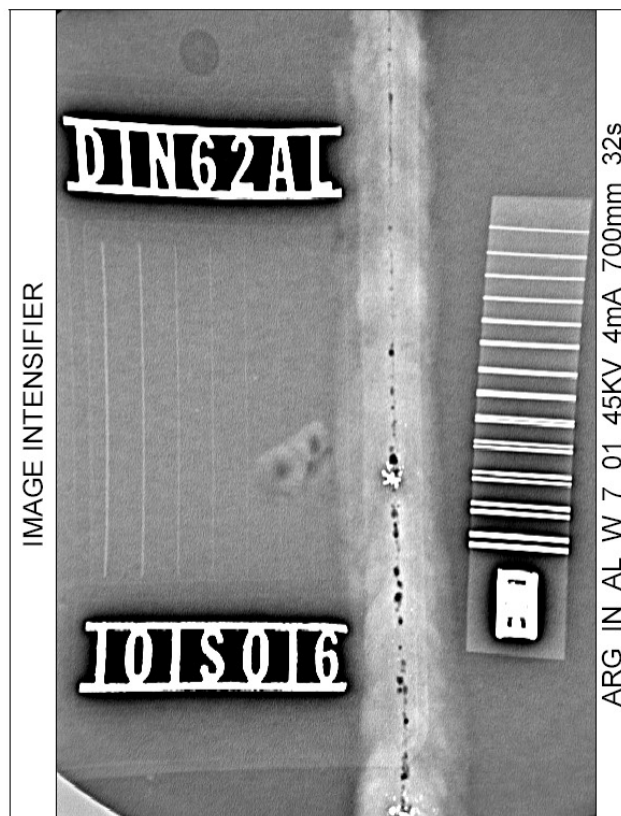
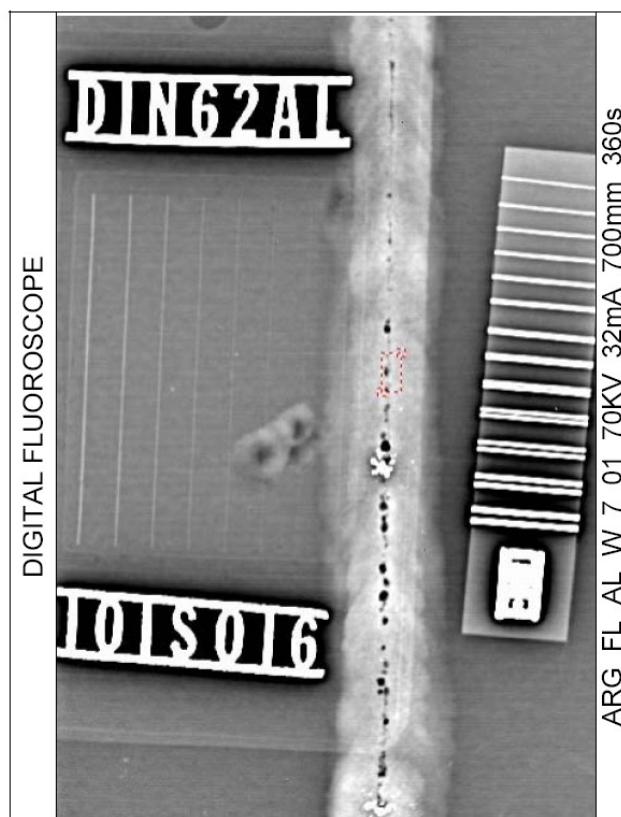
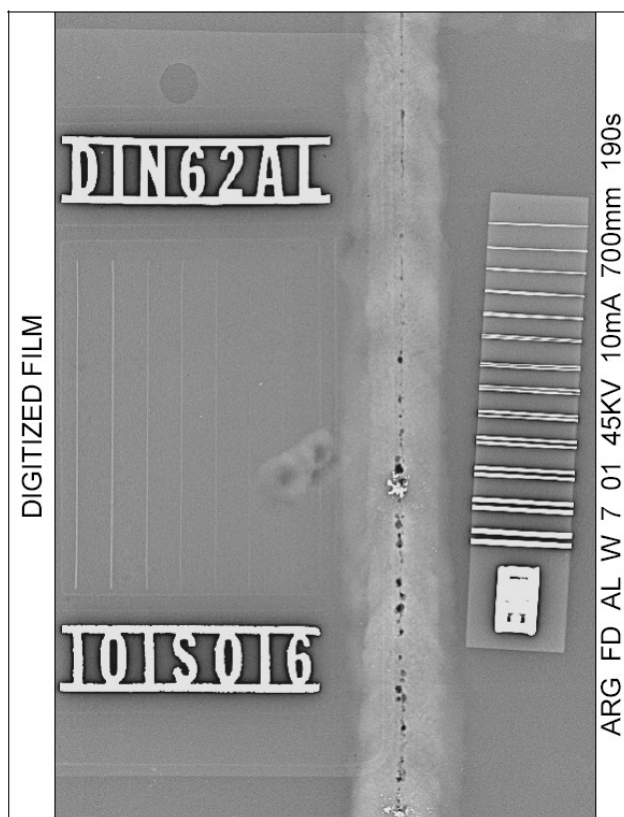
Discontinuities: Cracks, lack of penetration, porosity, lack of material, undercut

Catalogue Test Sample IAEA - 004		
Specimen: Weld	Welding Process: SMAW	Joint Preparation: Single V
Material: Carbon Steel	Nominal Thickness: 10 mm	Source: X - Ray

DIGITIZED FILM	
	
PAK-FR-FE-W10-03 140Kv 4mA 70Cm	
DIGITAL FLUOROSCOPE	
	
PAK-FL-FE-W10-03 140kV 4mA 50 2600	

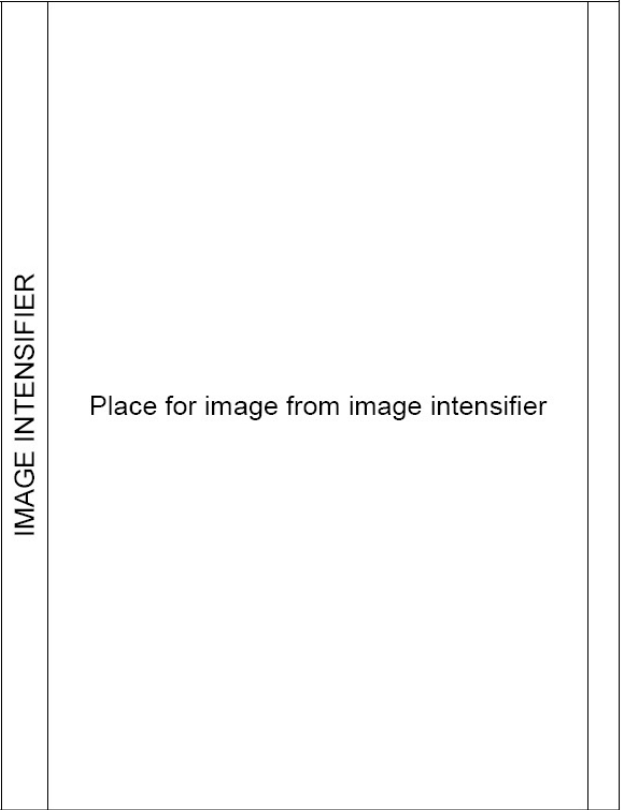
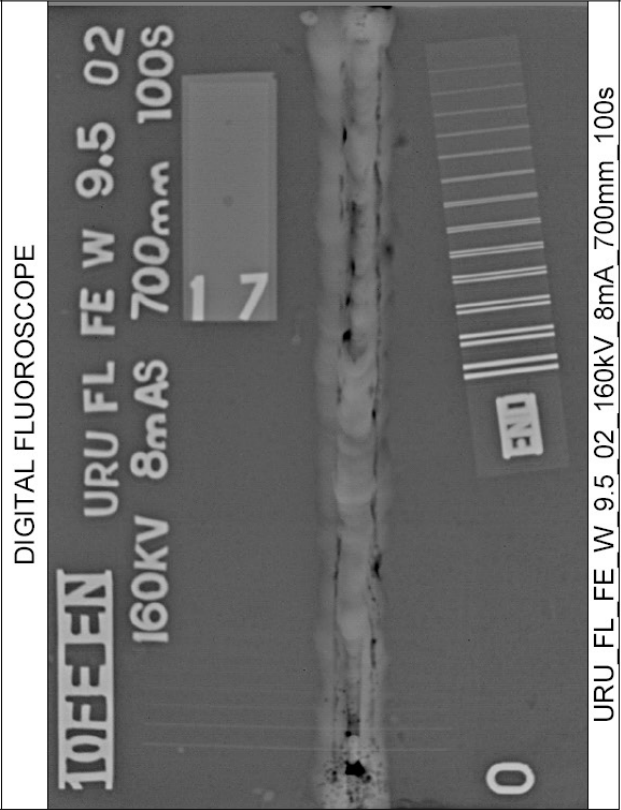
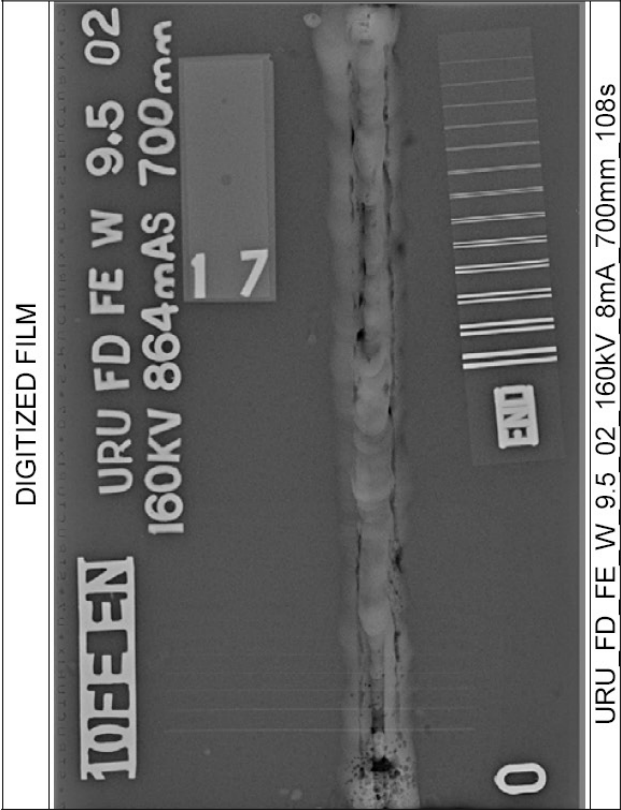
PHOTOGRAPH OF SPECIMEN	
	
PAK-FE-W-10-03	
PHOTOGRAPH OF BACK OF SPECIMEN	
	
PAK-II-FE-W10-03 111kV 4mA 100 Cm	

Catalogue Test Sample IAEA - 005		
Specimen: Weld	Welding Process: GTAW	Joint Preparation: Square
Material: Aluminium	Nominal Thickness: 7 mm	Source: X - Ray



Discontinuities: Vermicular pores, longitudinal crack, heavy metal inclusions

Catalogue Test Sample IAEA - 006		
Specimen: Weld	Welding Process: SMAW	Joint Preparation: Single V
Material: Carbon Steel	Nominal Thickness: 9.5 mm	Source: X - Ray



Discontinuities: Lack of penetration, undercut, porosity

7. SUMMARY

- (1) A low cost DFS for DIR can be built within the planned cost of €5000, and a step by step procedure is given in this publication.
- (2) The DFS provides image quality comparable with that of other commercial industrial systems for DIR. The achievable contrast sensitivity is better than or equal to that provided by computed radiography and digitized films in a certain material thickness range, but is less than that provided by modern DDAs.
- (3) The attractive features of this system include: the reduction of radiation dosage and inspection time; protection of the environment resulting from the elimination of chemical processing; long term storage of digital data without degradation; digital data analysis; quantitative defect detection and evaluation; and easy digital data transmission.
- (4) Because of the compact design of the DFS, it is suitable for mobile inspection of welds and castings.
- (5) The concept of a low cost DIR system has the potential for use in providing training in DIR technology. The IAEA may wish to consider supporting such training centres in developing countries.

REFERENCES

- [1] INTERNATIONAL ATOMIC ENERGY AGENCY, Radiation Protection and Safety of Radiation Sources: International Basic Safety Standards (Interim Edition), IAEA Safety Standards Series No. GSR Part 3 (Interim), IAEA, Vienna (2011).
- [2] INTERNATIONAL ATOMIC ENERGY AGENCY, Radiation Safety in Industrial Radiography, IAEA Safety Standards Series No. SSG-11, IAEA, Vienna (2011).

BIBLIOGRAPHY

ASTM INTERNATIONAL, E155-10 Standard Reference Radiographs for Inspection of Aluminum and Magnesium Castings, Book of Standards Volume 03.03, ASTM International (2012).

ASTM INTERNATIONAL, E747-04(2010) Standard Practice for Design, Manufacture and Material Grouping Classification of Wire Image Quality Indicators (IQI) Used for Radiology, Book of Standards Volume 03.03, ASTM International (2012).

ASTM INTERNATIONAL, E1025-11 Standard Practice for Design, Manufacture, and Material Grouping Classification of Hole-Type Image Quality Indicators (IQI) Used for Radiology, Book of Standards Volume 03.03, ASTM International (2012).

ASTM INTERNATIONAL, E1441 Standard Guide for Computed Tomography (CT) Imaging, Book of Standards Volume 03.03, ASTM International (2012).

ASTM INTERNATIONAL, E 1570-11 Standard Practice for Computed Tomographic (CT) Examination, Book of Standards Volume 03.03, ASTM International (2012).

ASTM INTERNATIONAL, E1742/E1742M-12 Standard Practice for Radiographic Examination, Book of Standards Volume 03.03, ASTM International (2012).

ASTM INTERNATIONAL, E2002-98(2009) Standard Practice for Determining Total Image Unsharpness in Radiology, Book of Standards Volume 03.03, ASTM International (2012).

ASTM INTERNATIONAL, E2007-00 Standard guide for computed radiology (Photostimulable Luminescence (PSL) Method), Book of Standards Volume 03.03, ASTM International (2012).

ASTM INTERNATIONAL, E2033-99 Standard practice for computed radiology, Book of Standards Volume 03.03 ASTM International (2012).

ASTM INTERNATIONAL, E2422-11 Standard Digital Reference Images for Inspection of Aluminum Castings, Book of Standards Volume 03.03, ASTM International (2012).

ASTM INTERNATIONAL, E2445 and E2446, Qualification for computed radiology, Book of Standards Volume 03.03, ASTM International (2012).

ASTM INTERNATIONAL, E2445-05(2010) Standard Practice for Qualification and Long-Term Stability of Computed Radiology Systems, Book of Standards Volume 03.03, ASTM International (2012).

ASTM INTERNATIONAL, E2446-05(2010) Standard Practice for Classification of Computed Radiology Systems, Book of Standards Volume 03.03, ASTM International (2012).

ASTM INTERNATIONAL, E2597-07e1 Standard Practice for Manufacturing Characterization of Digital Detector Arrays, Book of Standards Volume 03.03, ASTM International (2012).

ASTM INTERNATIONAL, E2698-10 Standard Practice for Radiological Examination Using Digital Detector Arrays, Book of Standards Volume 03.03, ASTM International (2012).

ASTM INTERNATIONAL, E2736-10 Standard Guide for Digital Detector Array Radiology, Book of Standards Volume 03.03, ASTM International (2012).

ASTM INTERNATIONAL, E2737-10 Standard Practice for Digital Detector Array Performance Evaluation and Long-Term Stability, Book of Standards Volume 03.03, ASTM International (2012).

BAVENDIEK, K., et al., “New Digital Radiography Procedure Exceeds Film Sensitivity Considerably in Aerospace Applications”, 9th ECNDT, European Federation of Non-Destructive Testing, Berlin (2006).

BUENO, C., MATULA, A.D., “Digital Radiography for Gas Turbine Components”, Proceedings from ASM Gas Turbine Materials Conference, 1998, Rosemont, ASM International, Materials Park, OH (1994) 119–122.

CASAGRANDE, J.M., KOCH, A., MUNIER, B., DE GROOT, P., “High Resolution Digital Flat-Panel X ray Detector — Performance and NDT Application”, 15th World Conference on Nondestructive Testing, Rome (2000), <http://www.ndt.net/article/wcndt00/papers/idn615/idn615.htm>

COMPANY COMECH, Non Destructive Testing of Alumino-Thermic Rail Welds, Seminar on Radiographic testing and radiation protection, Dortmund (2002).

DOROBANTU, V., Double wall technique pipelines inspection using gamma rays, NDT.net, March 2005, **10** 3 (2005).
EU project “Film Free”, <http://www.filmfree.eu.com>, 200–2009.

EUROPEAN COMMITTEE FOR STANDARDIZATION, CEN EN 14874, NDT industrial computed radiography with storage phosphor imaging plates, CEN.

EUROPEAN COMMITTEE FOR STANDARDIZATION, EN 444:1994, Non-destructive testing — General principles for radiographic examination of metallic materials by X- and gamma-rays, CEN (2004).

EUROPEAN COMMITTEE FOR STANDARDIZATION, EN 462-1:1994, Non-destructive testing — Image quality of radiographs; Part 1: Image quality indicators (wire type) — Determination of image quality value, CEN (1994).

EUROPEAN COMMITTEE FOR STANDARDIZATION, EN 462-2:1994, Non-destructive testing — Image quality of radiographs; Part 2: Image quality indicators (step/hole type) — Determination of image quality value, CEN (1994).

EUROPEAN COMMITTEE FOR STANDARDIZATION, EN 462-5:1996, Non-destructive testing — Image quality of radiographs; Part 5: Image quality indicators (duplex wire type), determination of image unsharpness value, CEN (1996).

EUROPEAN COMMITTEE FOR STANDARDIZATION, EN 462-3:1997, Non-destructive testing — Image quality of radiographs; Part 3: Image quality classes for ferrous metals, CEN (1997).

EUROPEAN COMMITTEE FOR STANDARDIZATION, EN 1435:1997, Non-destructive examination of welds. Radiographic examination of welded joints, CEN (1997).

EUROPEAN COMMITTEE FOR STANDARDIZATION, EN 13068-3:2001, Non-destructive testing — Radioscopic testing; Part 3: General principles of radioscopic testing of metallic materials by X- and gamma rays, CEN (2001).

EUROPEAN COMMITTEE FOR STANDARDIZATION, EN 14784-1:2005, Non-destructive testing — Industrial computed radiography with storage phosphor imaging plates; Part 1: Classification of systems, CEN (2005).

EUROPEAN COMMITTEE FOR STANDARDIZATION, EN 14784-2:2005, Non-destructive testing — Industrial computed radiography with storage phosphor imaging plates; Part 2: General principles for testing of metallic materials using X-rays and gamma rays, CEN (2005).

EUROPEAN COMMITTEE FOR STANDARDIZATION, EN 16016-1:2011, Non destructive testing — Radiation methods — Computed tomography; Part 1: Terminology, CEN (2011).

EUROPEAN COMMITTEE FOR STANDARDIZATION, EN 16016-2:2011, Non destructive testing — Radiation methods — Computed tomography; Part 2: Principle, equipment and samples, CEN (2011).

EUROPEAN COMMITTEE FOR STANDARDIZATION, EN 16016-3:2011, Non destructive testing — Radiation methods — Computed Tomography; Part 3: Operation and interpretation, CEN (2011).

EUROPEAN COMMITTEE FOR STANDARDIZATION, EN 16016-4:2011, Non destructive testing — Radiation methods — Computed tomography; Part 4: Qualification, CEN (2011).

EWERT, U., et al., Digital Laminography, *Materialforschung* **37** 6 (1995) 218–222.

EWERT, U., et al., New compensation principles for enhanced image quality in industrial radiology with digital detector arrays, *Materials Evaluation* **68** (2010) 163–168.

EWERT, U., et al., “Optimization of Digital Industrial Radiography (DIR) Techniques for Specific Applications: An IAEA Coordinated Research Project”, IV Conferencia Panamericana de END, Buenos Aires, October 2007, Argentinian Society of NDT (2007), <http://www.ndt.net/article/panndt2007/papers/151.pdf>

EWERT, U., et al., “Strategies for film replacement in radiography — Film and digital detectors in comparison”, 17th World Conference on Nondestructive Testing, Shanghai, China, 2008, International Committee of NDT (2008).

EWERT, U., STADE, J., ZSCHERPEL, U., KALING, M., Lumineszenz-Speicherfolien für die Radiographie, *Materialprüfung* **37** (1995) 474–478.

EWERT, U., ZSCHERPEL, U., Proceedings of the NAARRI International Conference on Applications of Radioisotopes and Radiation Technology in the 21st Century (2001) 1–17.

FLISCH, A., et al., “Industrial Computed Tomography in Reverse Engineering Applications”, Proc. Int. Symp. on Computerized Tomography for Industrial Applications and Image Processing in Radiology, Berlin, 1999 (BB67-CD), Deutsche Gesellschaft für Zerstörungsfreie Prüfung e.V (DGZFP), (1999) 45–53.

GOEBBELS, J., et al., “Functionally Graded Porosity in Ceramics — Analysis with High Resolution Computed Tomography”, Proc. 103rd Annual Meeting of the American Ceramic Society, April 2001, Indianapolis, Indiana, J. Ceramic Transactions **129** (2002) 103–124.

GONZALEZ, R.C., WOODS, R.E., Digital Image Processing, 2nd edn, Prentice Hall, New Jersey (2002).

HAMMAR, L., WIRDELIUS, H., “Radiographic sensitivity improved by optimized high resolution X- ray detector design”, Int. Symp. on Digital Industrial Radiology and Computed Tomography, Lyon, France (2007).

HANKE, R., et al., “Automated high speed volume computed tomography for inline quality control”, 16th World Conference on Nondestructive Testing, International Committee and Canadian Society of NDT, Montreal, Canada (2004).

HARARA, W., “Digital radiography in industry”, 17th World Conference on Nondestructive Testing, Shanghai, China (2008).

HARBICH, K.W., HENTSCHEL, M.P., SCHORS, J., X ray refraction characterisation of non-metallic materials, *NDT&E International* **34** (2001) 297–302.

HEIDT, H., GOEBBELS, J., REIMERS, P., KETTSCHAU, A., “Development and application of a universal CAT scanner”, Proc. 11th World Conference on NDT, Las Vegas (1985) 664–671.

HENTSCHEL, M.P., et al., “New development in X-Ray Topography of advanced non-metallic materials”, 15th World Conference on Nondestructive Testing, Rome (2000)
<http://www.ndt.net/article/wcndt00/papers/idn258/idn258.htm>

HOUNSFIELD, G.N., A Method and Apparatus for Examination of a Body by Radiation such as X or Gamma Radiation, Patent Specification 1283915, The Patent Office, London (1972).

INSIGHT, Special Edition on Rail Inspection 44 6 (2002).

INTERNATIONAL ORGANIZATION FOR STANDARDIZATION, ISO 5579:1998, Non-destructive testing — Radiographic examination of metallic materials by X- and gamma rays — Basic rules, ISO (1998).

INTERNATIONAL ORGANIZATION FOR STANDARDIZATION, ISO 15708-1:2002, Non-destructive testing — Radiation methods — Computed tomography — Part 1: Principles, ISO (2002).

INTERNATIONAL ORGANIZATION FOR STANDARDIZATION, ISO 15708-2:2002, Non-destructive testing — Radiation methods — Computed tomography — Part 2: Examination practices, ISO (2002).

INTERNATIONAL ORGANIZATION FOR STANDARDIZATION, ISO 19232-1:2004, Non-destructive testing — Image quality of radiographs — Part 1: Image quality indicators (wire type) — Determination of image quality value, ISO (2004).

INTERNATIONAL ORGANIZATION FOR STANDARDIZATION, ISO 19232-2:2004, Non-destructive testing — Image quality of radiographs — Part 2: Image quality indicators (step/hole type) — Determination of image quality value, ISO (2004).

INTERNATIONAL ORGANIZATION FOR STANDARDIZATION, ISO 19232-5:2004, Non-destructive testing — Image quality of radiographs — Part 5: Image quality indicators (duplex wire type) — Determination of image unsharpness value, ISO (2004).

INTERNATIONAL ORGANIZATION FOR STANDARDIZATION, ISO 10893-1:2011, Non-destructive testing of steel tubes — Part 1: Automated electromagnetic testing of seamless and welded (except submerged arc-welded) steel tubes for the verification of hydraulic leaktightness, ISO (2011).

INTERNATIONAL ORGANIZATION FOR STANDARDIZATION, EN ISO 10893-12:2011, Non-destructive testing of steel tubes — Automated full peripheral ultrasonic thickness testing of seamless and welded (except submerged arc-welded) steel tubes, ISO (2012).

INTERNATIONAL ORGANIZATION FOR STANDARDIZATION, ISO 11699-2:2012, Non-destructive testing — Industrial radiographic films - Part 2: Control of film processing by means of reference values (ISO 11699-2:1998); German version EN ISO 11699-2:2011 (Foreign Standard)

INTERNATIONAL ORGANIZATION FOR STANDARDIZATION, EN ISO 17636-1:2013, Non-destructive testing of welds — Radiographic testing — X- and gamma-ray techniques with film, ISO (2013).

INTERNATIONAL ORGANIZATION FOR STANDARDIZATION, EN ISO 17636-2:2013, Non-destructive testing of welds — Radiographic testing — X- and gamma-ray techniques with digital detectors, ISO (2013).

KAK, A.C., SLANEY, M., Principles of Computerized Tomographic Imaging, IEEE Press, New York (1988).

KONONV, N.K., et al., A digital system for production X ray images with a high spatial resolution, Instruments and Experimental Techniques **45** 5 (2006).

LINDLEY, C.A., Practical Image Processing in C: Acquisition, Manipulation, Storage, J. Wiley & Sons, New York (1991).

MEADE, B., KIDWELL, C., WARREN, G., Reliability and cost study of digital radiography, film and radioscopy, ASNT Digital Imaging Topical **6** (2003).

OIS ENGINEERING, “Freshex: A combined System for Ultrasonic and X ray Inspection of welds”, 15th World Conference on Nondestructive Testing, Rome (2000), <http://www.ndt.net/article/wcndt00/papers/idn286/idn286.htm>

PATEL, R.J., “Digital application of radiography”, 3rd Middle East Non-Destructive Testing Conference & Exhibition, Bahrain, Manama, 2005, Saudi Arabian Section of the American Society for Nondestructive Testing (SAS-ASNT) and Bahrain Society of Engineers (BSE) (2005).

REDMER, B., EWERT, U., ONEL, Y., BARANOV, V., “Untersuchungen zur Optimierung der Aufnahmeanordnung für die Tomosynthese und strukturabhängige Vorfilterung”, Jahreskonferenz der Deutsche Gesellschaft für Zerstörungsfreie Prüfung e.V (DGZFP), Berichtsband (1996) 637–647.

REDMER, B., et al., “Sensitive Detection of planar Defects by a Mechanised Radiometric Weld Inspection System”, 15th World Conference on Nondestructive Testing, Rome (2000), <http://www.ndt.net/article/wcndt00/papers/idn370/idn370.htm>

REIMERS, P., KETTSCHAU, A., GOEBBELS, J., Region-of-interest (ROI) mode in industrial X ray computed tomography, NDT International 23 (1990) 255–261.

RIESEMEIER, H., GOEBBELS, J., ILLERHAUS, B., “Development and application of cone beam tomography for materials research”, Proc. Int. Symp. Computerized Tomography for Industrial Applications, Berlin, 1994, Deutsche Gesellschaft für Zerstörungsfreie Prüfung e.V (DGZFP) (1994) 44:112–119.

SOLTANI, P.K., WYSNEWSKI, D., SWARTZ, K., “Amorphous Selenium Direct Radiography for Industrial Imaging”, DGZfP Symposium, Berlin (1999) CD-ROM.

VENGRINOVICH, V.L., DENKEVICH, Y.B., TILLACK, G.-R., NOCKEMANN, C., “Multistep 3D X ray Tomography for a Limited Number of Projections and Views”, Rev. Prog. in QNDE (THOMPSON, D.O., CHIMENTI, D.E., Eds), Vol. 16, Plenum Press, New York (1997) 317–323.

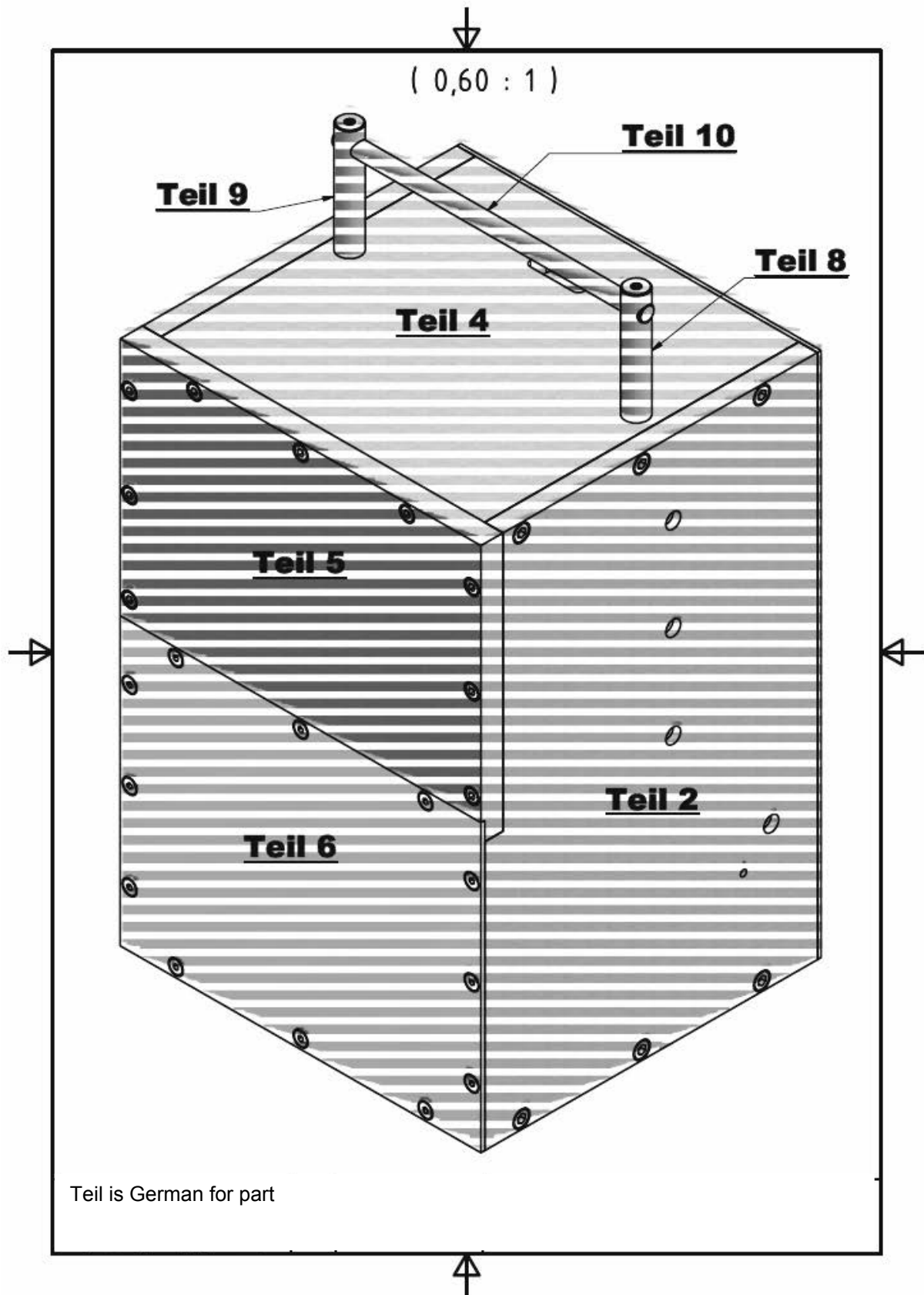
ZSCHERPEL, U., et al., “Comparative analysis of radiological detector systems”, 8th ECNDT, Barcelona, 2002, Vol. 1, No. 12, NDT.net (2002).

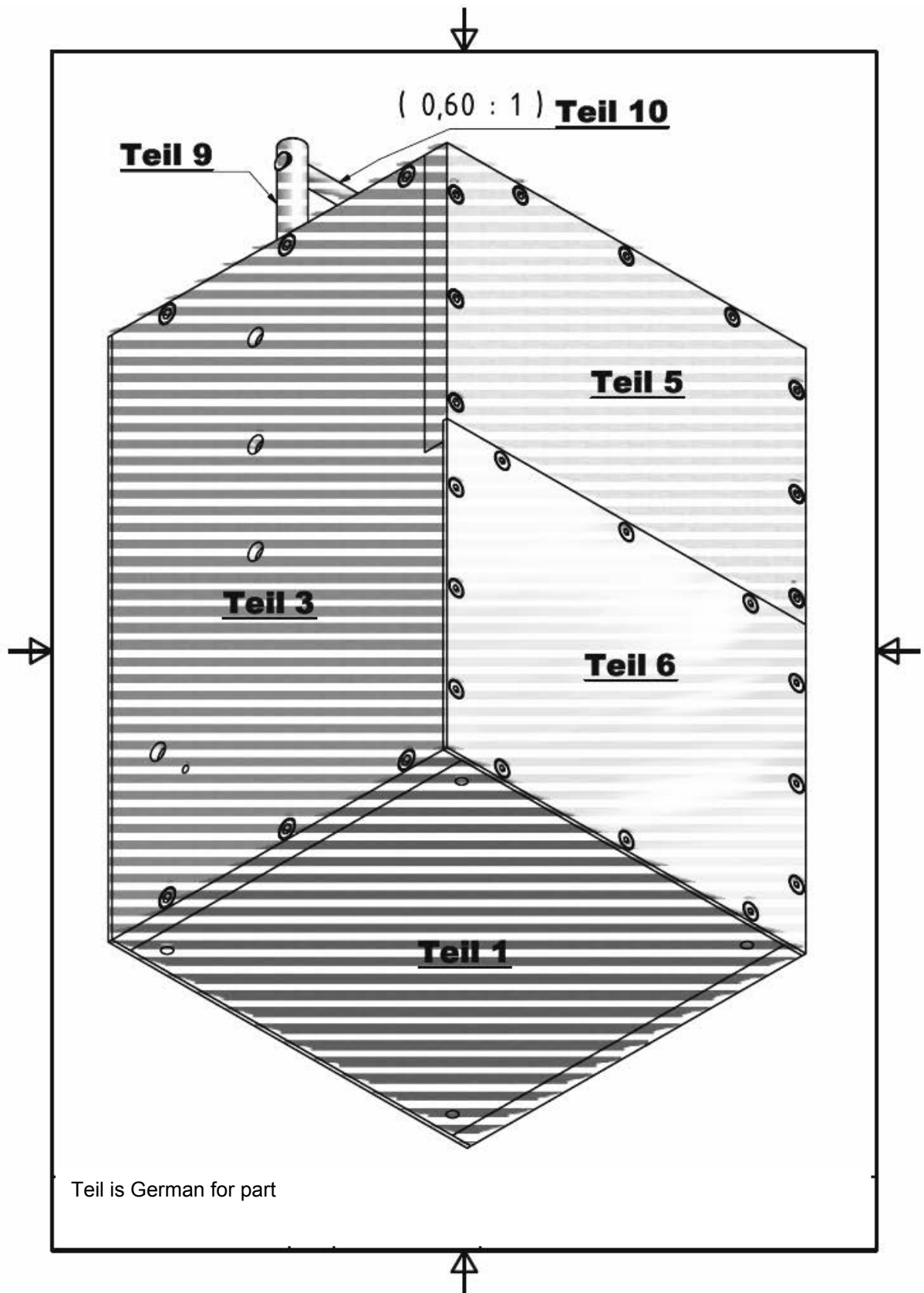
ZSCHERPEL, U., et al., “Possibilities and limits of digital industrial radiology — The new high contrast sensitivity technique — Examples and system theoretical analysis”, Int. Symp. Digital Industrial Radiology and Computed Tomography, Lyon, France, (2007).

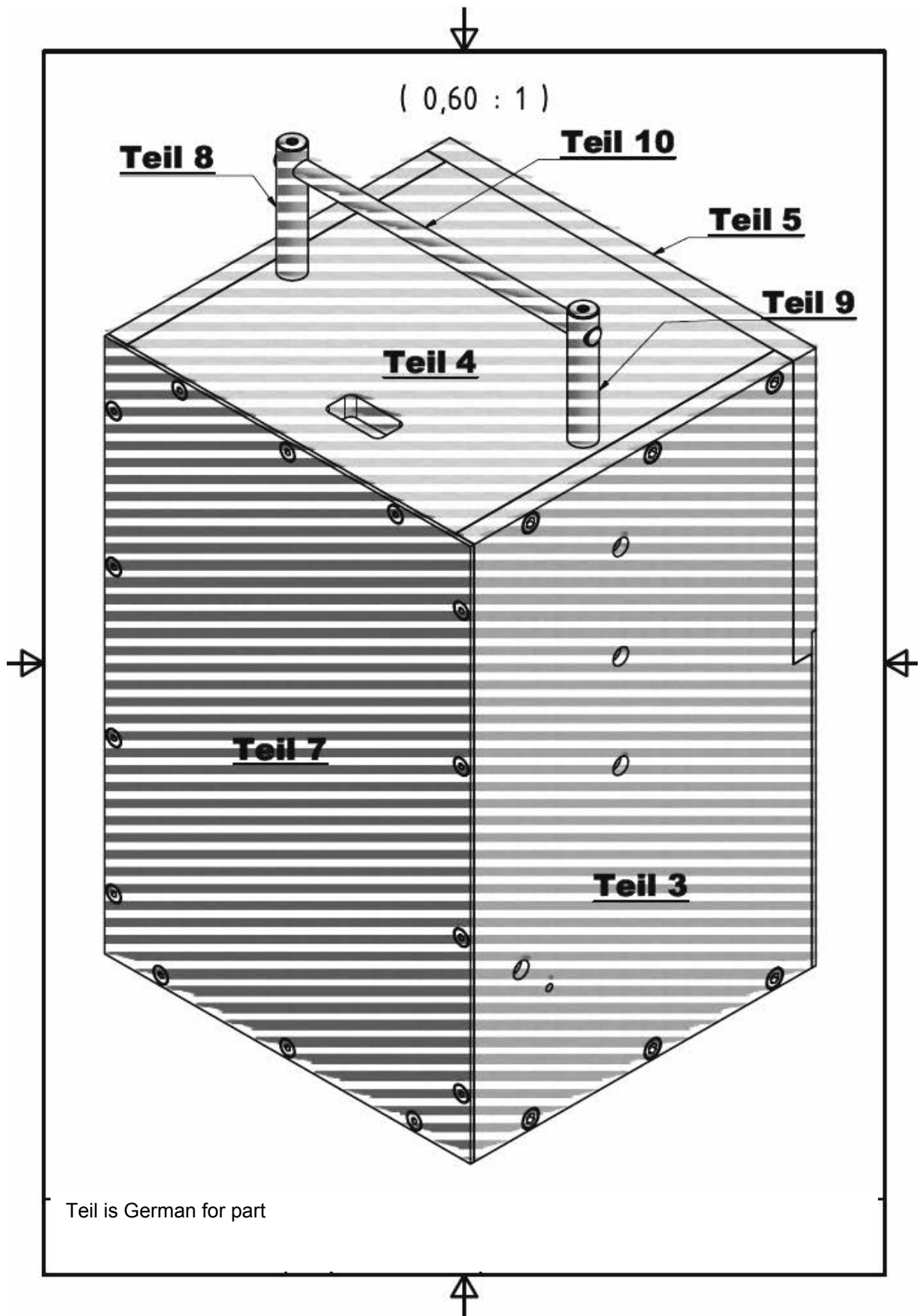
ZSCHERPEL, U., “Film digitization systems for DIR: Standards, Requirements, Archiving and Printing”, NDT.net 5 5 (2000), <http://www.ndt.net/article/v05n05/zscherp/zscherp.htm>

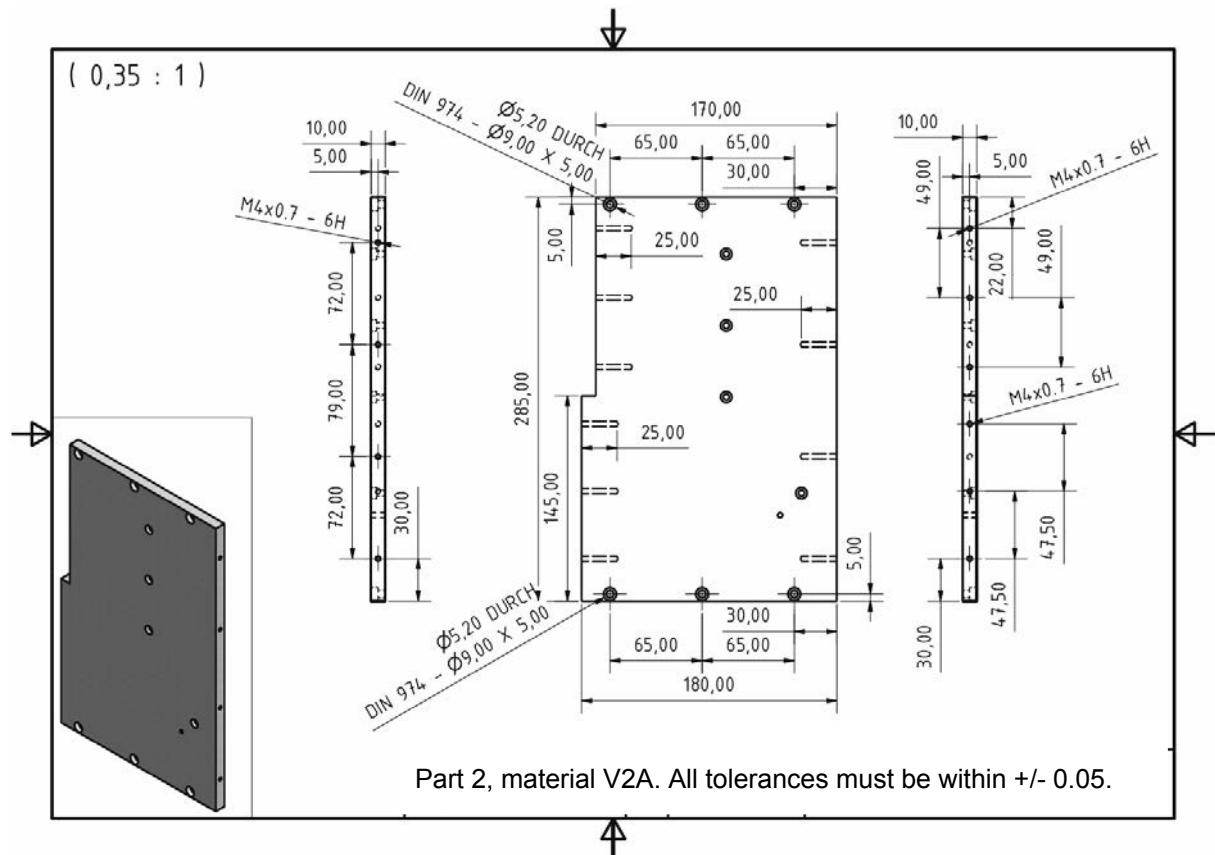
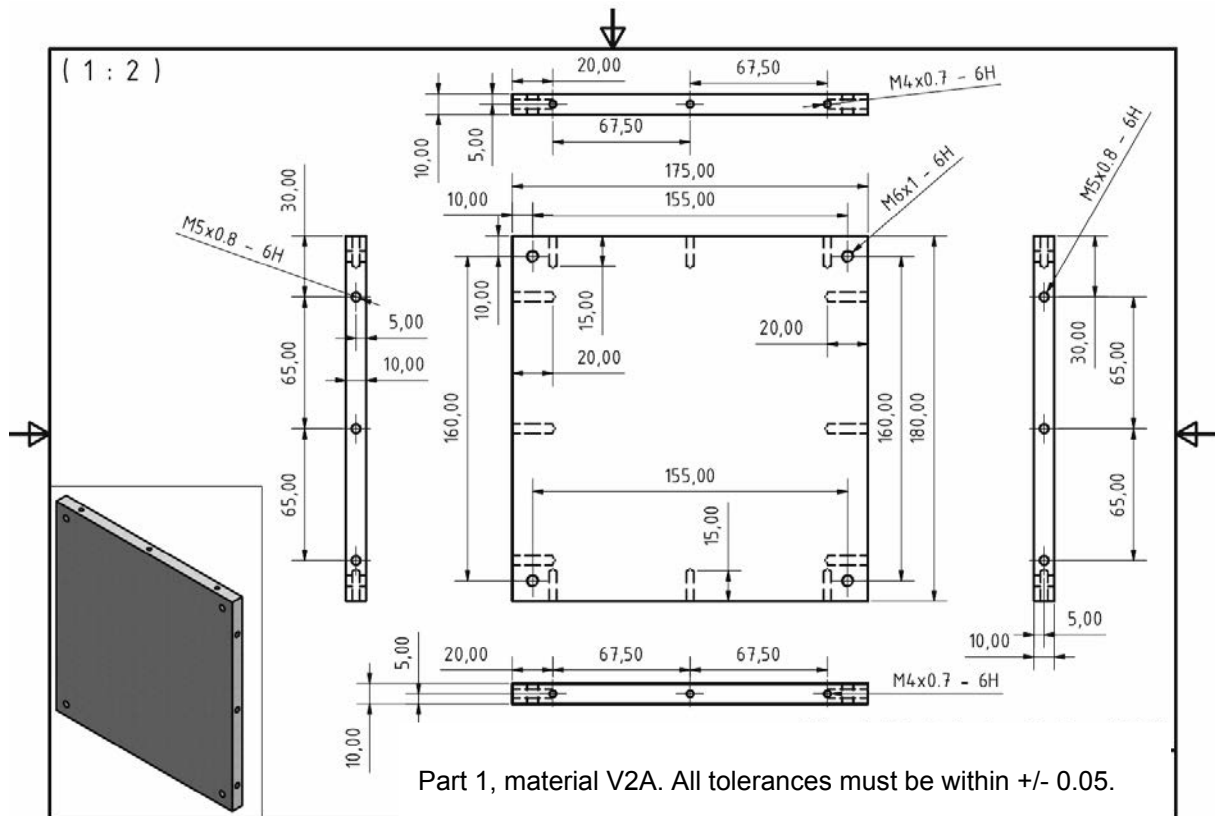
Annex
**BAM CONSTRUCTION DRAWINGS FOR PRODUCING A
CASING FOR THE DIGITAL FLUOROSCOPE**

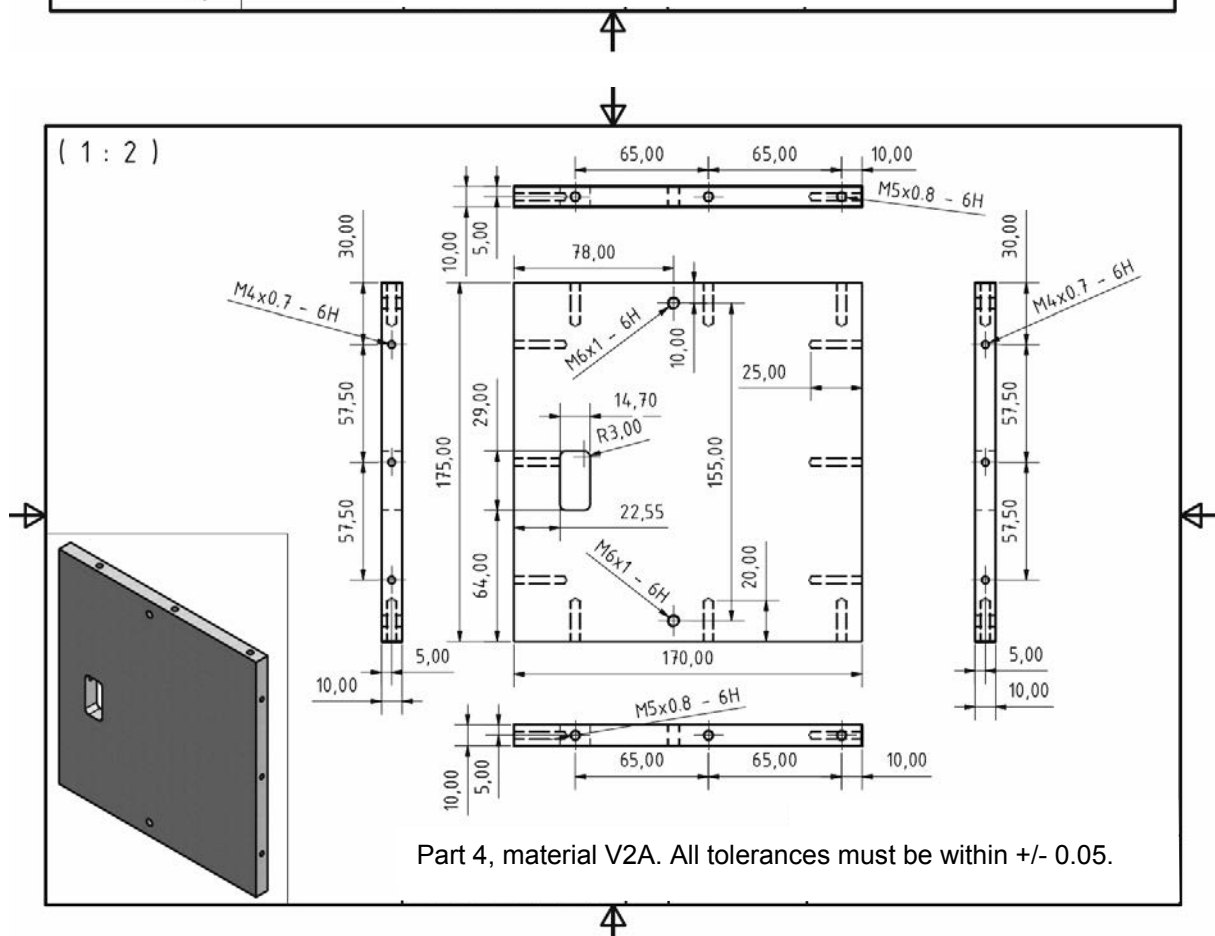
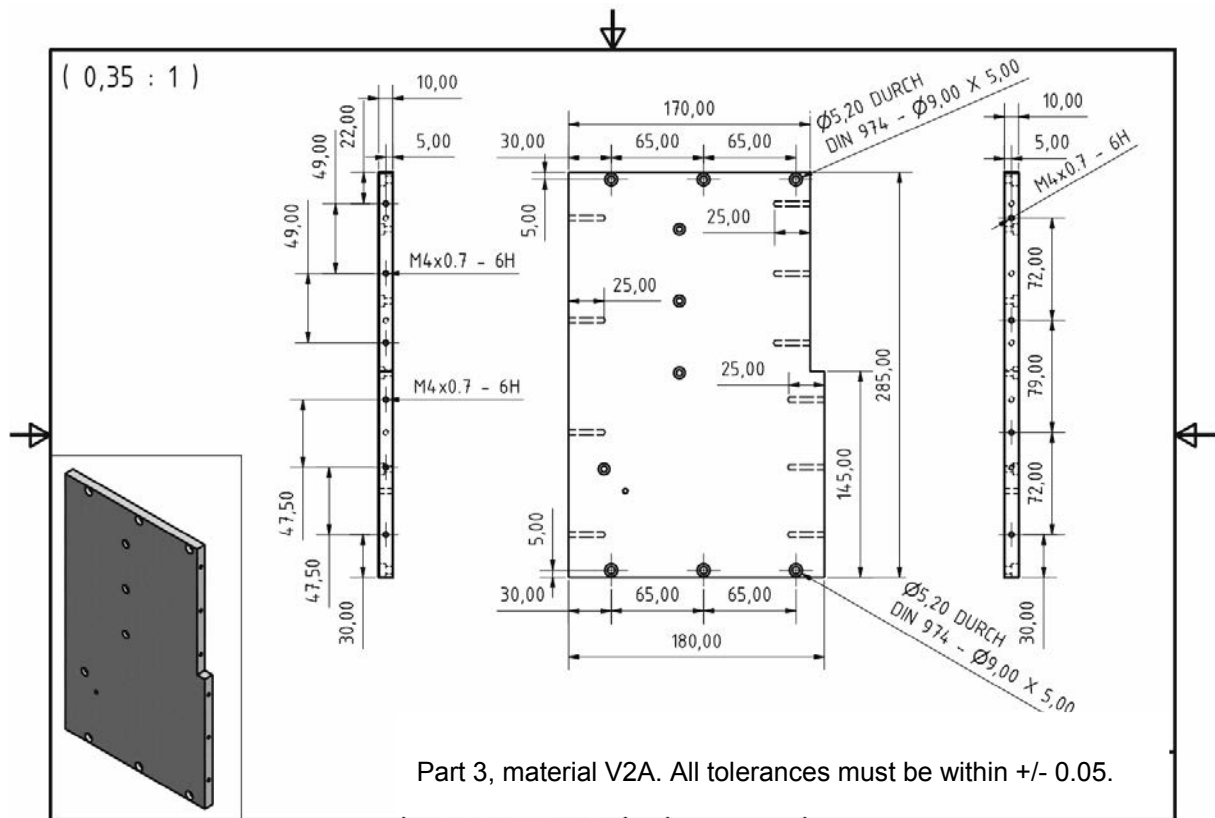
The drawings reproduced in this Annex are for a typical low cost system for digital industrial radiology (courtesy of the Federal Institute for Materials Research and Testing (BAM), Germany).

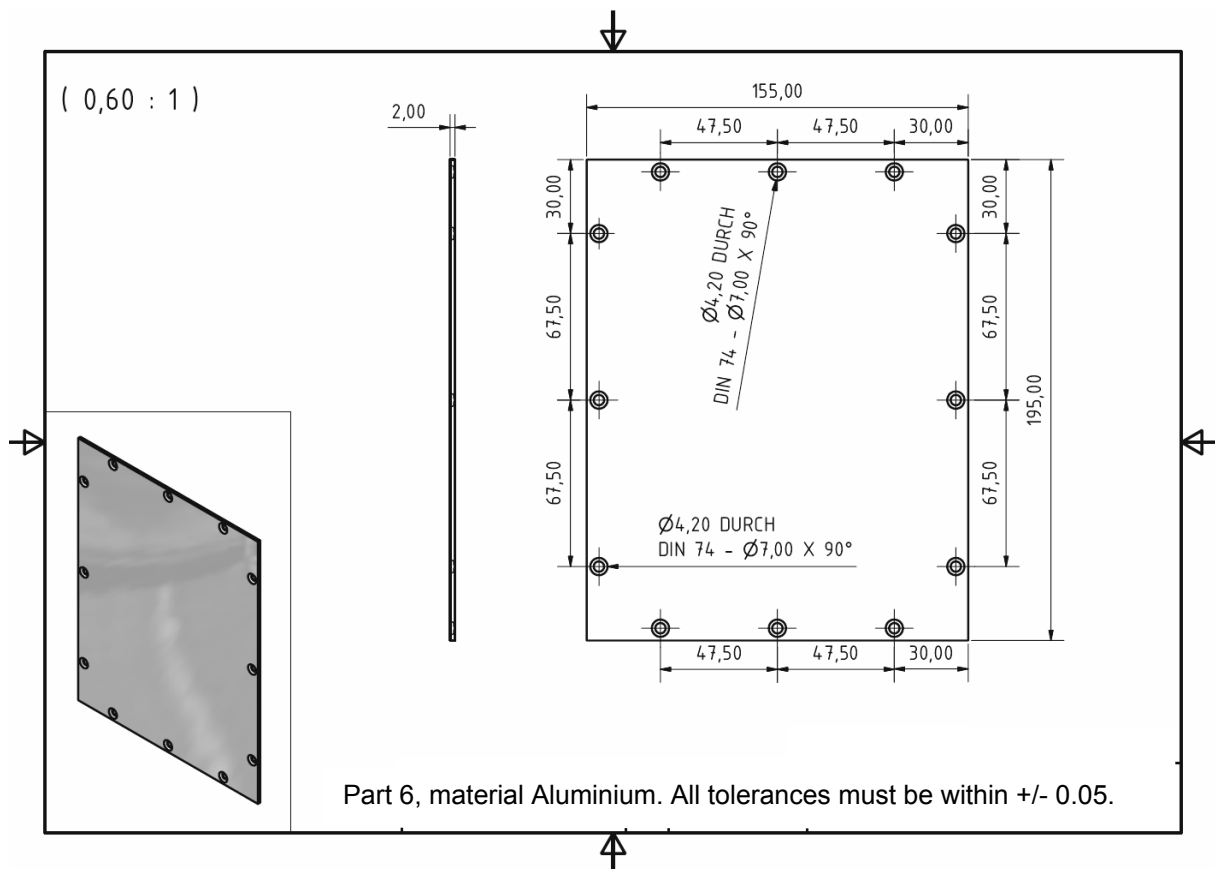
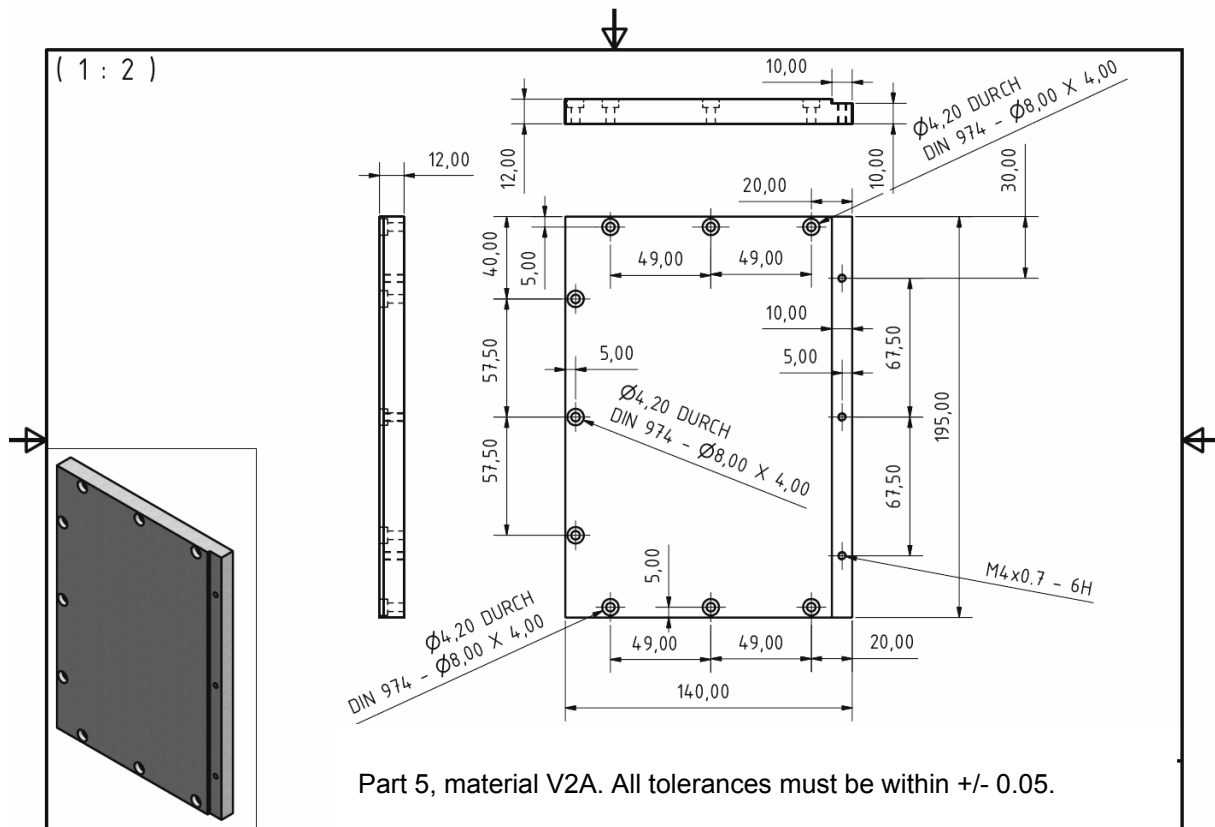


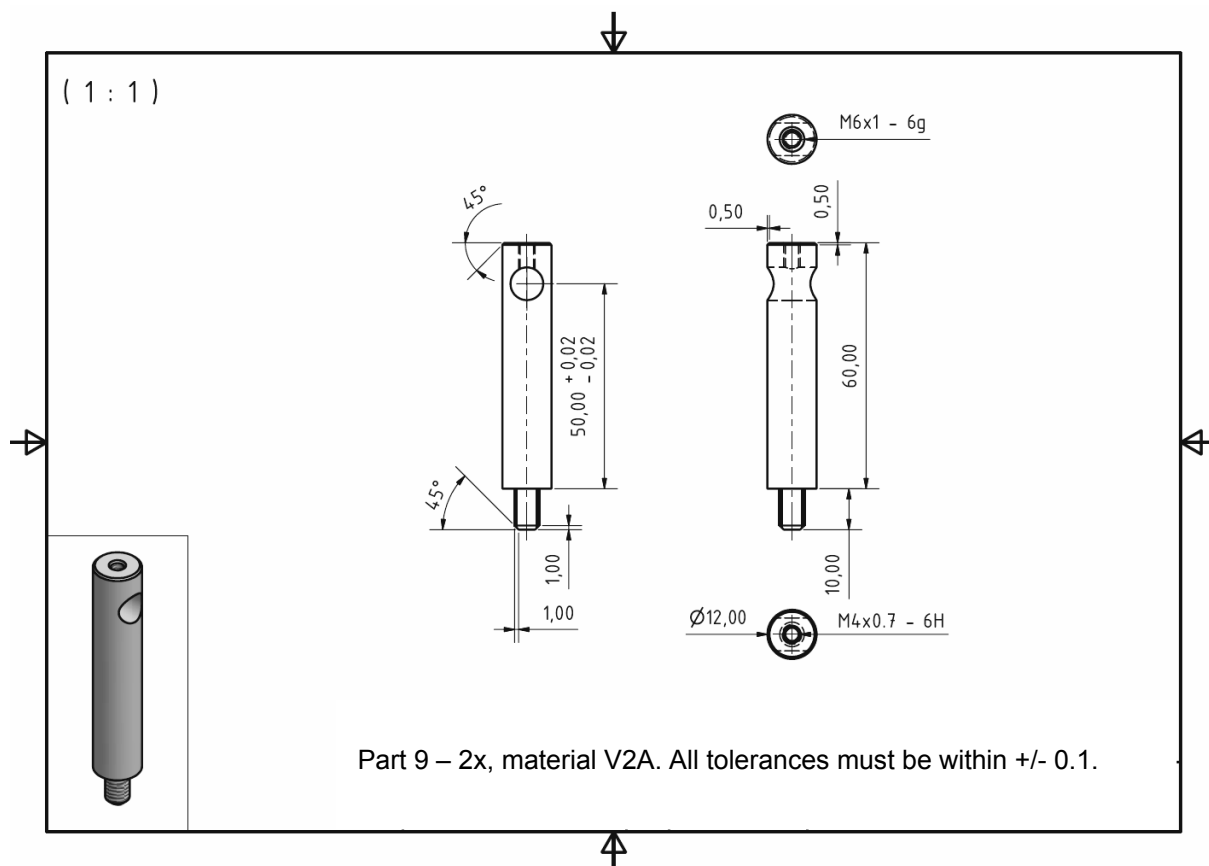
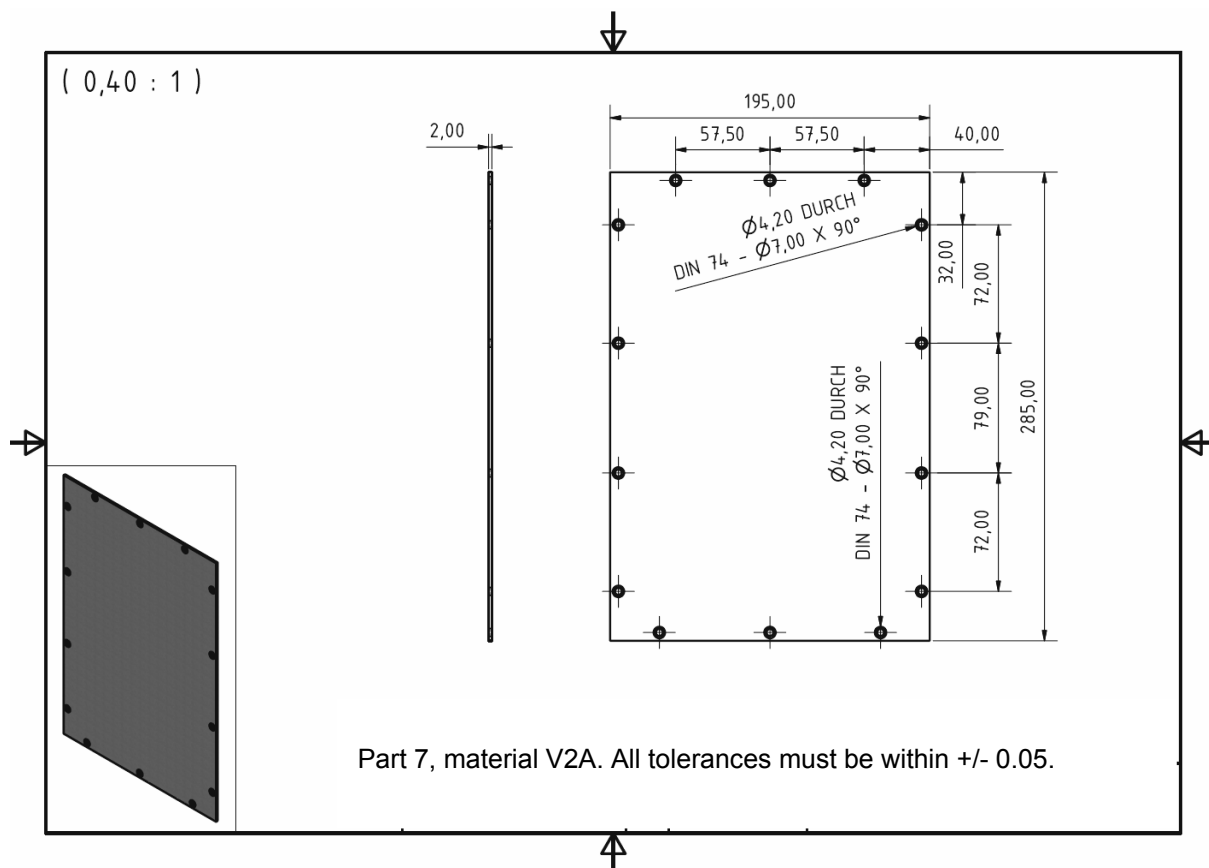


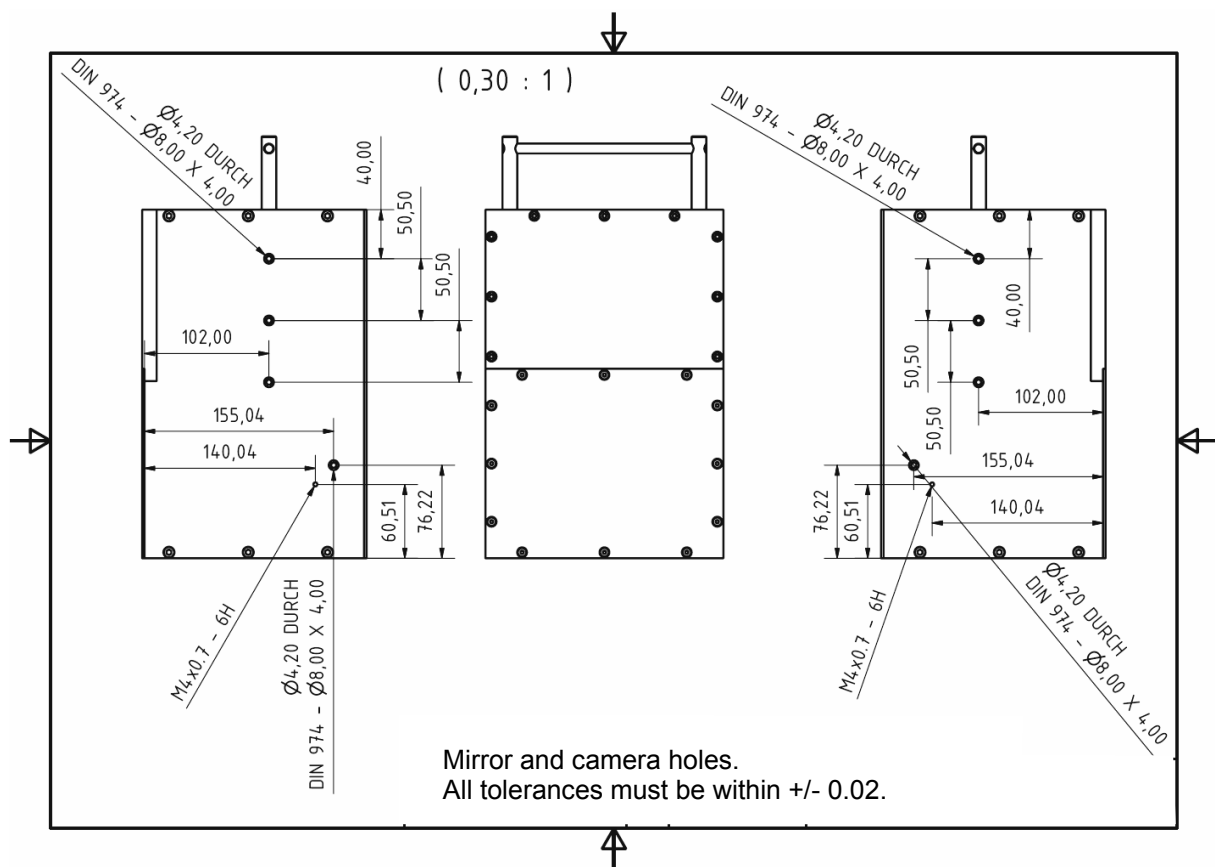
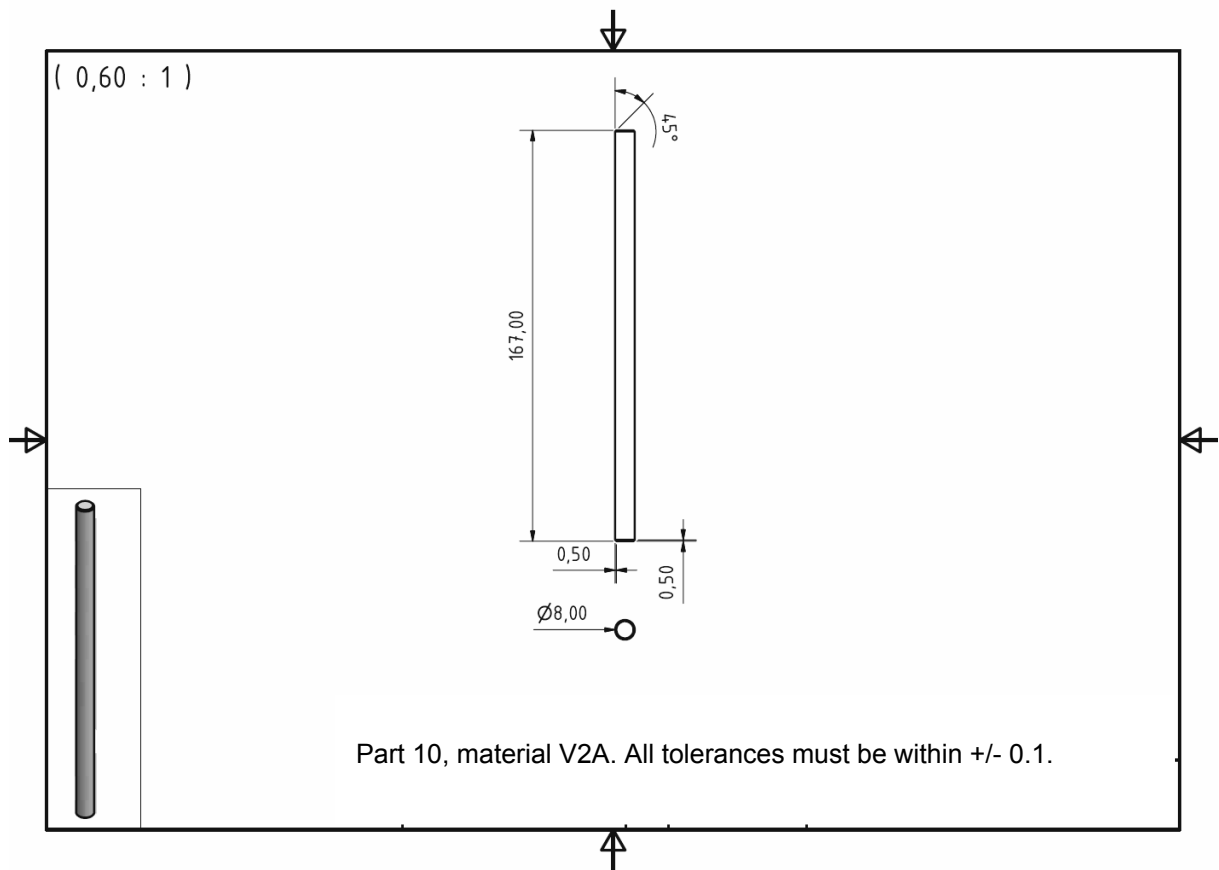


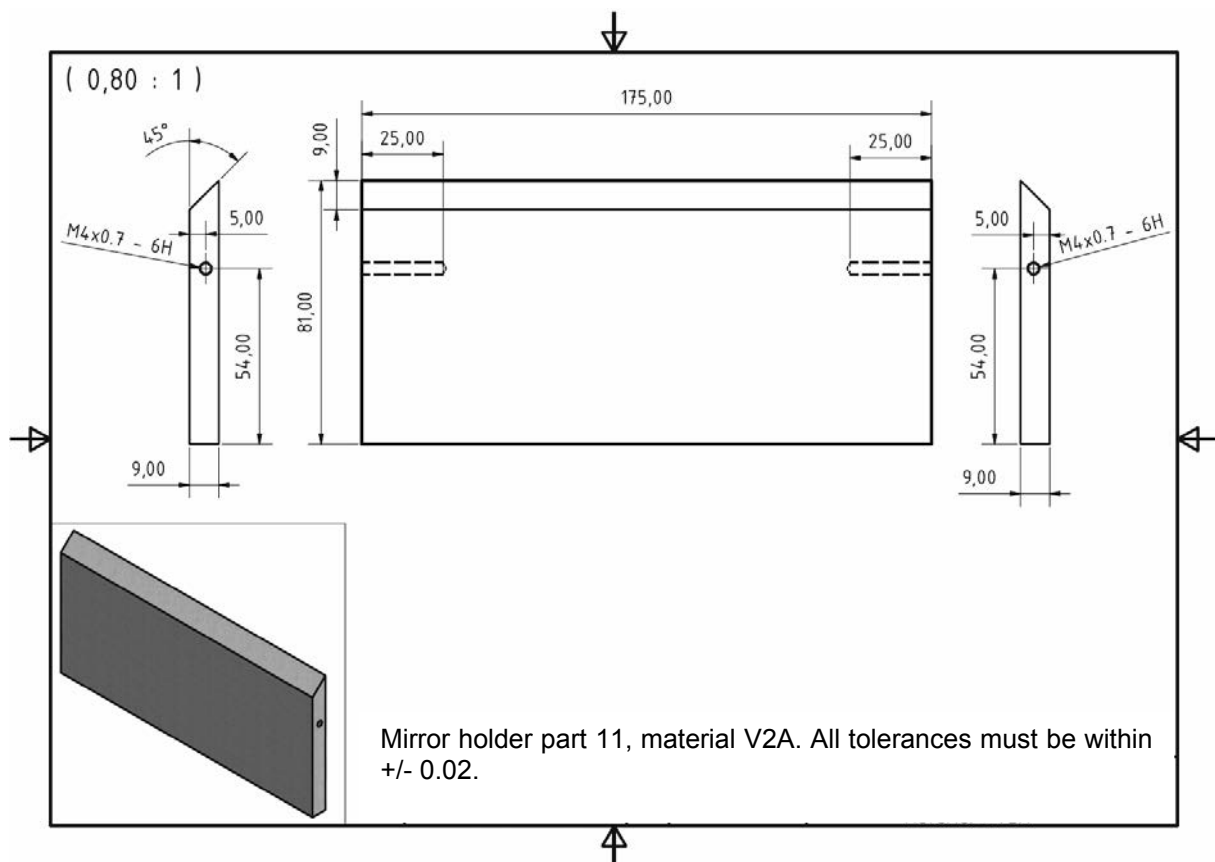
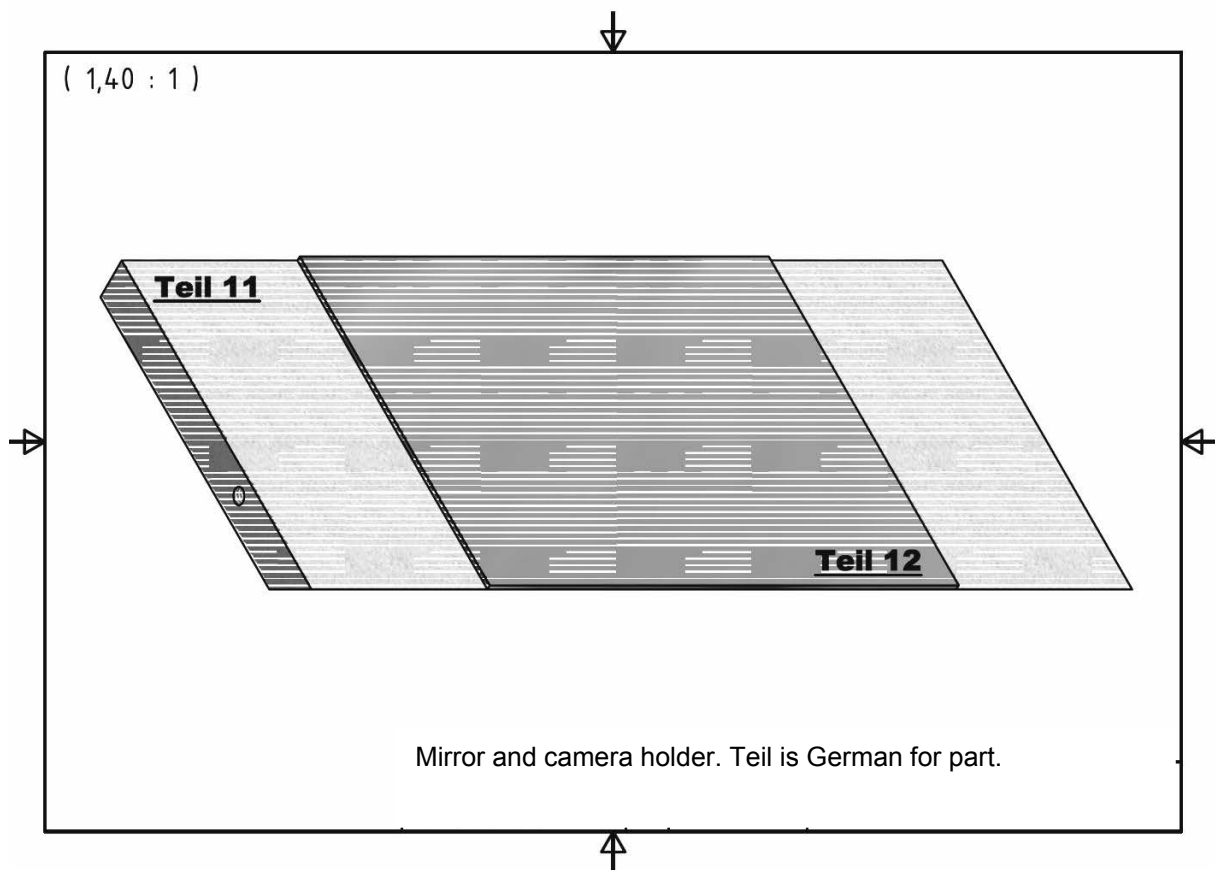


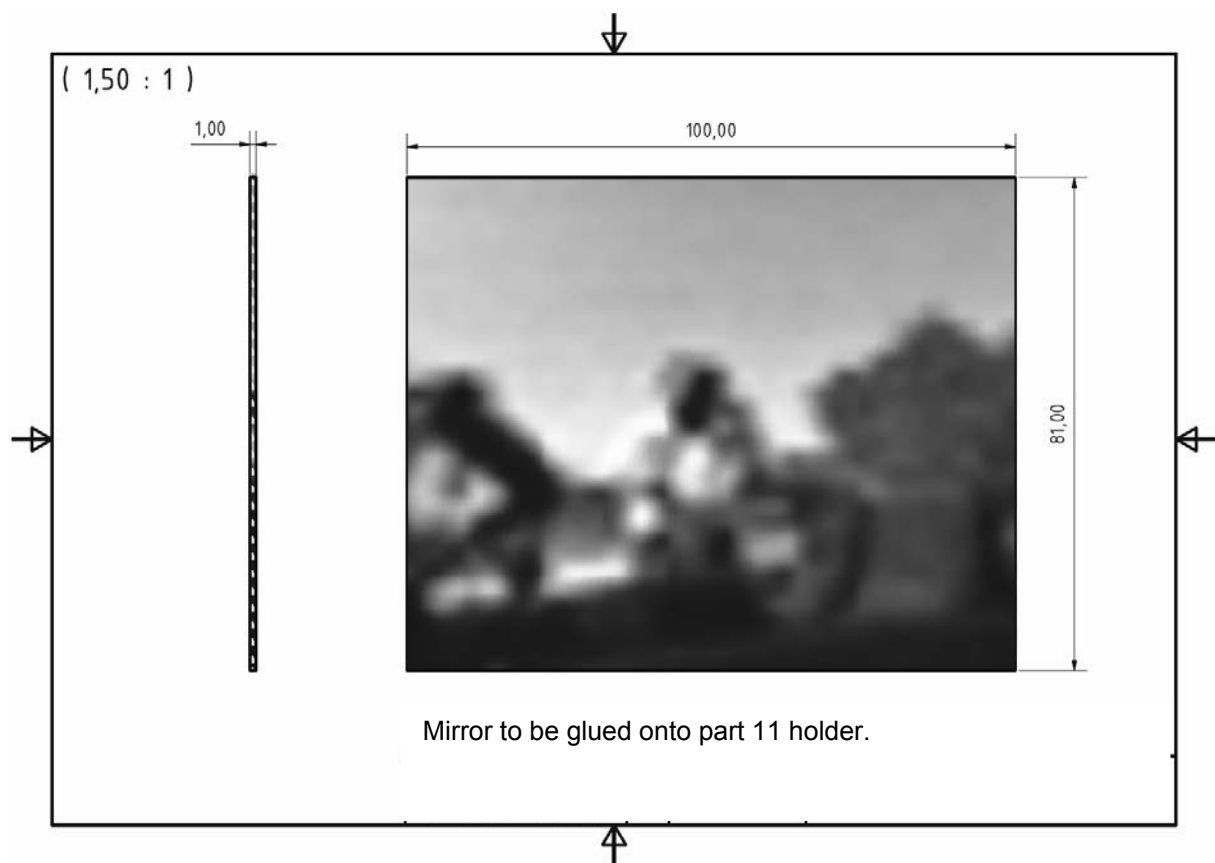


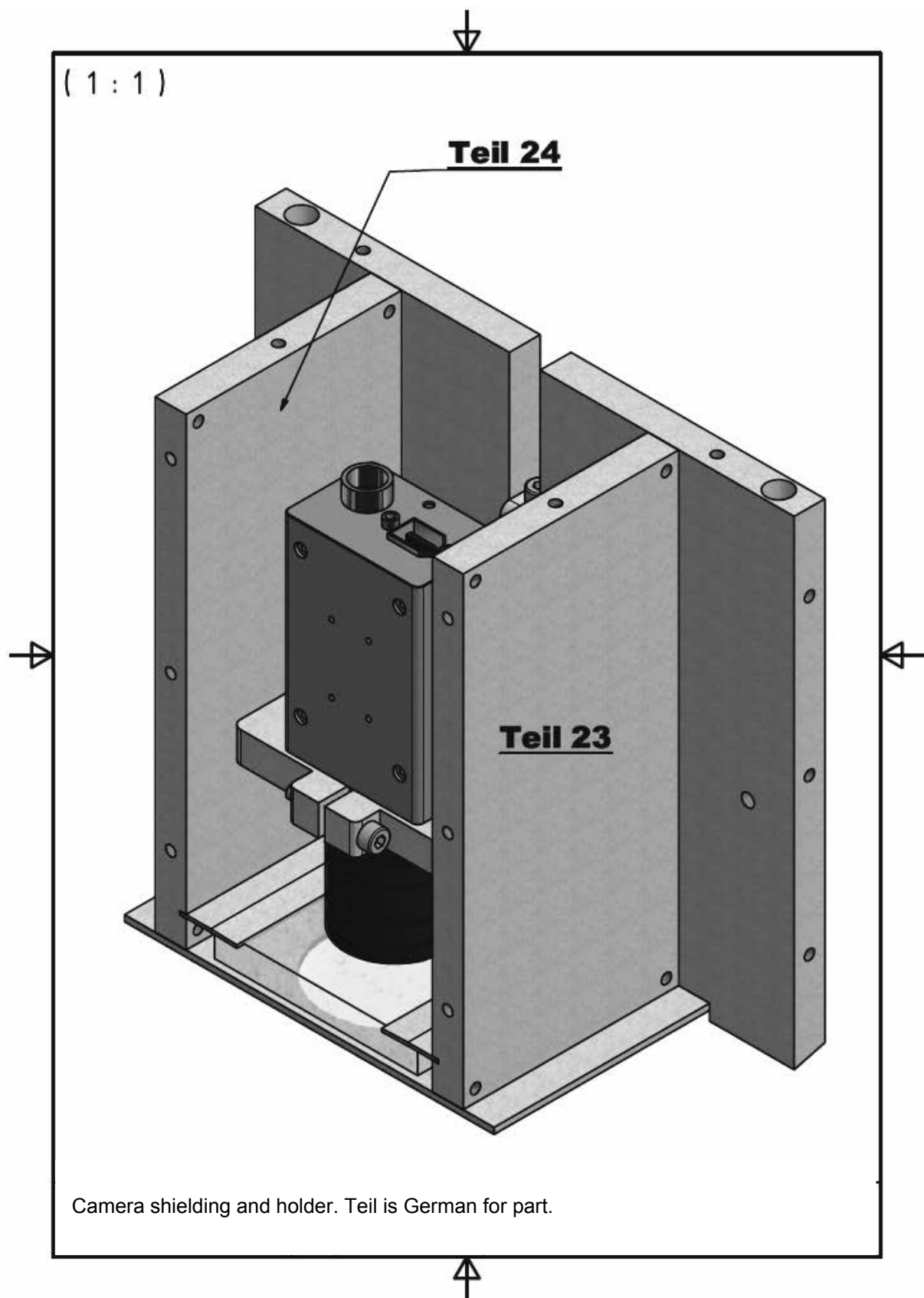


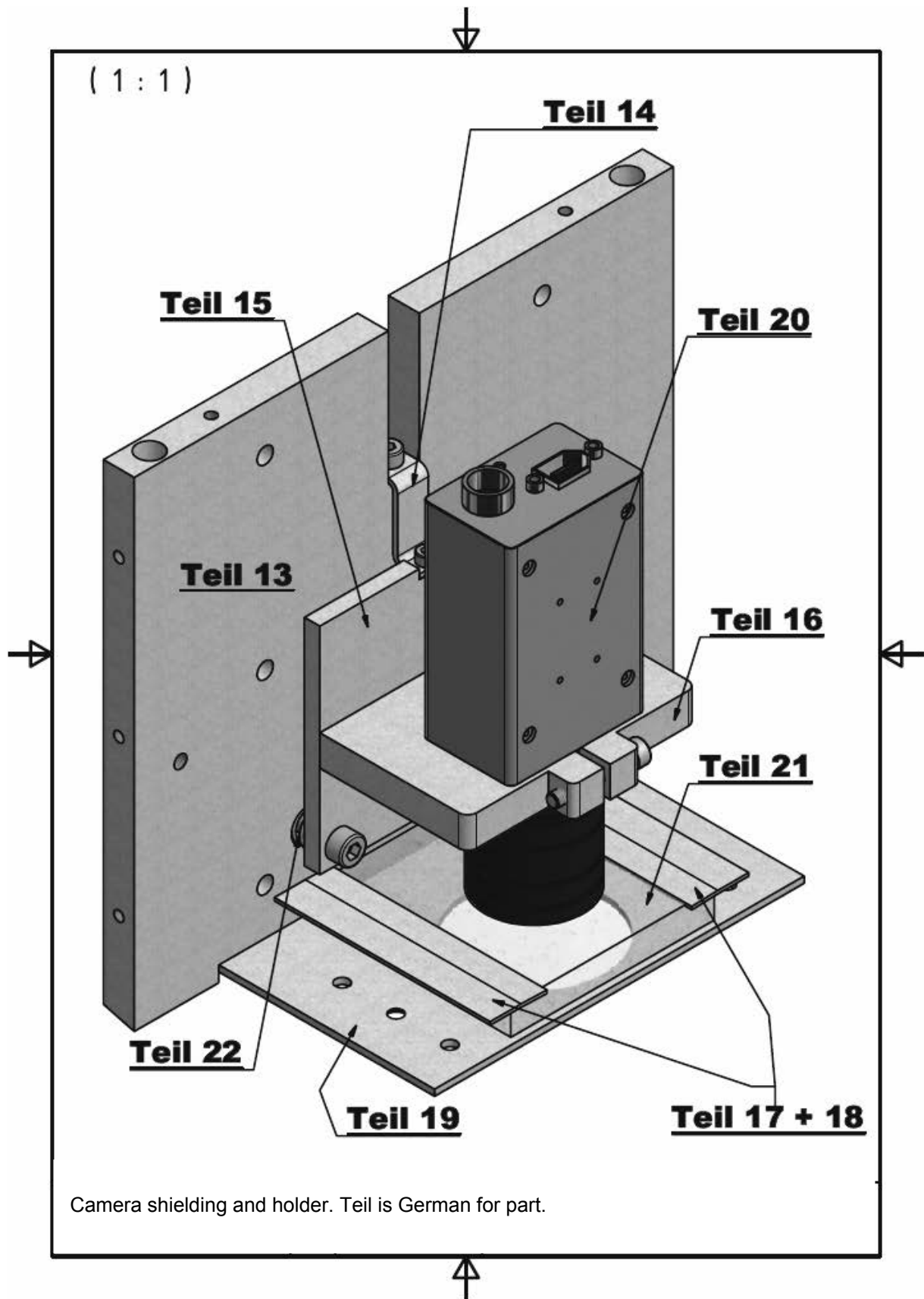


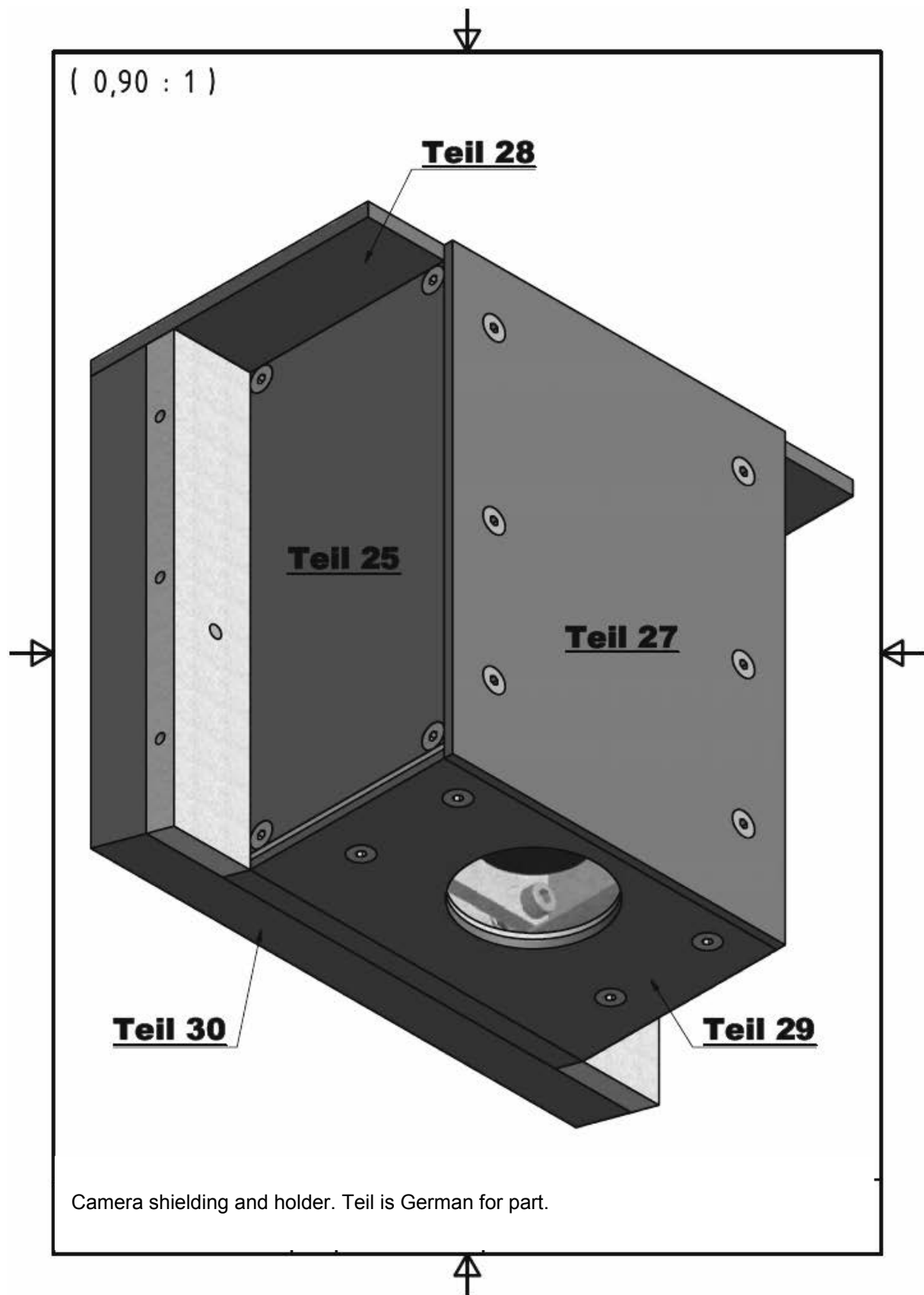


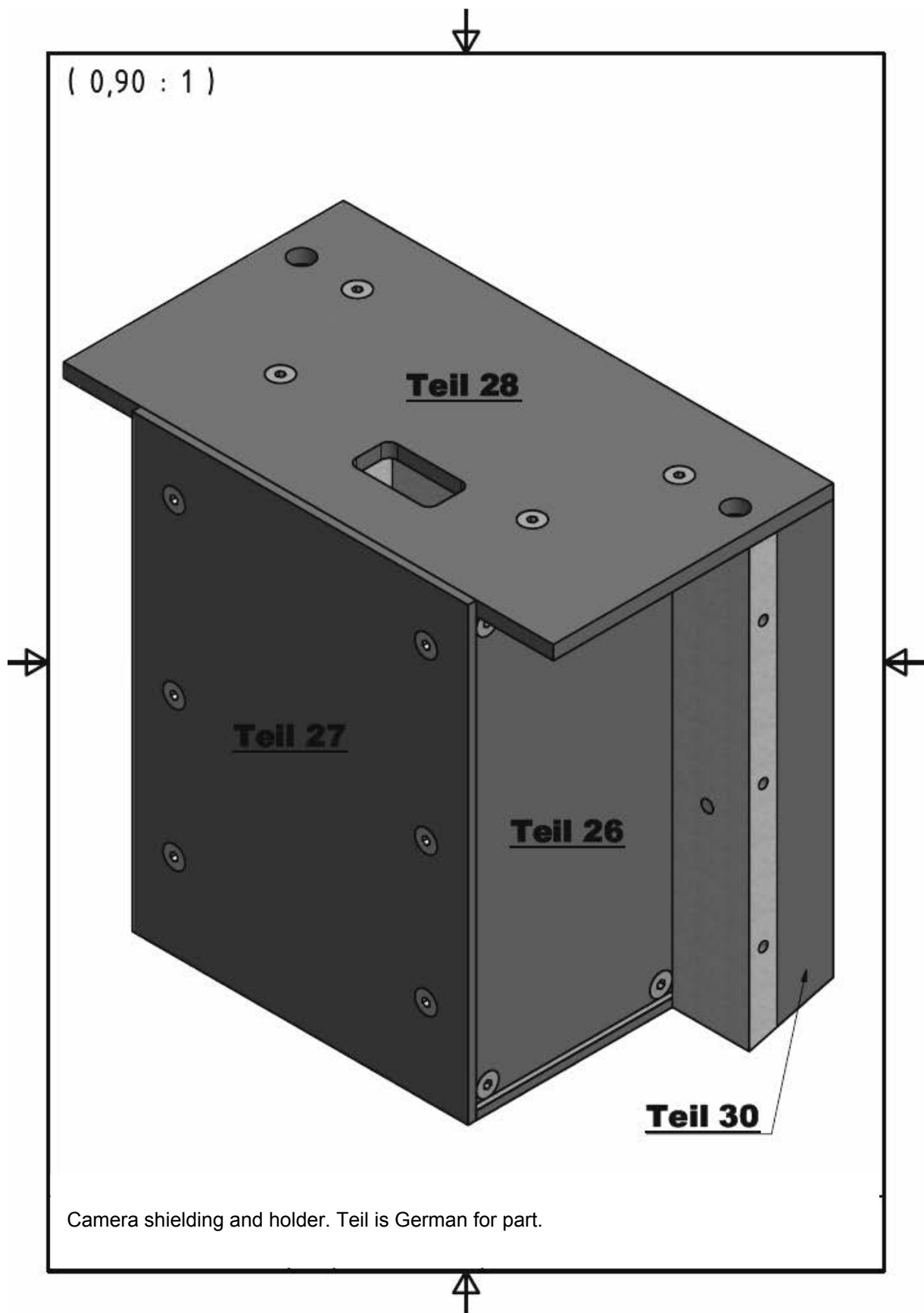


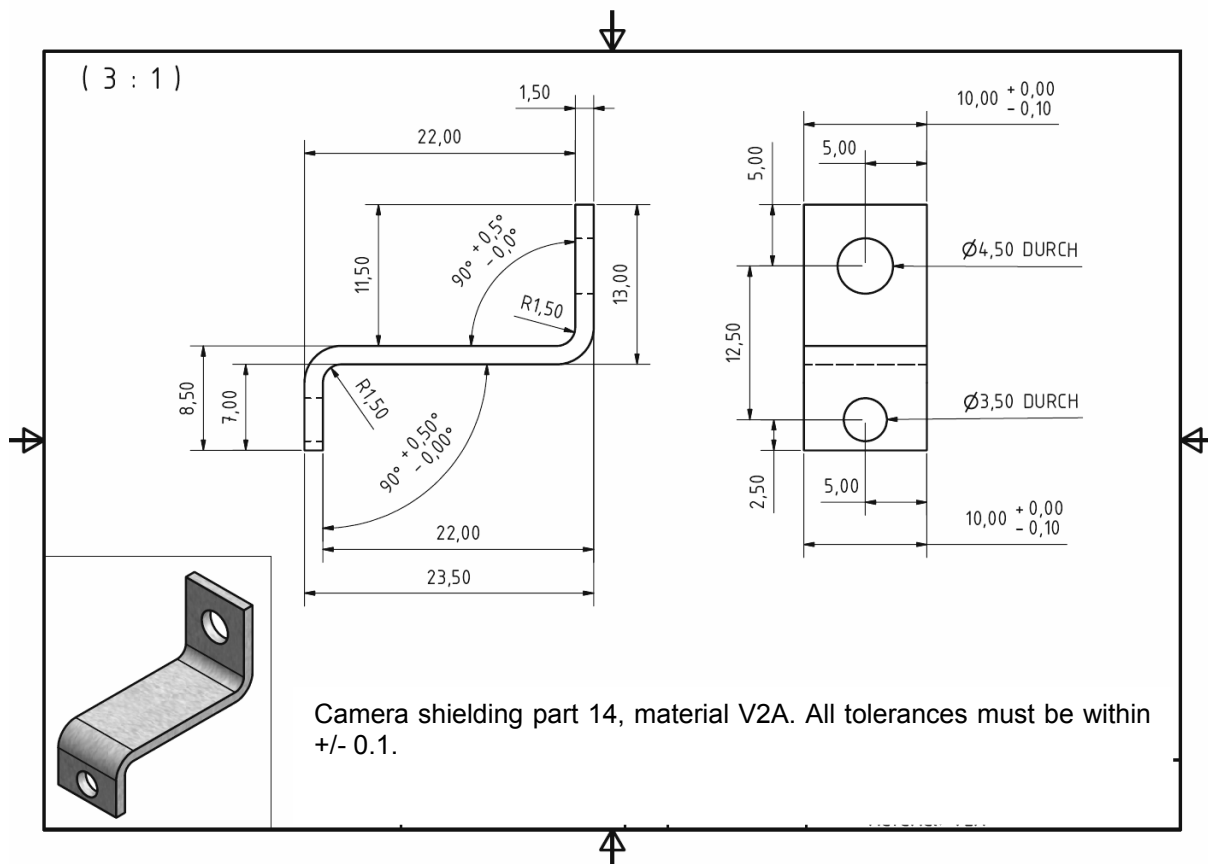
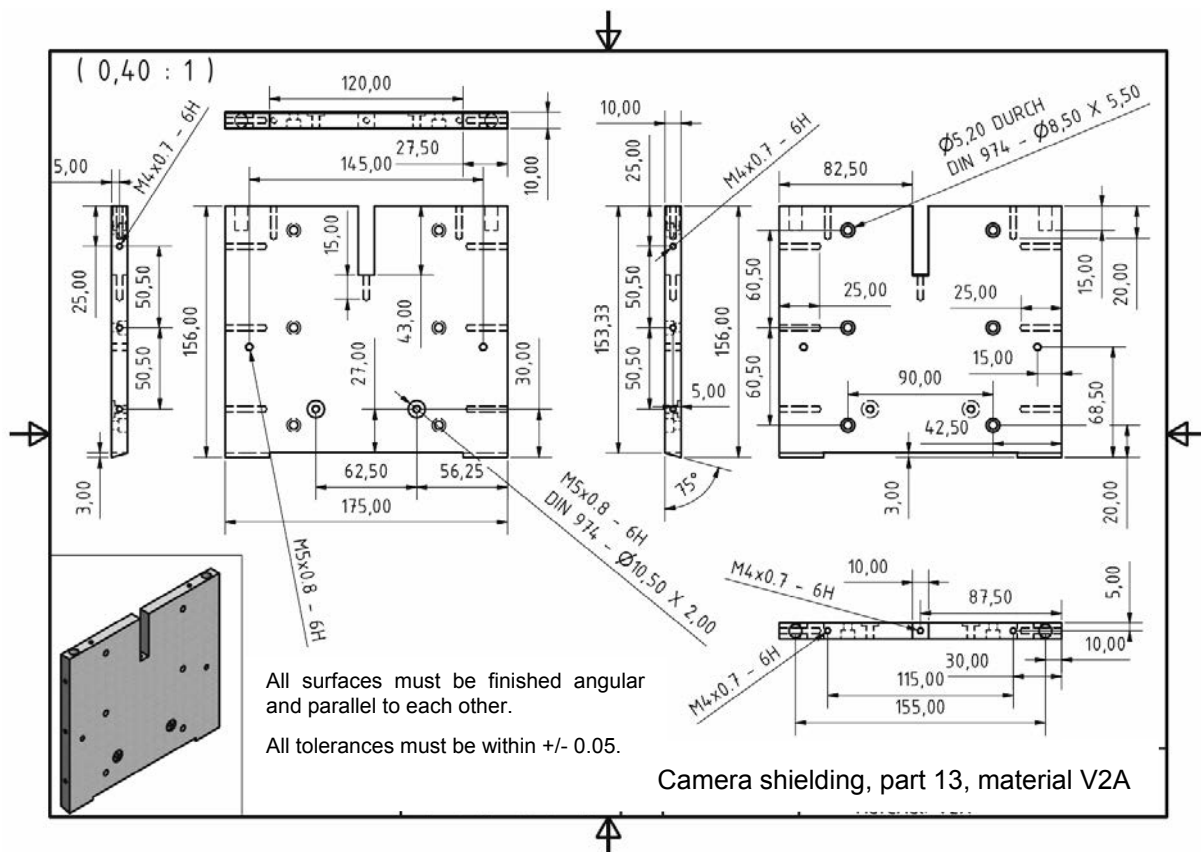


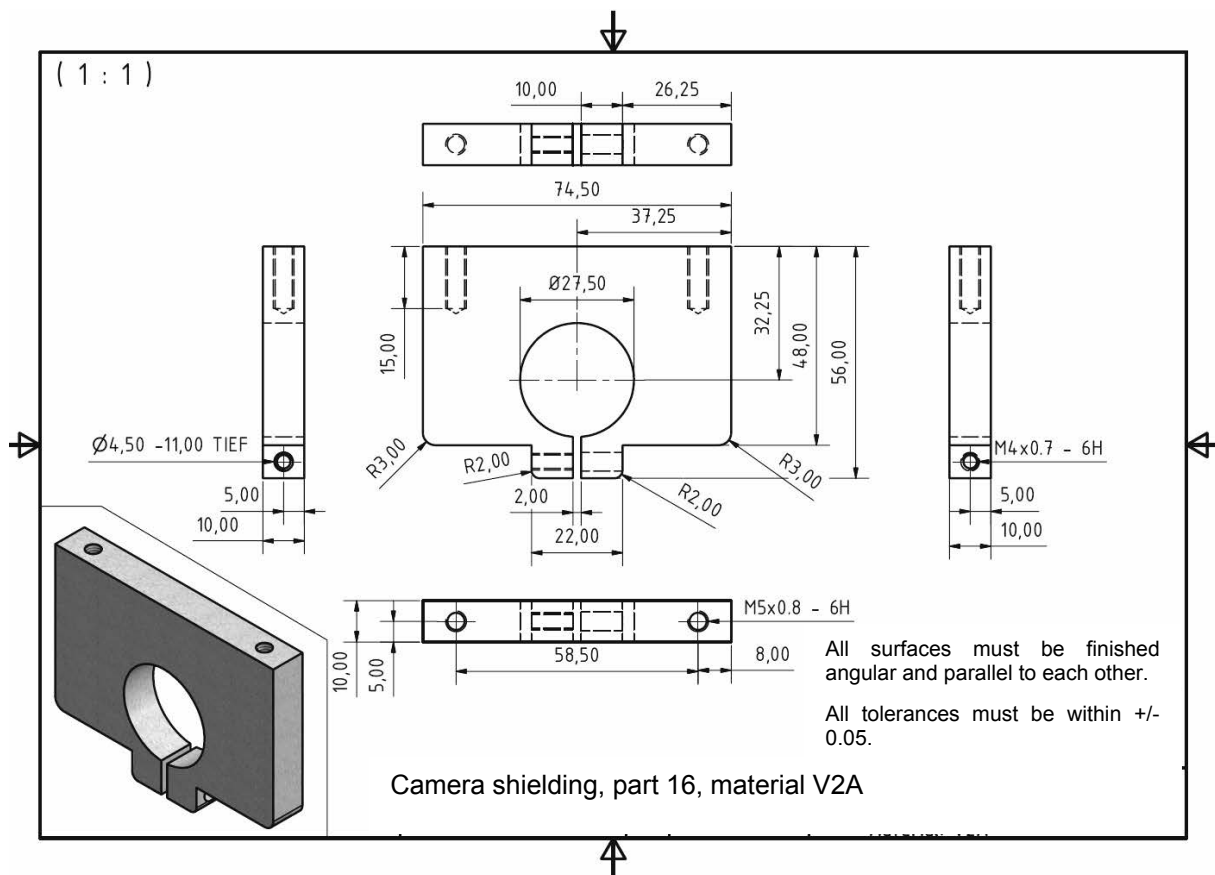
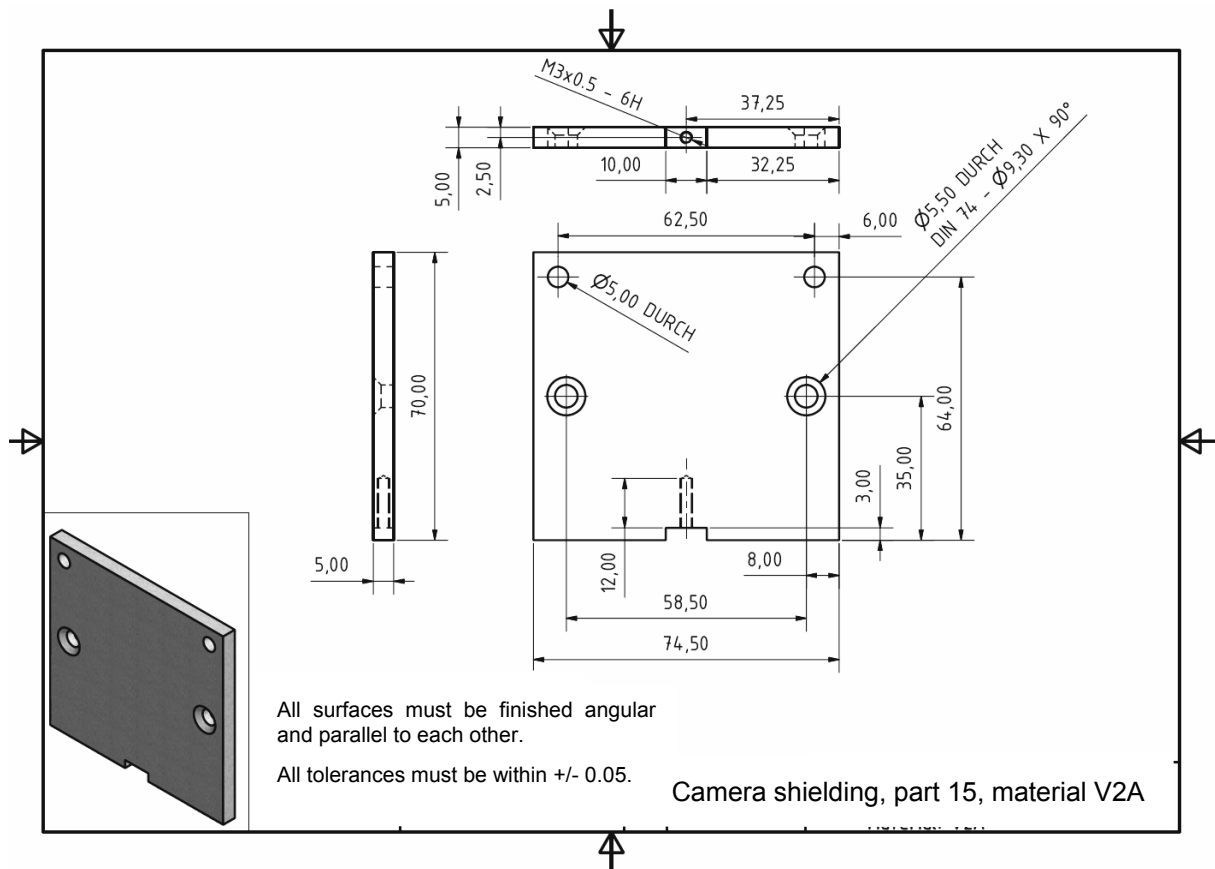


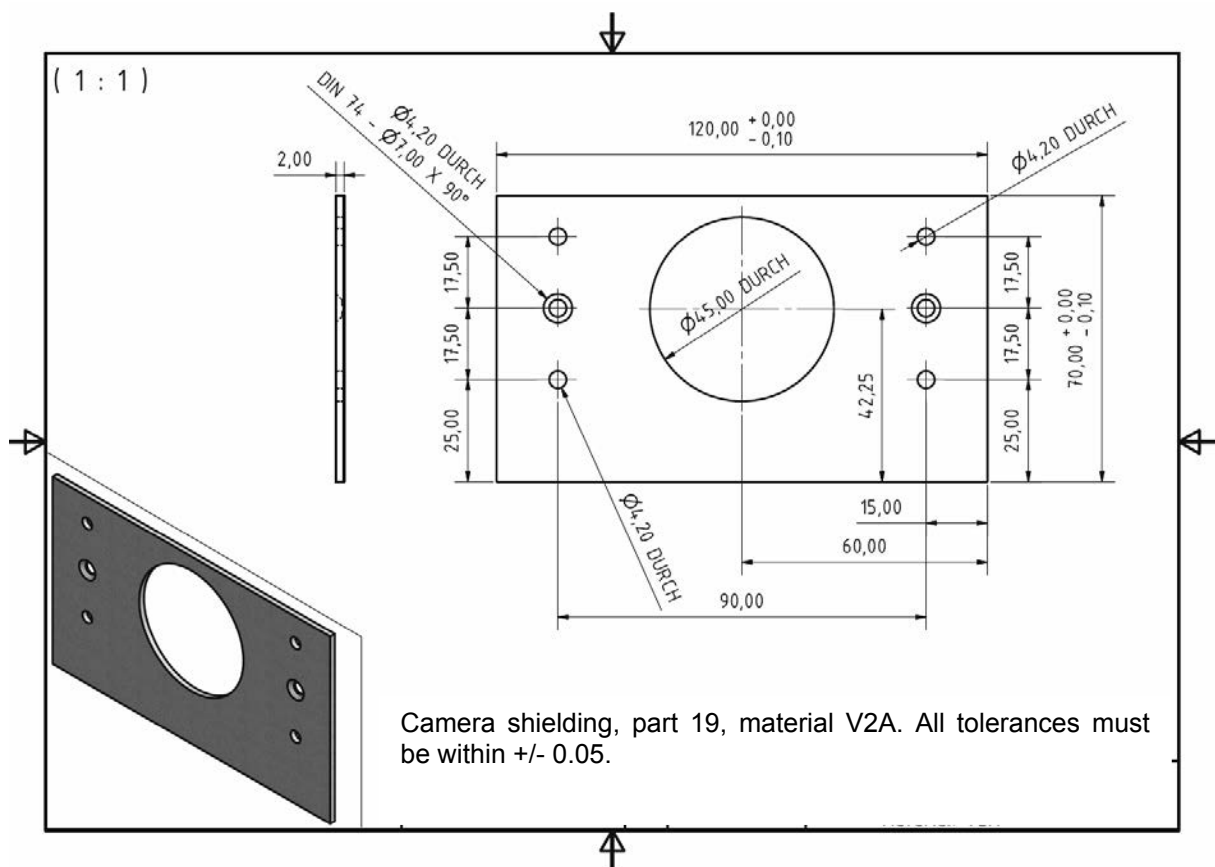
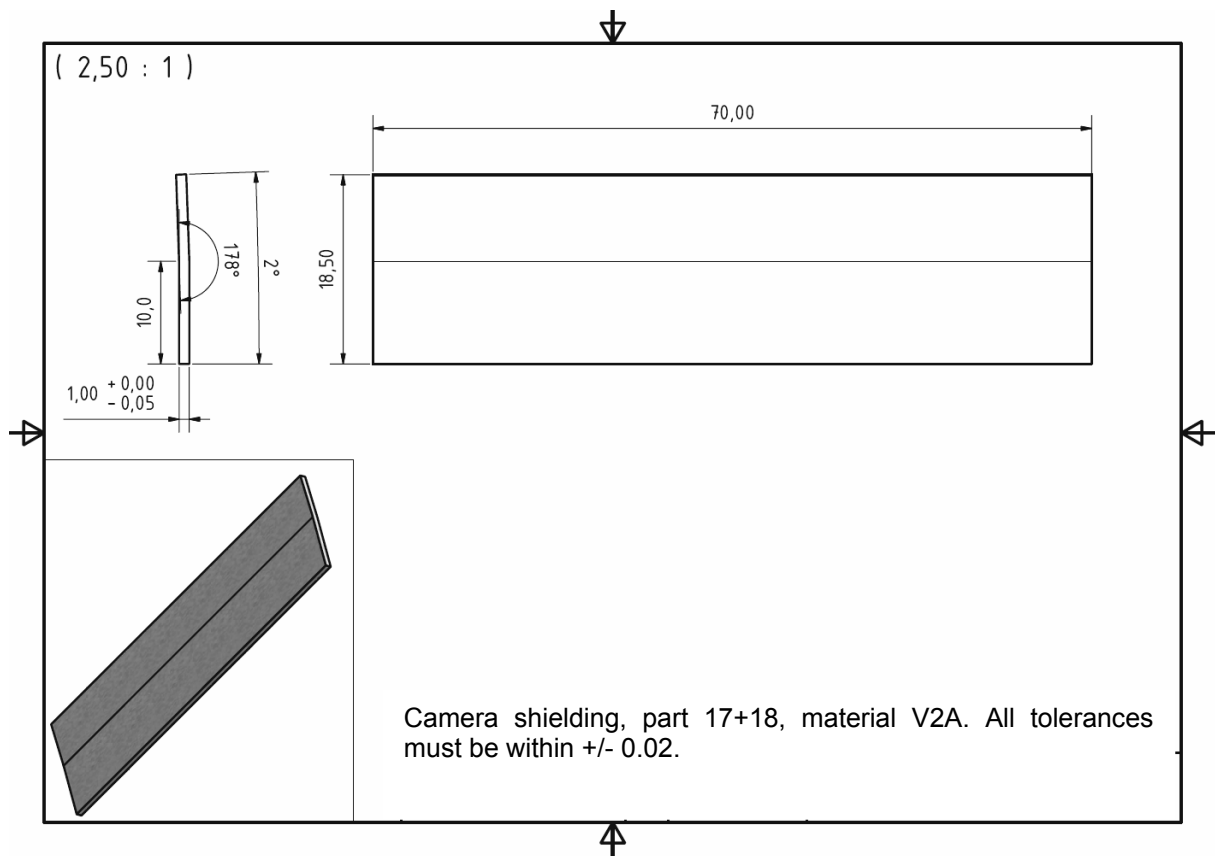


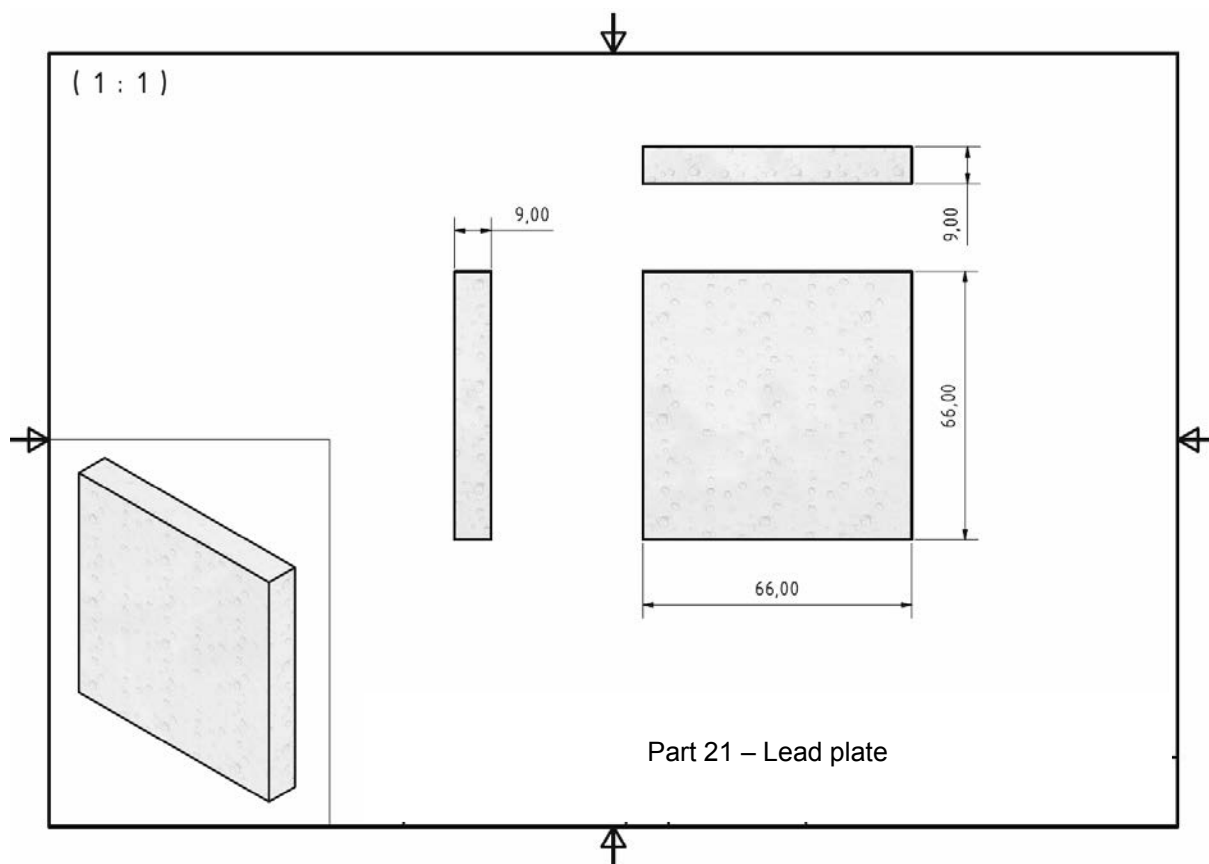
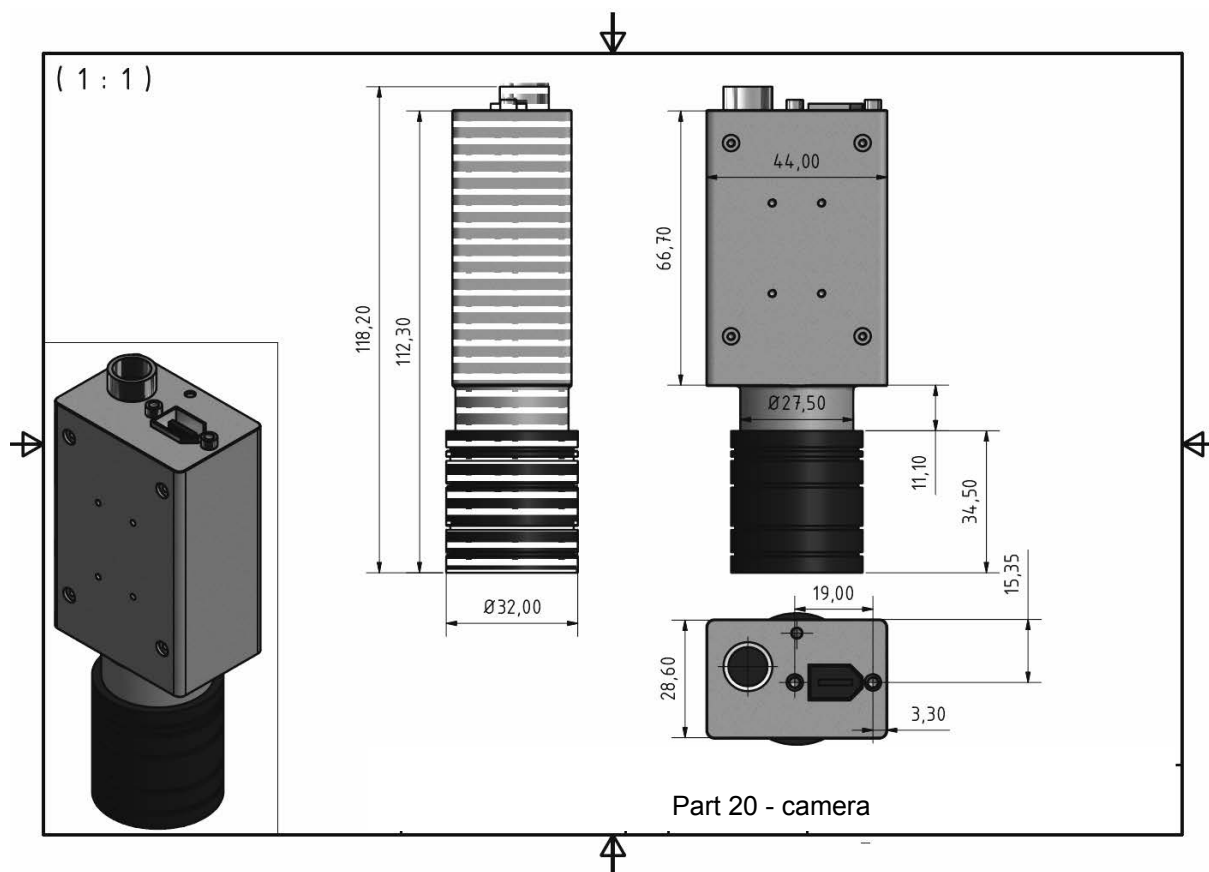


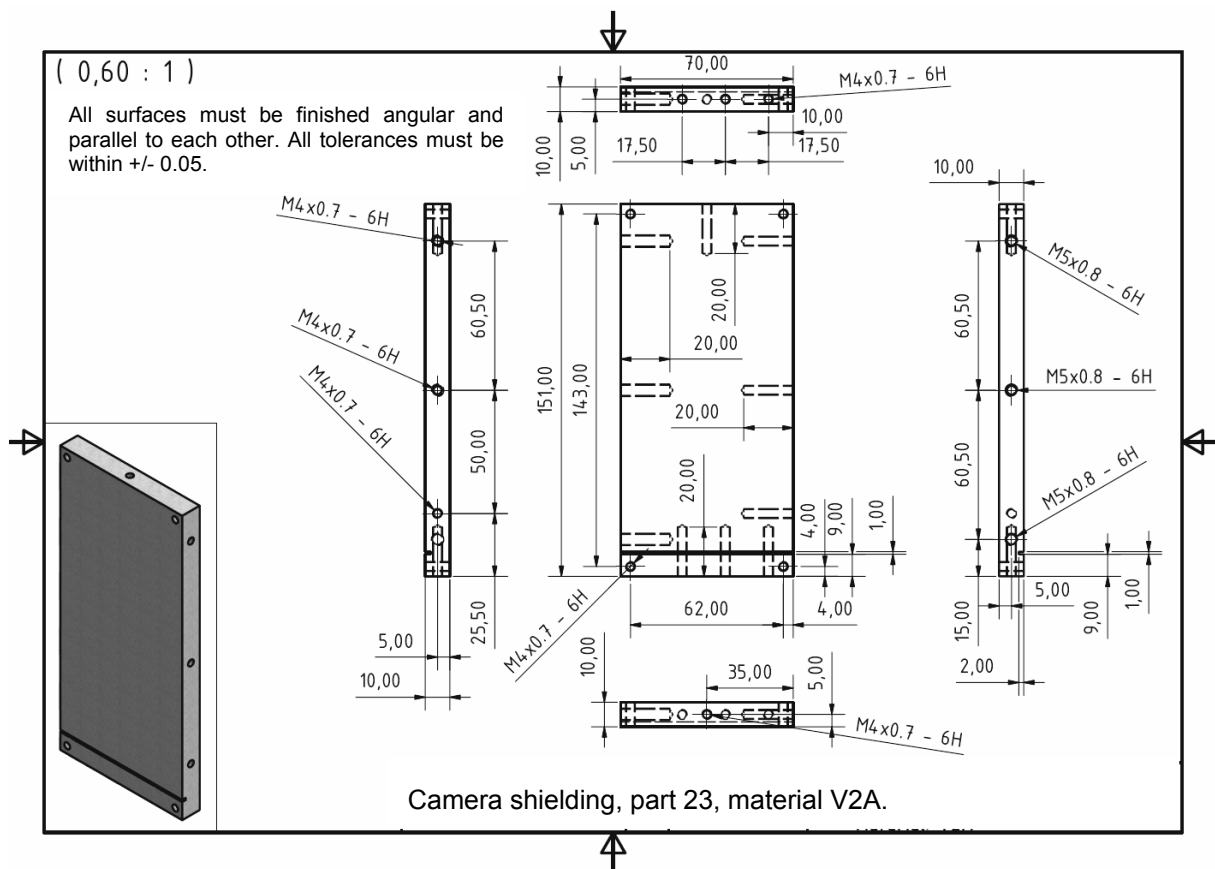
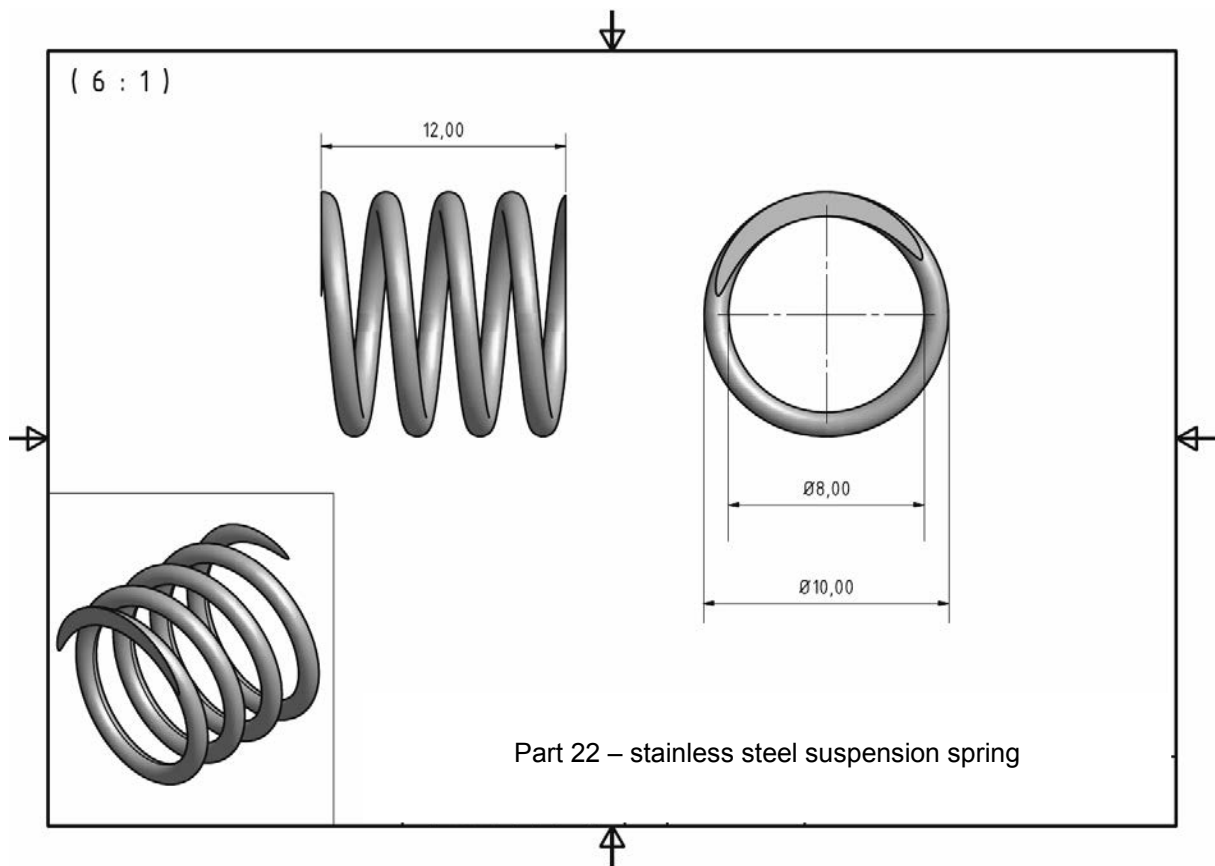


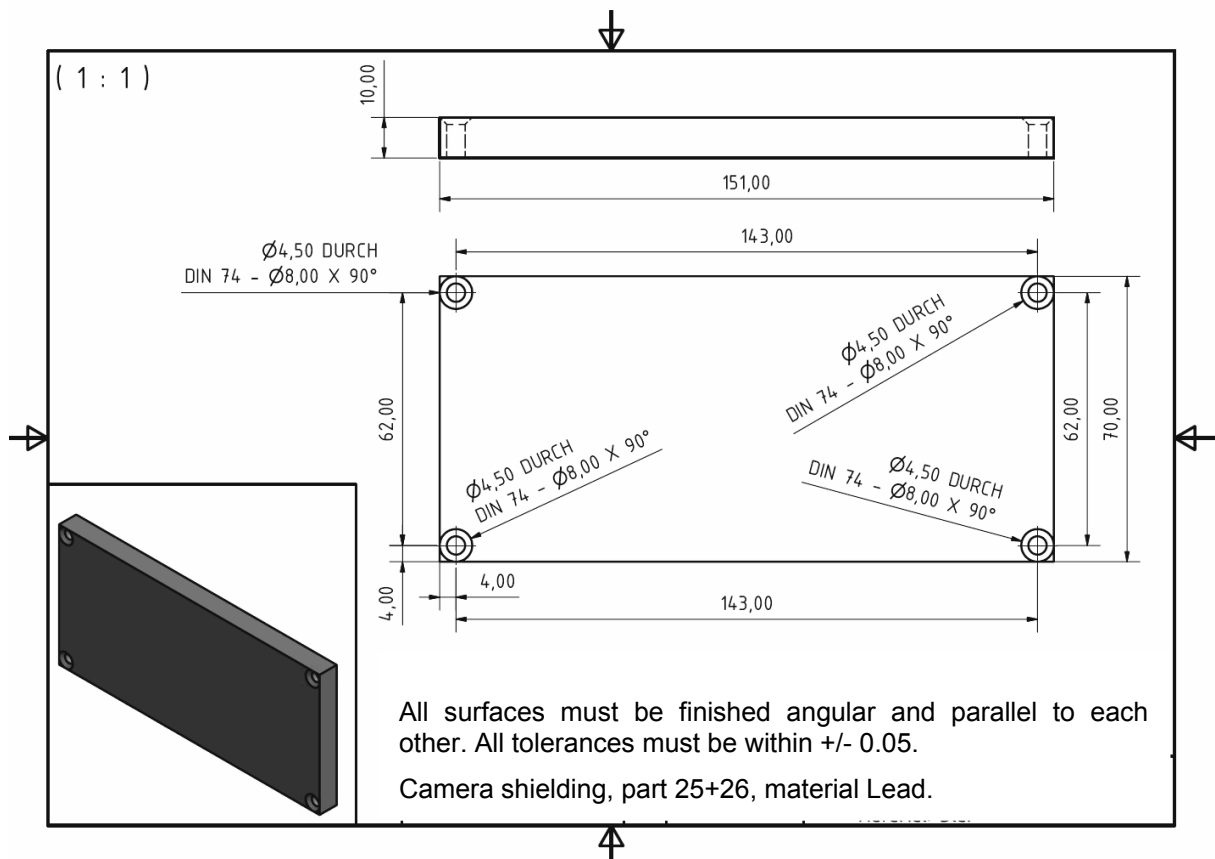
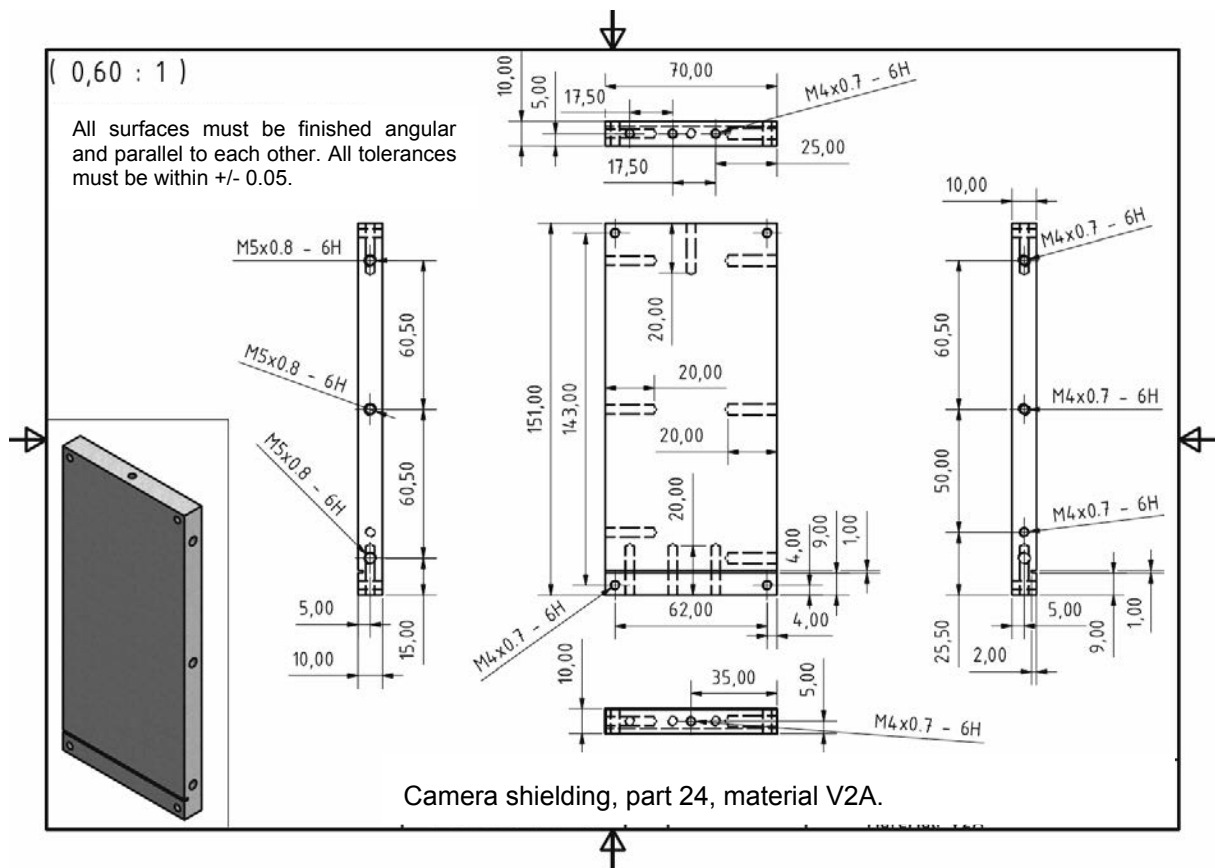


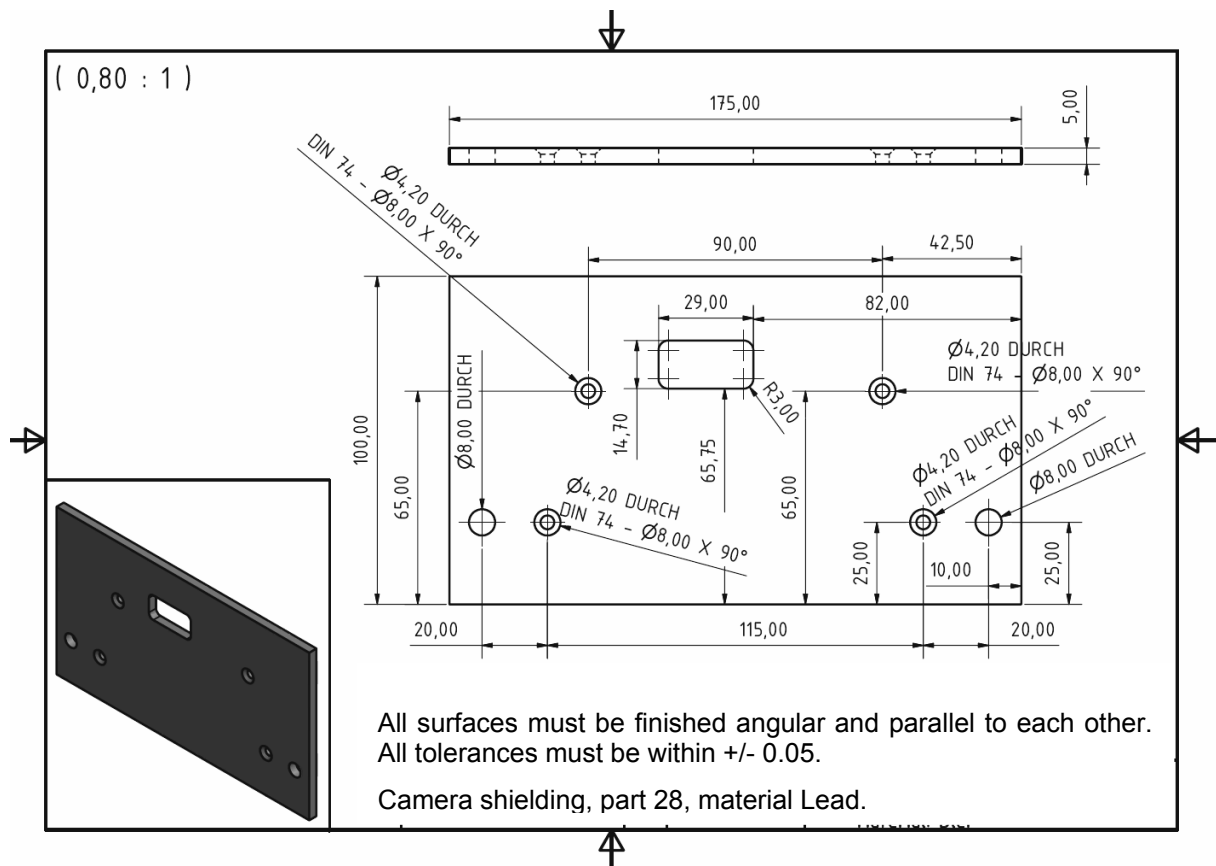
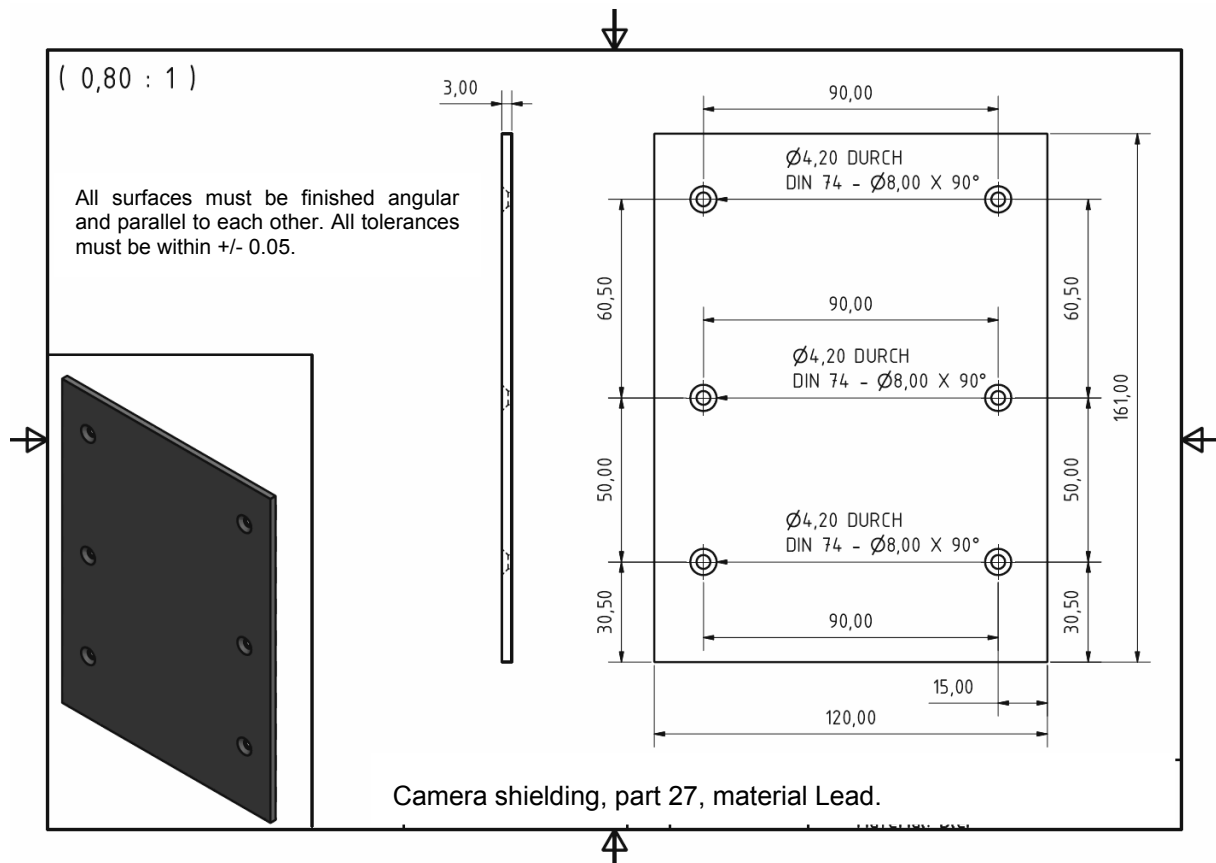


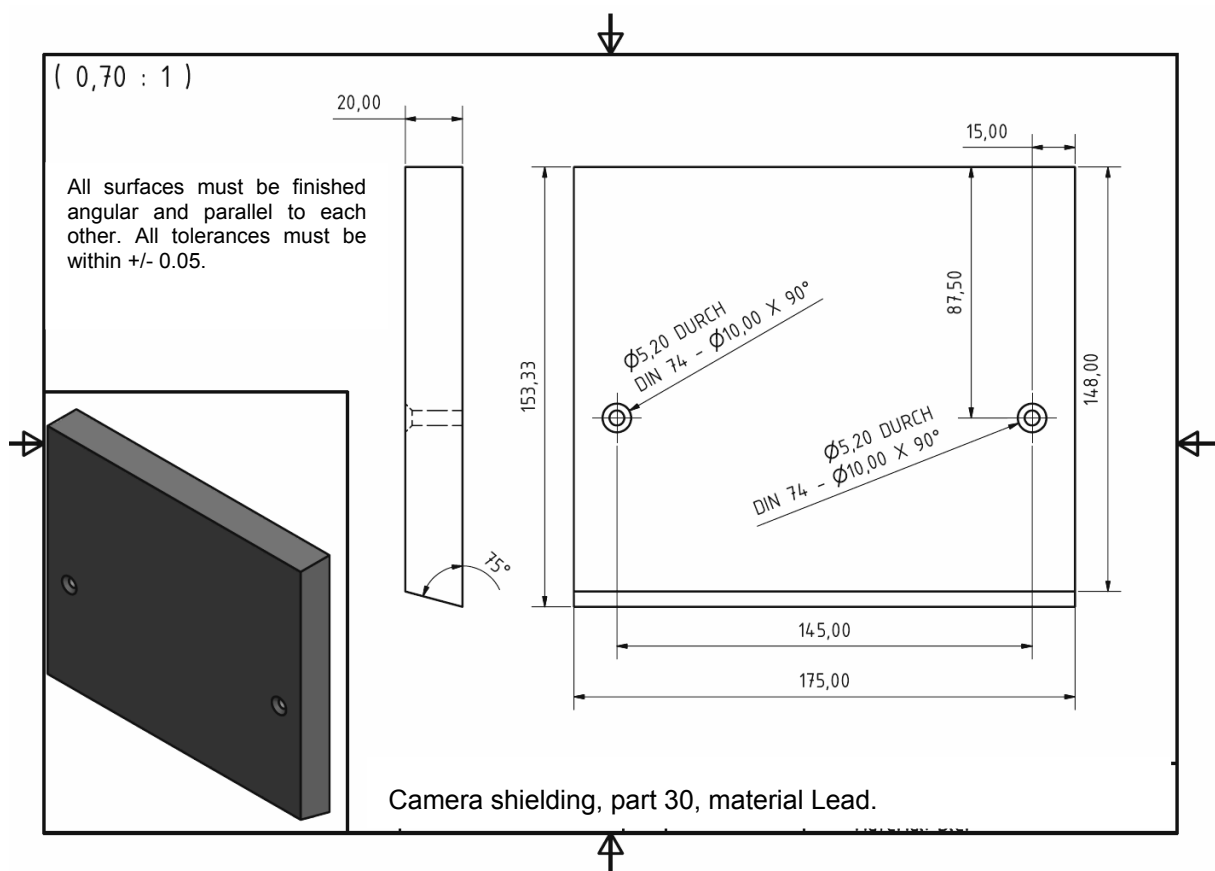
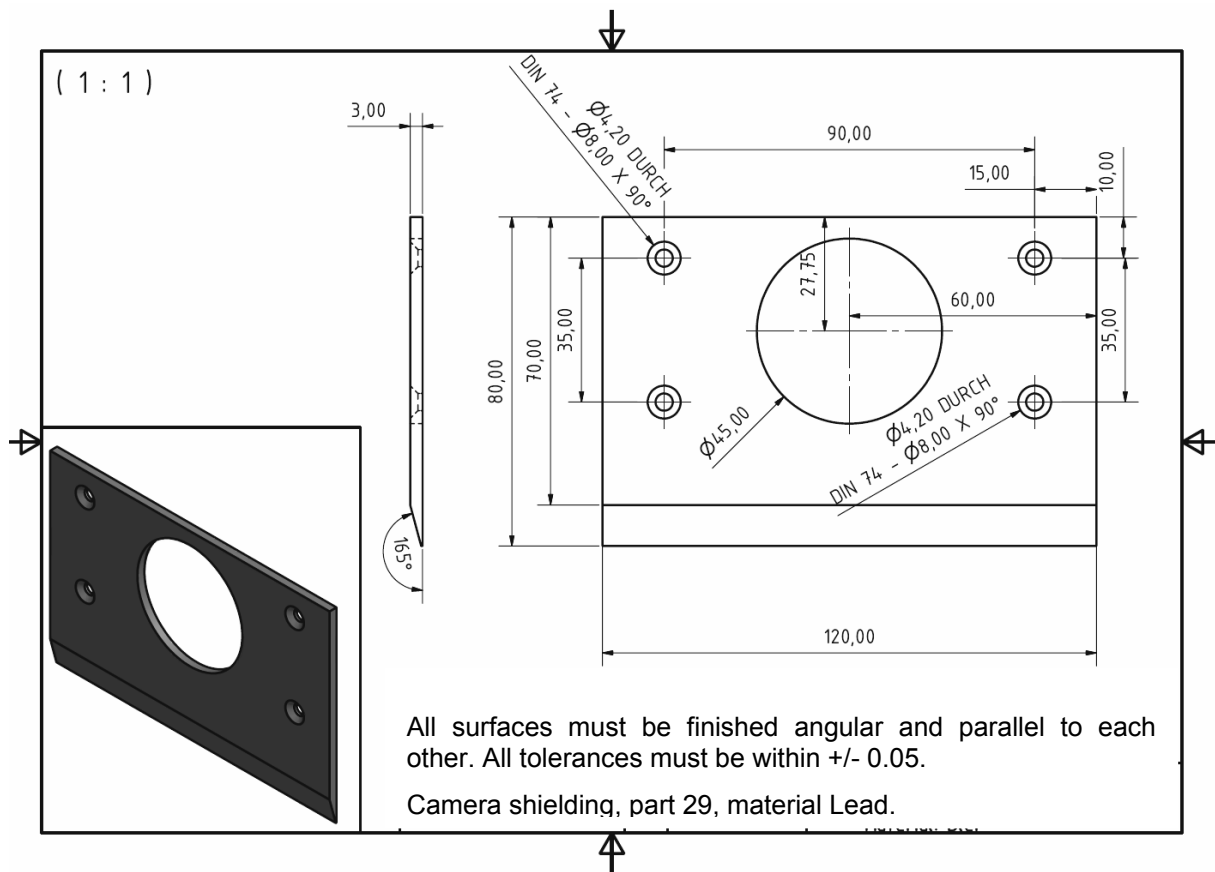












CONTRIBUTORS TO DRAFTING AND REVIEW

Azizova, A.	Navoi Mining and Metallurgy Combine, Uzbekistan
Dorobantu, V	Timisoara Politechnica University, Romania
Ewert, U.	Federal Institute for Materials Research and Testing, Germany
Garci, A.	National Atomic Energy Commission, Argentina
Hamzah, A.R.	Ministry of Science, Technology and Innovation, Malaysia
Harara, W.	Atomic Energy Commission, Syrian Arab Republic
Infanzon, S.	Uruguayan Society for NDT, AENDUR, ANCAP, Uruguay
Jin, Joon-Ha	International Atomic Energy Agency
Khan, A.A.	International Atomic Energy Agency
Rao, B.P.C.	International Atomic Energy Agency
Venkatraman, B.	Indira Gandhi Centre for Atomic Research, India
Zaheer, A.	National Centre for Non-Destructive Testing, Pakistan
Zscherpel, U.	Federal Institute for Materials Research and Testing, Germany



IAEA

International Atomic Energy Agency

No. 22

Where to order IAEA publications

In the following countries IAEA publications may be purchased from the sources listed below, or from major local booksellers. Payment may be made in local currency or with UNESCO coupons.

AUSTRALIA

DA Information Services, 648 Whitehorse Road, MITCHAM 3132
Telephone: +61 3 9210 7777 • Fax: +61 3 9210 7788
Email: service@dadirect.com.au • Web site: <http://www.dadirect.com.au>

BELGIUM

Jean de Lannoy, avenue du Roi 202, B-1190 Brussels
Telephone: +32 2 538 43 08 • Fax: +32 2 538 08 41
Email: jean.de.lannoy@infoboard.be • Web site: <http://www.jean-de-lannoy.be>

CANADA

Bernan Associates, 4501 Forbes Blvd, Suite 200, Lanham, MD 20706-4346, USA
Telephone: 1-800-865-3457 • Fax: 1-800-865-3450
Email: customercare@bernandirect.com • Web site: <http://www.bernandirect.com>

Renouf Publishing Company Ltd., 1-5369 Canotek Rd., Ottawa, Ontario, K1J 9J3
Telephone: +613 745 2665 • Fax: +613 745 7660
Email: order.dept@renoufbooks.com • Web site: <http://www.renoufbooks.com>

CHINA

IAEA Publications in Chinese: China Nuclear Energy Industry Corporation, Translation Section, P.O. Box 2103, Beijing

CZECH REPUBLIC

Suweco CZ, S.R.O., Klecakova 347, 180 21 Praha 9
Telephone: +420 26603 5364 • Fax: +420 28482 1646
Email: nakup@suweco.cz • Web site: <http://www.suweco.cz>

FINLAND

Akateeminen Kirjakauppa, PO BOX 128 (Keskuskatu 1), FIN-00101 Helsinki
Telephone: +358 9 121 41 • Fax: +358 9 121 4450
Email: akatilauk@akateeminen.com • Web site: <http://www.akateeminen.com>

FRANCE

Form-Edit, 5, rue Janssen, P.O. Box 25, F-75921 Paris Cedex 19
Telephone: +33 1 42 01 49 49 • Fax: +33 1 42 01 90 90
Email: formedit@formedit.fr • Web site: <http://www.formedit.fr>

Lavoisier SAS, 145 rue de Provigny, 94236 Cachan Cedex
Telephone: + 33 1 47 40 67 02 • Fax +33 1 47 40 67 02
Email: romuald.verrier@lavoisier.fr • Web site: <http://www.lavoisier.fr>

GERMANY

UNO-Verlag, Vertriebs- und Verlags GmbH, Am Hofgarten 10, D-53113 Bonn
Telephone: + 49 228 94 90 20 • Fax: +49 228 94 90 20 or +49 228 94 90 222
Email: bestellung@uno-verlag.de • Web site: <http://www.uno-verlag.de>

HUNGARY

Librotrade Ltd., Book Import, P.O. Box 126, H-1656 Budapest
Telephone: +36 1 257 7777 • Fax: +36 1 257 7472 • Email: books@librotrade.hu

INDIA

Allied Publishers Group, 1st Floor, Dubash House, 15, J. N. Heredia Marg, Ballard Estate, Mumbai 400 001,
Telephone: +91 22 22617926/27 • Fax: +91 22 22617928
Email: alliedpl@vsnl.com • Web site: <http://www.alliedpublishers.com>

Bookwell, 2/72, Nirankari Colony, Delhi 110009
Telephone: +91 11 23268786, +91 11 23257264 • Fax: +91 11 23281315
Email: bookwell@vsnl.net

ITALY

Libreria Scientifica Dott. Lucio di Biasio "AEIOU", Via Coronelli 6, I-20146 Milan
Telephone: +39 02 48 95 45 52 or 48 95 45 62 • Fax: +39 02 48 95 45 48
Email: info@libreriaaeiou.eu • Website: www.libreriaaeiou.eu

JAPAN

Maruzen Company Ltd, 1-9-18, Kaigan, Minato-ku, Tokyo, 105-0022
Telephone: +81 3 6367 6079 • Fax: +81 3 6367 6207
Email: journal@maruzen.co.jp • Web site: <http://www.maruzen.co.jp>

REPUBLIC OF KOREA

KINS Inc., Information Business Dept. Samho Bldg. 2nd Floor, 275-1 Yang Jae-dong SeoCho-G, Seoul 137-130
Telephone: +02 589 1740 • Fax: +02 589 1746 • Web site: <http://www.kins.re.kr>

NETHERLANDS

De Lindeboom Internationale Publicaties B.V., M.A. de Ruyterstraat 20A, NL-7482 BZ Haaksbergen
Telephone: +31 (0) 53 5740004 • Fax: +31 (0) 53 5729296
Email: books@delindeboom.com • Web site: <http://www.delindeboom.com>

Martinus Nijhoff International, Koraalrood 50, P.O. Box 1853, 2700 CZ Zoetermeer
Telephone: +31 793 684 400 • Fax: +31 793 615 698
Email: info@nijhoff.nl • Web site: <http://www.nijhoff.nl>

Swets and Zeitlinger b.v., P.O. Box 830, 2160 SZ Lisse
Telephone: +31 252 435 111 • Fax: +31 252 415 888
Email: info@swets.nl • Web site: <http://www.swets.nl>

NEW ZEALAND

DA Information Services, 648 Whitehorse Road, MITCHAM 3132, Australia
Telephone: +61 3 9210 7777 • Fax: +61 3 9210 7788
Email: service@dadirect.com.au • Web site: <http://www.dadirect.com.au>

SLOVENIA

Cankarjeva Založba d.d., Kopitarjeva 2, SI-1512 Ljubljana
Telephone: +386 1 432 31 44 • Fax: +386 1 230 14 35
Email: import.books@cankarjeva-z.si • Web site: <http://www.cankarjeva-z.si/uvvoz>

SPAIN

Díaz de Santos, S.A., c/ Juan Bravo, 3A, E-28006 Madrid
Telephone: +34 91 781 94 80 • Fax: +34 91 575 55 63
Email: compras@diazdesantos.es, carmela@diazdesantos.es, barcelona@diazdesantos.es, julio@diazdesantos.es
Web site: <http://www.diazdesantos.es>

UNITED KINGDOM

The Stationery Office Ltd, International Sales Agency, PO Box 29, Norwich, NR3 1 GN
Telephone (orders): +44 870 600 5552 • (enquiries): +44 207 873 8372 • Fax: +44 207 873 8203
Email (orders): book.orders@tso.co.uk • (enquiries): book.enquiries@tso.co.uk • Web site: <http://www.tso.co.uk>

On-line orders

DELTA Int. Book Wholesalers Ltd., 39 Alexandra Road, Addlestone, Surrey, KT15 2PQ
Email: info@profbooks.com • Web site: <http://www.profbooks.com>

Books on the Environment

Earthprint Ltd., P.O. Box 119, Stevenage SG1 4TP
Telephone: +44 1438748111 • Fax: +44 1438748844
Email: orders@earthprint.com • Web site: <http://www.earthprint.com>

UNITED NATIONS

Dept. I004, Room DC2-0853, First Avenue at 46th Street, New York, N.Y. 10017, USA
(UN) Telephone: +800 253-9646 or +212 963-8302 • Fax: +212 963-3489
Email: publications@un.org • Web site: <http://www.un.org>

UNITED STATES OF AMERICA

Bernan Associates, 4501 Forbes Blvd., Suite 200, Lanham, MD 20706-4346
Telephone: 1-800-865-3457 • Fax: 1-800-865-3450
Email: customercare@bernan.com • Web site: <http://www.bernan.com>

Renouf Publishing Company Ltd., 812 Proctor Ave., Ogdensburg, NY, 13669
Telephone: +888 551 7470 (toll-free) • Fax: +888 568 8546 (toll-free)
Email: order.dept@renoufbooks.com • Web site: <http://www.renoufbooks.com>

Orders and requests for information may also be addressed directly to:

Marketing and Sales Unit, International Atomic Energy Agency

Vienna International Centre, PO Box 100, 1400 Vienna, Austria
Telephone: +43 1 2600 22529 (or 22530) • Fax: +43 1 2600 29302
Email: sales.publications@iaea.org • Web site: <http://www.iaea.org/books>

The introduction of powerful computers and reliable imaging technologies has had a significant impact on traditional radiation based non-destructive testing (NDT) techniques. In particular, digitization of images provides economy of storage, efficiency of communication, and increased speed of inspection and evaluation. NDT laboratories in developed countries are progressing rapidly with the digitization of radiation inspection data. New imaging techniques using image intensifier systems, imaging plates and flat panel detectors have increased the capacity for visualization of surface and internal defects in welds, castings, forging composite materials and concrete, revealing new potential for accurate evaluation of such defects by radiation techniques. This publication describes the design, development and optimization of an affordable, low cost digital industrial radiology (DIR) fluoroscopic system. It provides guidelines on building an economically viable, easily assembled DIR system, providing interested Member States — including developing Member States — access to DIR technology.

INTERNATIONAL ATOMIC ENERGY AGENCY
VIENNA

ISBN 978-92-0-129310-7
ISSN 2225-8833